University of South Carolina
Scholar Commons

Theses and Dissertations

2016

A Mechanical Approach to the Characterization of Material Failure of Atherosclerotic Lesions

Lindsey A. Davis
University of South Carolina

Follow this and additional works at: http://scholarcommons.sc.edu/etd

 Part of the Biomedical Engineering and Bioengineering Commons

Recommended Citation
Davis, L. A.(2016). *A Mechanical Approach to the Characterization of Material Failure of Atherosclerotic Lesions.* (Doctoral dissertation). Retrieved from http://scholarcommons.sc.edu/etd/3547

This Open Access Dissertation is brought to you for free and open access by Scholar Commons. It has been accepted for inclusion in Theses and Dissertations by an authorized administrator of Scholar Commons. For more information, please contact SCHOLARC@mailbox.sc.edu.

A Mechanical Approach to the Characterization of Material Failure of Atherosclerotic Lesions

by

Lindsey A. Davis

Bachelor of Science
Virginia Tech, 2012

Submitted in Partial Fulfillment of the Requirements

For the Degree of Doctor of Philosophy in

Biomedical Engineering

College of Engineering and Computing

University of South Carolina

2016

Accepted by:

Susan M. Lessner, Major Professor

Michael A. Sutton, Committee Member

John F. Eberth, Committee Member

Richard L. Goodwin, Committee Member

Lacy Ford, Senior Vice Provost and Dean of Graduate Studies

© Copyright by Lindsey A. Davis, 2016
All Rights Reserved.

DEDICATION

To my parents, my brothers, Matt and Brian, and to a very special aunt, Lisa, who encouraged me to pursue a PhD.

ACKNOWLEDGEMENTS

I would especially like to thank my advisor, Dr. Susan Lessner, for all of the advice and guidance she has given me over the past four years. She has been a great mentor and teacher and I am truly thankful for the opportunity to work with her. I would also like the thank committee members, Dr. Michael Sutton, Dr. John Eberth, and Dr. Rich Goodwin for all of their help and support along the way. Each of them have answered countless questions and provided valuable advice throughout this process.

I have collaborated on projects with several different groups including Dr. Michelle Bendeck and Joshua Lopes, Dr. Tarek Shazly and Will Torres, Dr. Daping Fan and Fatma Saaoud, and Dr. Xiaomin Deng and Xiaochang Leng. I appreciate all of their feedback and advice and I enjoyed working working with people with expertise in other fields.

Lastly, I would like to thank past and present members of Dr. Lessner's lab specifically, Shana Watson, John Johnson, Mo Gabr, Taylor Shaw, and Bilal Merei for their encouragement, support, and advice. Each of them also helped make the lab an enjoyable place to work. I would also like to thank Samm Stewart, an undergraduate student who assisted my research projects for nearly two years. She was vital in helping me complete all of my research.

ABSTRACT

Failure of atherosclerotic plaques can lead to potentially life threatening clinical events such as myocardial infarction (MI), stroke, or transient ischemic attack (TIA). The most frequently described plaque failure mechanism is tensile rupture of the fibrous cap; however, often during angioplasty another plaque failure mechanism occurs in which the atherosclerotic plaque separates from the internal elastic lamina (IEL). This study aims assess the material strength of atherosclerotic lesions using mechanical concepts.

To assess likelihood of plaque dissection at the vessel wall, adhesion strength was assessed in both mouse and human specimens using plaque delamination experiments. Measuring plaque adhesion in transgenic mouse models can be useful in understanding the contributions to plaque adhesion from specific proteins. Comparing these results to similar delamination experiments in human plaques aids in understanding the similarities between mechanical properties of plaques in the two species.

To further understand adhesive failure at the plaque-IEL interface, the contributions of adhesive proteins to the mechanical strength of the plaque-IEL interface were investigated. The results from a novel semi-quantitative plaque immunoblotting technique and measurements of adhesive strength of thin protein films combine to provide an estimate of the adhesive strength of relevant matrix

proteins at approximate ex vivo concentrations. The adhesion strength in thin protein films is much lower than that determined from in situ plaque adhesion experiments and suggests that bridging fibers, rather than adhesive proteins, are likely to be responsible for the adhesive strength of the plaque-IEL interface.

In addition to plaque adhesion strength, plaque stability was also assessed by investigating the resistance to tensile rupture of the fibrous caps in human carotid endarterectomy specimens. Mechanical strength of fibrous caps was assessed during failure by calculating crack tip opening displacement (CTOD) and stress in the uncracked segment (UCS) in miniature single edge notched tensile (MSENT) specimens. The results show that fibrous caps with greater collagen content exhibit more brittle behavior and fail at a higher stress and a smaller CTOD than those with a lower collagen content, which exhibit a more ductile response. Knowledge of the collagen content in the fibrous cap prior to surgical intervention could predict the mechanical response of the fibrous cap and aid in determining the optimal treatment plan.

Fracture toughness was used to assess plaque resistance to two different failure mechanisms: 1) plaque delamination at the plaque-IEL interface and 2) tensile rupture of the fibrous cap. Collagen is a vital structural component of atherosclerotic plaques and is crucial in determining the mechanical response of fibrous caps. Fibrillar forms of collagen, such as collagen I, or other fibrillar proteins, such as fibrillin-1, are likely responsible for the mechanical strength of the plaque-IEL interface.

TABLE OF CONTENTS

LIST OF TABLES

LIST OF FIGURES

CHAPTER 1

INTRODUCTION

Atherosclerotic plaque rupture can lead to myocardial infarction (MI) or ischemic stroke, which are two of the leading causes of death in the United States [1]. There were approximately 7.6 million MIs in 2014 in the US alone. It is estimated that by 2030 there will be 3.4 million strokes in American adults, a 20% increase in prevalence since 2012. The total cost of cardiovascular disease and stroke in the United States in 2010 is estimated to be over $315 billion [2].

1.1 Structure and composition of the arterial wall

There are two main types of arteries: elastic arteries and muscular arteries. Elastic arteries, such as the aorta, typically consist of three concentric tissue layers: the intima, the media, and the adventitia. Figure 1, used with permission from reference [3], shows a diagram of a typical elastic artery. The intima is the innermost layer and primarily consists of a single layer of endothelial cells which rest on a basement membrane and subendothelial layer. In diseased atherosclerotic arteries, the intima thickens in the subendothelial layer with inflammatory cells, lipids, calcium deposits, and collagen fibers. This thickening can be so severe that in these cases the intima actually bears a significant portion of the load in these regions [3]. The middle layer of the artery, the media, consists

of a network of collagen fibers, elastin, and smooth muscle cells (SMCs). A series of elastic lamellae separate the media into several layers of a fiber reinforced material. The innermost elastic layer, the internal elastic lamina, separates the media from the intima, and the outermost, the external elastic lamina, separates the media from the adventitia. Collagen and elastin are the major load bearing extracellular matrix (ECM) proteins present in arteries [3]–[5]. Elastin, a primary component of the media, allows for the reversible stretching of the artery, which repeatedly occurs in elastic arteries due to the pulsatile blood flow originating from the heart. Elastic fibers appear wavy and unengaged at low pressures; however, they straighten at physiological blood pressures and are likely the primary load bearing elements [5], [6]. The adventitia is the outermost layer of the artery and is primarily composed of thick bundles of collagen, fibroblasts (fibrocytes), macrophages, and resident stem cells. Collagen, unlike elastin, primarily engages at higher than normal physiological pressures to prevent rupture of the artery [3], [5] - [7].

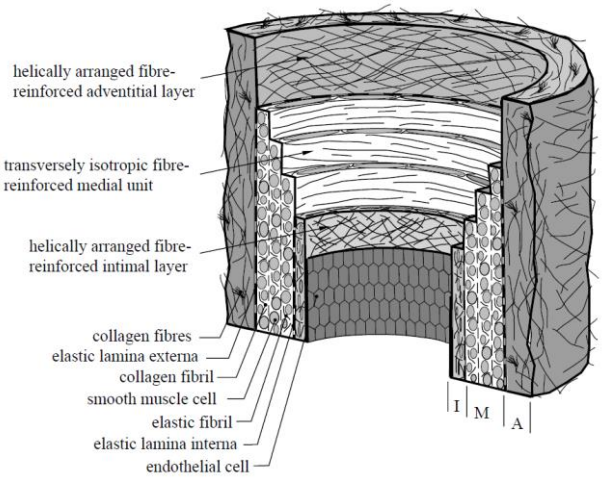

Figure 1.1 A typical elastic artery. The intima is designated by ‘I’, the media ‘M’, and the adventitia, ‘A’. This figure was reused with permission from [3].

Though collagen and elastin provide most of the load bearing support, glycoproteins, such as fibrillin-1, fibronectin, or other glycoproteins with adhesive properties, may be involved in physically binding the layers of the artery together. Fibrillin-1 is the major component of individual microfibrils which associate with mature elastic fibers [8]; however, they are found in the absence of elastin in some locations, such as the ciliary zonula of the eye and superficial regions of the skin [9]. Microfibrils, even without the presence of elastin, have been shown to contribute to the structural integrity of the tissue [10]. They have been found linking the abluminal surface of endothelial cells to the internal elastic lamina in neonatal rat aorta [11]. Therefore, microfibrils may be important structural elements in vascular tissue, even in the absence of elastin. There is also evidence to support adhesive proteins, such as fibronectin, as important structural proteins in vascular tissue. Fibronectin has a multidomain structure which enables binding to cell surfaces as well as to other ECM molecules, such as collagen, microfibrils, and proteoglycans [11]–[13]. Therefore, fibronectin may be a structural link between cells and ECM components. Other, unidentified adhesive and fibrillar proteins may also contribute to the structural integrity of healthy and diseased vasculature. There are many adhesive glycoproteins, e.g. laminin, osteopontin, thrombospondin, in tissue. In fact, an entire class of proteins, matricellular proteins, may be important to consider. While matricellular proteins are not primary structural proteins like collagen or elastin, they can modulate cell-matrix interactions and therefore may affect adhesion strength [14].

1.2 Atherosclerosis

Development and progression of atherosclerotic lesions

The development of atherosclerosis is a decades-long process that begins with thickening of the intima. This thickening, known at adaptive intimal thickening, primarily consists of SMCs, proteoglycans, and elastin, and is likely an adaptation to maintain homeostatic flow and shear stress [15]. In 1995 Williams and Tabas described the “response-to-retention” hypothesis, still a valid hypothesis of atherogenesis today [16]. The first step of atherogenesis, according to the response-to-retention hypothesis, is sequestration of lipoproteins in the thickened intima by binding to proteoglycans in the ECM. Lipoproteins bound to proteoglycans are more likely to be oxidized, which leads to uptake by macrophage cells. The process is advanced by macrophages secreting additional proteoglycans that further increase lipid retention in the vascular wall [17]. Macrophages ingest and store lipoproteins, which are rich in cholesterol, resulting in the formation of foam cells [18], [19]. Foam cells sometimes ingest too much cholesterol to store as cholesterol esters, resulting in high levels of free cholesterol. High levels of free cholesterol trigger apoptosis in cells, resulting in necrosis of the foam cells [19]. When the resulting necrotic core is covered by a thin fibrous cap, the plaque configuration is particularly vulnerable to plaque rupture, potentially leading to myocardial infarction and stroke [20]–[22].

There are several key processes involved in the development of atherosclerosis, such as lipoprotein retention, macrophage infiltration, apoptosis,

and necrosis of the lipid core. The order and interaction between these processes is not well understood. Repeated cycles of atherogenic events at different time points during plaque development likely contribute to the heterogeneous nature and unpredictable progression of atherosclerotic plaques. One potential sequence of atherosclerotic lesion development is shown in Figure 1.2.

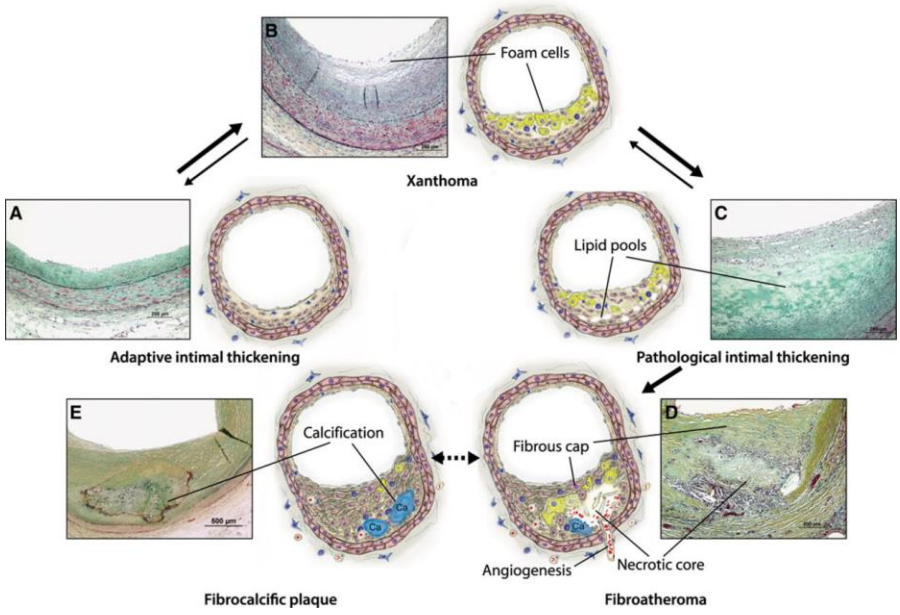

Figure 1.2 The progression of atherosclerosis. The histological images were stained with Movat's pentachrome. This image is reused with permission from [22].

There is some disagreement regarding the initiation of atherosclerotic lesions. While intimal xanthoma and adaptive intimal thickening are both considered non-atherosclerotic due to their limited clinical impact, the sequence and interaction between these two states is not well known. Some studies argue that intimal xanthomas are a separate initiation pathway to atherosclerotic lesions [20], while other studies hypothesize that xanthomas develop at sites of adaptive intimal thickening [22] (and as shown in Figure 1.2). Atherosclerotic lesions

progress by accumulating lipids and macrophages within the intima, developing a distinct fibrous cap composed of SMCs and collagen, and accumulating calcium deposits within the lesion [22]. Many of these processes are concurrent and the exact processes are difficult to sequence; however, various stages can be classified using the morphological characteristics described in the next section.

Classification of atherosclerotic lesions

There are several methods of classification of atherosclerotic lesions; however, the most widely referenced classification scheme linking plaque morphology to clinical disease state was first introduced by Virmani, et al. in 2000 [20]. Based on this classification, there are seven categories of lesions.

Virmani, et al. proposed two potential initiation mechanisms in atherosclerosis: intimal thickening and intimal xanthoma. An intimal xanthoma is characterized by an accumulation of macrophages in the intima of the vessel, whereas intimal thickening primarily consists of SMCs, proteoglycans, and elastin. The intermediate stage is termed pathologic intimal thickening (PIT) and is characterized by lipid presence in the lesion without necrosis. The lipid pools are covered with a thin layer of proteoglycans and SMCs, with small numbers of macrophages [18], [20]. The fibrous cap atheroma contains a true necrotic core along with a distinct fibrous cap which consists of SMCs, collagen, proteoglycans, and typically higher levels of macrophages and lymphocytes than those in PIT lesions. The thin cap fibroatheroma (TCFA) is given a special distinction because of its increased likelihood of plaque rupture. The presence of significant amounts

of calcification within the lesion leads to two additional morphological classifications. The first is calcified nodules, which are dense nodules of calcium that disrupt the fibrous cap and are associated with thrombi. Fibrocalcific plaques, on the other hand, are characterized by a heavily calcified plaque with a relatively small necrotic core and an intact fibrous cap without any thrombus present [20].

Material failure of atherosclerotic lesions

As the atherosclerotic disease state progresses, the likelihood increases of plaque failure resulting in a clinical event, such as myocardial infarction or stroke. The most frequent and well described mechanism of plaque failure is plaque rupture, during which a tear in the fibrous cap exposes the highly thrombogenic necrotic core material. This mechanism generally occurs in lesions characterized as a thin-cap fibroatheroma (TCFA) and is responsible for about 60% of all cases involving thrombotic sudden coronary death. A second mechanism is plaque erosion, which typically occurs in intimal thickening or fibroatheromas with little to no necrotic core. However, the exact mechanism underlying plaque erosion is unknown [20]–[23].

The size of the necrotic core is thought to play an important role in the risk associated with TCFAs. Necrotic core material is lacking sufficient collagen to provide mechanical support to the vessel which can lead to a greater stress applied to the fibrous cap. Additionally, the necrotic core may erode the thin fibrous cap, increasing the stress even further. Ultimately, higher stresses in a material increase the likelihood of material failure [21]–[23].

Oftentimes, the thrombosis resulting from plaque rupture or plaque erosion does not result in vessel occlusion and remains clinically silent. However, the healing of the rupture or erosion sites promotes further occlusion of the vessel, and subsequent ruptures or erosions frequently occur. Healed rupture sites are generally characterized by a disrupted fibrous cap filled in with proteoglycans or collagen III. There also may be multi-layering of necrotic core and lipid. Healed erosion sites, on the other hand, typically do not have a necrotic core or a disrupted fibrous cap. Instead, multi-layering of collagen and SMCs with proteoglycans is evident [22], [23].

1.3 Current clinical interventions

The two most common interventional treatments for atherosclerotic carotid artery stenosis are carotid artery stenting (CAS) and carotid endarterectomy (CEA). CEA is an invasive surgical procedure in which the plaque and the underlying media are dissected from the carotid artery and a vascular patch is placed over the remaining adventitia. Carotid endarterectomy (CEA) is generally considered the standard treatment for carotid artery stenosis, but recently carotid artery stenting (CAS) has been suggested as an alternative, less invasive, technique.

In CAS, a catheter is inserted into the carotid artery and a small balloon is inflated at the lesion site. The goal is to flatten the plaque and to increase the lumen area; however, in some cases this results in plaque dissection at the plaque shoulder. The resulting damage is commonly treated with the implantation of a

stent over the dissected tissue to hold the intimal and medial surfaces together to recreate a smooth lumen [24]–[26]. CAS has been shown to result in more strokes during the periprocedural period than CEA [27]–[29].

Estimation of the plaque mechanical properties could help assess the optimal treatment for carotid artery stenosis. The increased risk of stroke during the periprocedural period following CAS may be reduced if the material properties of the plaque are considered prior to selecting a treatment. The timing of the procedure can be optimized if we can predict which plaques are more prone to rupture.

1.4 Fracture mechanics and biological tissues

The goal of this study is to use the principles of fracture mechanics and material failure to gain an understanding of the failure of atherosclerotic lesions. Assessing the adhesion strength between atherosclerotic plaques and the underlying arterial wall may provide insight into the mechanism of plaque dissection or delamination that sometimes occurs during balloon angioplasty. Additionally, measuring the fracture toughness through the fibrous cap will characterize its ability to resist a tear and ultimately to avoid rupture.

Fracture mechanics can be used to characterize the cohesive behavior of materials, such as the tissue within the fibrous cap, as well as the properties of the interface between two adhesive materials, such as the plaque-internal elastic lamina (IEL) interface. Fracture toughness can be described by several metrics.

Two that will be used in this study are energy release rate and crack tip opening displacement (CTOD).

The energy release rate is defined as the energy required to extend a crack, per unit of crack extension, and is based on the concept that crack extension will occur when the energy available for crack growth exceeds the resistance of the material [30]–[33]. Though not used previously to characterize fracture toughness in vascular tissue, CTOD was first proposed by Wells at the British Welding Institute to characterize failure under elastic-plastic yielding conditions [14]. Wells observed that plastic deformation resulted in blunting at the crack tip, and that the extent of crack-tip blunting increased in proportion to the toughness of the material. Later, Dawes showed that CTOD is linearly related to the J-integral in elastic-plastic conditions and that both are valid fracture parameters [15].

1.5 Previous Studies

Fracture mechanics has been used to characterize biological tissues in the past. Several groups have previously used energy release rate to characterize fracture toughness within biological tissues [30], [34], [35]. Wang et al. developed a protocol to measure the plaque adhesion strength in mice and to determine the effects of specific proteins on plaque adhesion using transgenic mice [36], [37]. This technique can be applied to investigate the potential contributions of additional proteins to plaque adhesion strength.

Collagen VIII is a non-fibrillar collagen upregulated during atherosclerotic lesion development that may impact plaque stability [38]–[40] and therefore it may

be important to investigate the effect of collagen VIII on plaque adhesion strength. SMC migration and proliferation are both decreased in apolipoprotein E; collagen VIII triple knockout ($ApoE^{-/-}$;$Col8^{-/-}$) mice when compared to apolipoprotein E knockout ($ApoE^{-/-}$) mice [41], [42]. SMCs adhere less strongly to collagen VIII than to collagen I, and it is hypothesized that increased deposition of collagen VIII masks collagen I and allows increased migration of SMCs in atherosclerotic lesions [41]. Atherosclerotic lesions of $ApoE^{-/-}$;$Col8^{-/-}$ mice have thinner fibrous caps and larger necrotic cores than those of $ApoE^{-/-}$ $Col\ 8^{+/+}$ mice due to decreased migration and proliferation of SMCs [42]. Morphological characteristics including larger necrotic cores and thinner fibrous caps are associated with increased plaque vulnerability in humans [21], [43] and this may also be true in mice. In order to truly assess the effects of collagen VIII on plaque stability, however, mechanical testing of the atherosclerotic plaques must be conducted in both $ApoE^{-/-}$ and $ApoE^{-/-}$;$Col8^{-/-}$ mice. Additionally, in order for the mouse plaque adhesion strength results to be considered clinically relevant, plaque adhesion strength must also be measured in human atherosclerotic plaques.

Measurements of plaque adhesion strength can provide some insights into failure at the plaque-IEL or fibrous cap-lipid core interfaces, but further investigation is necessary in order to understand the more detailed failure mechanism. Potential failure mechanisms include breakage of fibers that bind two tissue layers or breakage of bonds between adhesive proteins and other ECM components. There is little known about which proteins are present at the plaque-

IEL interface and even less known about the mechanical properties of these proteins.

There have been several studies that have investigated the mechanical properties of human atherosclerotic plaques using uniaxial extension tests [44]–[49], compression tests [49]–[51], and uniaxial extension tests in both circumferential and axial orientations [52], [53]. Most of these studies have determined the stress-strain response under specified loading conditions; however, few studies have measured other mechanical properties of these tissues. Ultimate tensile strength (UTS) has been measured by a few groups in whole plaques [46]–[48], and once in isolated fibrous caps [54]. While knowledge of the mechanical properties of whole plaques has some utility, properties of isolated fibrous cap specimens are more relevant to assessing plaque vulnerability to rupture. In general, both strength and toughness need to be assessed to understand material failure. Many engineering materials that exhibit high strength are brittle and exhibit low fracture toughness and vice versa, though this is not always the case, especially in complex materials such as atherosclerotic plaques. To the author's knowledge, there have been no reports of fracture toughness measurements in human fibrous caps. Thus, this represents an important gap in the literature.

1.6 Specific Aims

The overall goal of this project is to assess the mechanical failure of atherosclerotic lesions. Mechanical characterization of these tissues may provide

insight into the failure mechanisms and potentially determine the relevant failure criteria. Understanding the mechanism of plaque failure is the first step in developing a method or treatment to prevent plaque failure. Therefore, this work may be an important step in advancing the therapeutic treatment options for atherosclerosis.

Specific Aim 1*: Determine the effects of collagen VIII on plaque adhesion strength in mice and compare plaque adhesion strength in mice to fibrous cap adhesion strength in human carotid endarterectomy specimens.*

In order to build on previous plaque adhesion strength measurements, two additional sets of experiments were performed. The first set of experiments measured plaque adhesion strength in transgenic mice to assess the contributions of collagen VIII to adhesion strength. The second set of experiments was performed on human atherosclerotic plaques to determine whether or not the mouse plaque adhesion strength measurements are representative of plaque adhesion strength in humans.

Specific Aim 2: *Determine the role of adhesive proteins at the plaque-IEL interface.*

The goal of specific aim 2 is to investigate separation of adhesive proteins as a potential failure mechanism at the plaque-IEL interface using a novel approach. Immunohistochemistry and semi-quantitative plaque immunoblotting were used to identify and to approximately quantify several adhesive proteins at the interface between atherosclerotic plaques and the underlying IEL in a mouse

model of atherosclerosis. The adhesive strength between thin films of these proteins and vascular ECM was measured using rigid double cantilever beam (RDCB) experiments. By comparing the energy release rate in these experiments to the energy release rate calculated from previous in situ measurements of plaque delamination from the IEL, the role of the adhesive proteins can be determined. If the energy release rates are greatly different between these two sets of experiments, we can conclude that other structures, such as bridging fibers, may play a significant role in the adhesion strength between the plaque and the IEL.

Specific Aim 3: *Characterize the fracture toughness of atherosclerotic fibrous caps in human carotid endarterectomy (CEA) specimens.*

Fracture mechanics concepts were used to characterize fracture toughness in atherosclerotic fibrous caps for the first time. In particular, crack tip opening displacement (CTOD) and the stress in the uncracked segment (UCS) at failure initiation were evaluated in each fibrous cap specimen. Additionally, the collagen content was measured in each fibrous cap and compared to the mechanical testing results.

CHAPTER 2

ATHEROSCLEROTIC PLAQUE ADHESION STRENGTH IN TRANSGENIC MICE AND HUMAN CAROTID ENDARTERECTOMY SPECIMENS

2.1 Introduction

Atherosclerotic plaque failure is one of the leading causes of myocardial infarction and stroke. There are at least two potential failure mechanisms for atherosclerotic plaques. The first involves tensile rupture of the fibrous cap and the second, which is prominent during angioplasty, involves plaque delamination from the internal elastic lamina (IEL) at the plaque shoulder. During balloon angioplasty, a catheter is inserted into the blood vessel and a small balloon is inflated at the lesion site. The goal is to flatten the plaque and increase the lumen area; however, in some cases this procedure results in intimal dissection at the plaque shoulder. These localized dissections are commonly treated with the implantation of a stent over the dissected tissue to hold the intimal and medial surfaces together and to recreate a smooth lumen [24]–[26].

Plaque adhesion strength has previously been measured in apolipoprotein E knockout ($ApoE^{-/-}$) mice [36] and in apolipoprotein E matrix metalloproteinase-12 double knock out ($ApoE^{-/-}$ $MMP12^{-/-}$) mice [37], showing that MMP-12

strengthens plaque adhesion, potentially by increasing the formation of gaps in the IEL to allow for fiber bridging between the intima and the media. The methodology developed by Wang, et al. will be used in the present work to study the effects of collagen VIII on plaque adhesion strength by examining plaque adhesion strength in both ApoE$^{-/-}$ and apolipoprotein E; collagen VIII triple knockout (ApoE$^{-/-}$ Col8$^{-/-}$) mice.

Collagen VIII is a non-fibrillar collagen that is upregulated during atherosclerotic lesion development [38]–[40]. Smooth muscle cell (SMC) migration and proliferation are both decreased in ApoE$^{-/-}$ Col8$^{-/-}$ mice when compared to ApoE$^{-/-}$ mice [42], [55]. SMCs adhere less strongly to collagen VIII than to collagen I, and it is hypothesized that increased deposition of collagen VIII masks collagen I and allows increased migration of SMCs in atherosclerotic lesions [55]. Atherosclerotic lesions of ApoE$^{-/-}$ Col8$^{-/-}$ mice have thinner fibrous caps and larger necrotic cores than those of ApoE$^{-/-}$ Col 8$^{+/+}$ mice due to decreased SMC migration and proliferation [42]. Morphological characteristics including larger necrotic cores and thinner fibrous caps are associated with increased plaque vulnerability in humans [21] and this may also be true in mice. In order to truly assess plaque stability, however, mechanical testing of the atherosclerotic plaques must be conducted in both ApoE$^{-/-}$ and ApoE$^{-/-}$ Col8$^{-/-}$ mice.

The current study will build on the previous work by Wang et al. [36], [37] further by investigating adhesion strength of human fibrous caps in carotid endarterectomy specimens. Performing the experiments on human tissue allows for similarities between mouse and human plaque adhesion strength to be

assessed. This analysis will also assist in determining whether or not the results from mouse plaque adhesion strength experiments can be translated to human atherosclerotic plaques.

2.2 Materials and Methods

2.2.1 Plaque adhesion strength in transgenic mice

All procedures involving vertebrate animals were approved by the USC Institutional Animal Care and Use Committee. Four C57Bl6 congenic ApoE$^{-/-}$ mice and seven ApoE$^{-/-}$ Col8$^{-/-}$ mice were fed a high-fat (40% of total calories) diet for six months to develop advanced aortic atherosclerotic plaques. Mice were euthanized by carbon dioxide asphyxiation and perfused with heparinized saline at physiological pressure for five minutes. The adhesion strength between the atherosclerotic plaque and the IEL was measured with cyclic peeling experiments, based on a previously published protocol [36], [37]. In brief, the aorta was opened longitudinally to visualize the atherosclerotic plaques. A small initial flaw was made at the proximal end of one plaque and the free edge was gripped with forceps which were mounted in a Bose Electroforce 3200 Test Instrument (Bose Corp., Framingham, MA). The Bose Test Instrument has two grips. One grip clamps the plate which holds the mouse with exposed aorta. In the other grip, microclamps that hold the tip of the free edge of the plaque are mounted. A stereomicroscope equipped with a CCD camera was placed above the aorta to obtain a top-down view of the delamination process. Figure 2.1 shows a schematic of the side view of the experimental test setup.

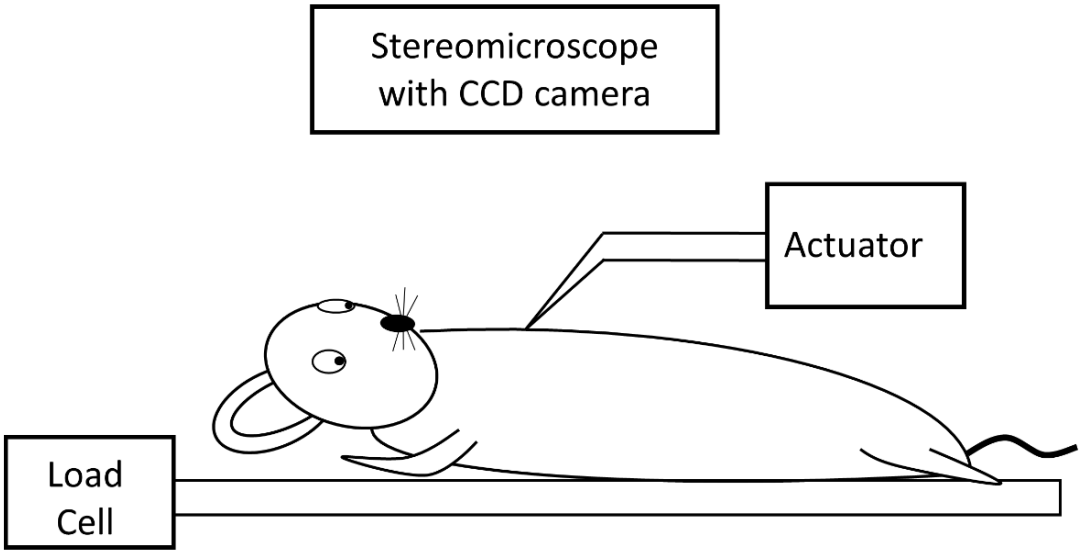

Figure 2.1 The experimental test setup. The Bose instrument prescribes a displacement (actuator) and records the resulting force (load cell). The microclamps are attached to the actuator and grip the tip of the plaque. A stereomicroscope with one CCD camera is mounted overhead to take images of the experiment.

2.2.1.1 Mechanical testing

The Bose Electroforce 3200 Test Instrument applied controlled displacement at a rate of 0.05 mm/s to detach the plaque in stages, and a stereomicroscope with a monochrome Q-Imaging QICAM CCD camera acquired images of the newly exposed area underneath the plaque at a frequency of 1 Hz. Consecutive cycles were run with increasing total displacement until the plaque completely separated from the vessel wall.

2.2.1.2 Histological studies

After complete delamination, the plaques were fixed in 10% neutral buffered formalin. The plaques were embedded in paraffin and sectioned transversely at 5 μm. Masson's trichrome staining was performed on several sections from each plaque.

2.2.1.3 Data analysis

The energy released during the delamination, ΔE, is the area under the load-displacement curve, shown in Figure 2.2, which is calculated from experimental data using the trapezoidal rule for integration

$$\Delta E = \sum_{i=1}^{\infty} \frac{(d_{i+1} - d_i) * (l_i + l_{i+1})}{2} \quad (2.1)$$

where d_i and d_{i+1} are incremental values of the displacement and l_i and l_{i+1} are incremental values of the load. The area exposed at the plaque-IEL interface during one delamination cycle, ΔA, is measured using ImageJ by determining the area before delamination, A_i, and the area after delamination, A_f.

$$\Delta A = A_f - A_i \quad (2.2)$$

The energy release rate, G, is a measure of adhesion strength and is calculated by dividing the energy released during delamination, ΔE, by the area exposed during the same delamination, ΔA.

$$G = \frac{\Delta E}{\Delta A} \quad (2.3)$$

The failure load of each cycle was determined by measuring the load when tearing initiated for each cycle, depicted in Figure 2.2.

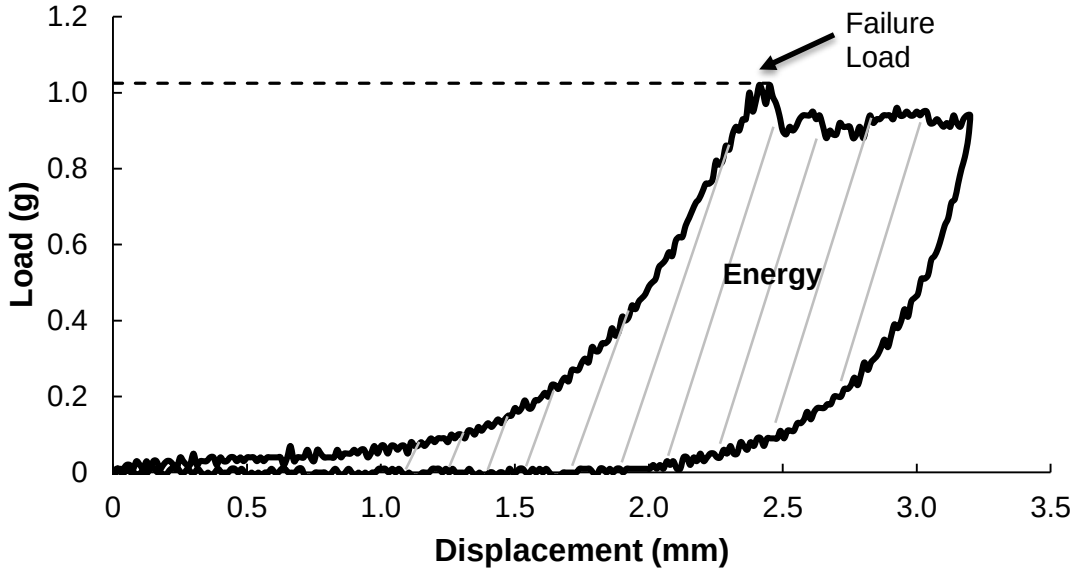

Figure 2.2 A representative image of the raw load versus displacement data. The area under the load-displacement curve represents the energy released during one delamination cycle. The failure load is the load at which tearing begins.

A stiffness parameter was caclulated for each delamination cycle. First, an exponential trendline was fitted to the loading region of the load-displacement curve. The exponetential trendline is of the form

$$F = ae^{b\delta} \tag{2.4}$$

where F is the force or load, δ is the displacement, and a and b are parameters. Taking the natural logarithm of equation 4, it becomes clear that b is responsible for the slope of this line and a is related to the intercept.

$$\ln(F) = \ln(a) + b\delta \tag{2.5}$$

Therefore, b is defined as the stiffness parameter for each cycle. When the natural logarithm of load is plotted versus displacement, the loading portion of the curve becomes linear, shown in Figure 2.3. The lines with a greater slope correspond to the cycles with a stiffer response.

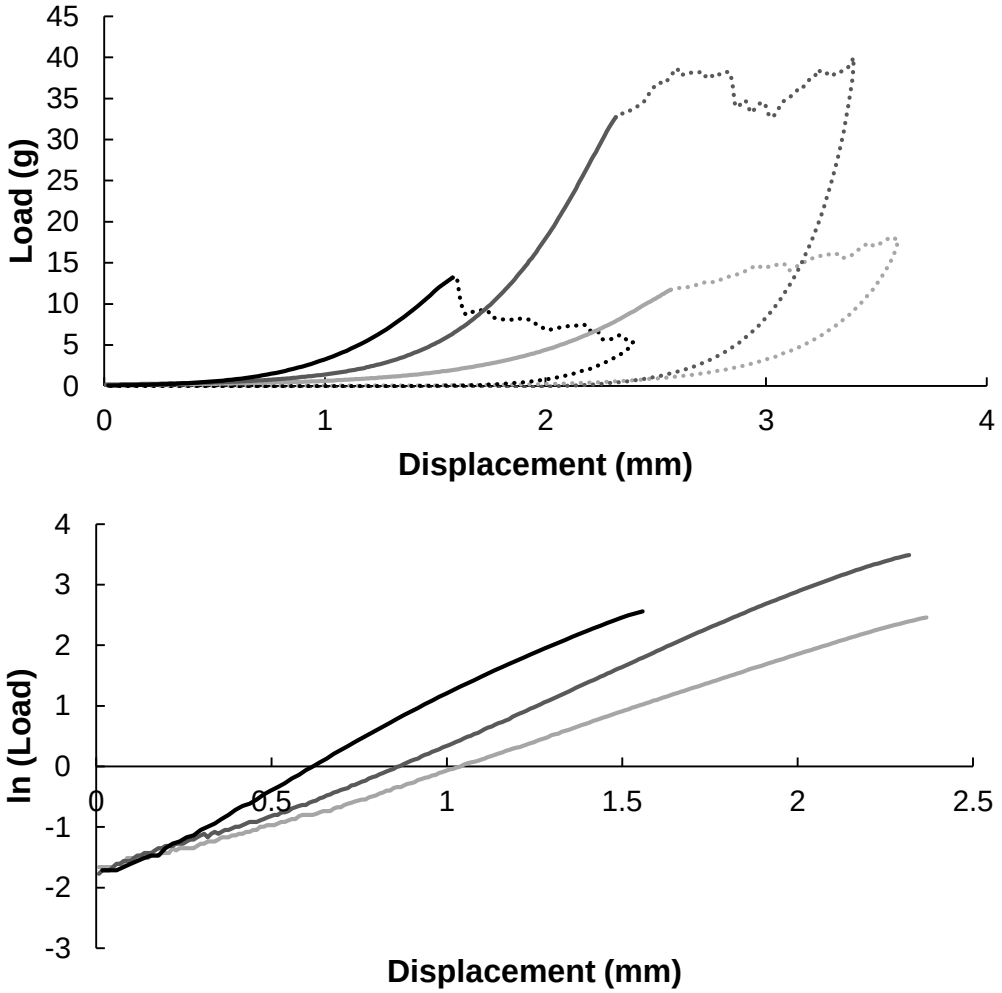

Figure 2.3 A set of representative load-displacement curves from three different plaques (loading regions in solid lines, tearing and unloading regions in dashed lines) with varied stiffness parameters (top). The natural logarithm of the load is plotted versus displacement for the loading region of each of these curves (bottom). The lines with steeper slopes correspond to the cycles with higher stiffness. Stiffness parameters equal 3.4, 2.4, and 1.8 for the black, medium grey, and light grey lines, respectively.

A Shapiro-Wilk test was used to test the normality of the distributions of results. For normally distributed data, a t-test was performed to test for differences between the two genotypes and for non-normally distributed data, a Mann-Whitney nonparametric test was used to compare the median values between the $ApoE^{-/-}$ mice and the $ApoE^{-/-}$ $Col8^{-/-}$ mice. The results were considered significant if P was less than 0.05.

2.2.2 Human fibrous cap adhesion strength

The plaque adhesion strength experiments conducted in mice, described in section 2.2.1, were adapted to human plaque specimens. Rather than measure the adhesion strength at the plaque-IEL interface as in the mouse studies, the adhesion strength between the fibrous cap and the underlying plaque was measured in human carotid endarterectomy plaque specimens.

The current study was approved by the IRB at Greenville Health System on September 3, 2013 and all patients gave written informed consent. Seven fresh carotid endarterectomy samples were obtained at the time of surgery from two local hospitals (6 specimens from Greenville Health System, Greenville, SC; 1 specimen from Palmetto Health, Columbia, SC). The carotid endarterectomy specimens were immersed in Belzer UW Cold Storage Solution (Bridge to Life Ltd., Columbia, SC, USA) immediately following excision from the patient and were kept cool until testing. All testing was completed within 48 hours of surgery. The specimens were sliced transversely into segments nominally 5 mm in width prior

to mechanical testing. Several specimens were large enough that multiple samples were prepared, resulting in a total of 11 fibrous cap delamination samples.

At the start of an experiment, the ring-shaped plaque sample was opened with a longitudinal cut. At this cut edge, a scalpel was used to carefully introduce a small initial delamination between the fibrous cap and the underlying plaque tissue. The medial side of the tissue was glued to a glass plate with Dermabond Advanced (Ethicon Inc., Somerville, NJ, USA), a topical skin adhesive. One of the grips in the Bose Test Instrument was used to securely mount the glass plate, while the opposite grip held a micro-clamp that gripped the delaminated tab of the fibrous cap, as shown in Figure 2.4.

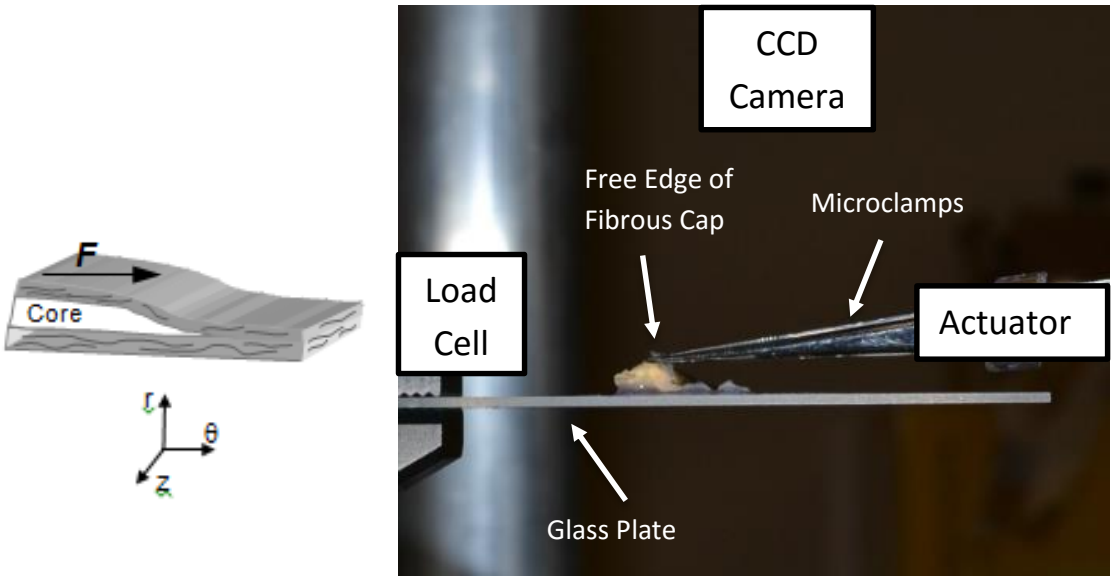

Figure 2.4 Human fibrous cap delamination experimental setup. A schematic of the sample prepared for mechanical testing is shown on the left; an actual sample mounted in our testing device is shown on the right.

Controlled displacement of the microclamps was used to further delaminate the free edge of the fibrous cap. A charge-coupled device (CCD) camera (Grasshopper GRAS-50S5M, Point Grey Research, Richmond, BC, Canada) was placed above the tissue to capture images at a frequency of 1 Hz during the delamination process.

2.2.2.1 Mechanical Testing

Consecutive delamination cycles at a rate of 0.05 mm/s were performed under displacement control. The actuator of the Bose Test Instrument prescribes a displacement for the microclamps which grip the plaque, and the resulting load is recorded by the grips that mount the glass plate. The cyclic loading-delamination-unloading cycles are performed until complete delamination of the fibrous cap is achieved.

2.2.2.2 Histological Studies

After delamination, each portion of the tissue (delaminated fibrous cap, underlying plaque and media) was fixed in 4% paraformaldehyde in 0.1 M phosphate buffer, pH 7.4. The samples were embedded in paraffin and sectioned transversely at 5 μm.

2.2.2.3 Data Analysis

The analysis of the results obtained in this section was performed identically to the mouse plaque adhesion strength data analysis (see section 2.2.1.3).

2.3 Results

2.3.1 Mouse plaque adhesion strength is unaffected by collagen VIII deficiency

Five plaques from ApoE$^{-/-}$ mice were tested in 17 peeling cycles, resulting in an average local energy release rate of 15.4 J/m^2. Twenty-two peeling cycles were obtained from nine plaques from ApoE$^{-/-}$ Col8$^{-/-}$ mice, with an average local energy release rate of 16.2 J/m^2. Figure 2.5 shows that the local energy release rates between ApoE$^{-/-}$ and ApoE$^{-/-}$ Col8$^{-/-}$ plaques have similar distributions, though the maximum energy release rate for ApoE$^{-/-}$ Col8$^{-/-}$ mice is higher than that in ApoE$^{-/-}$ mice.

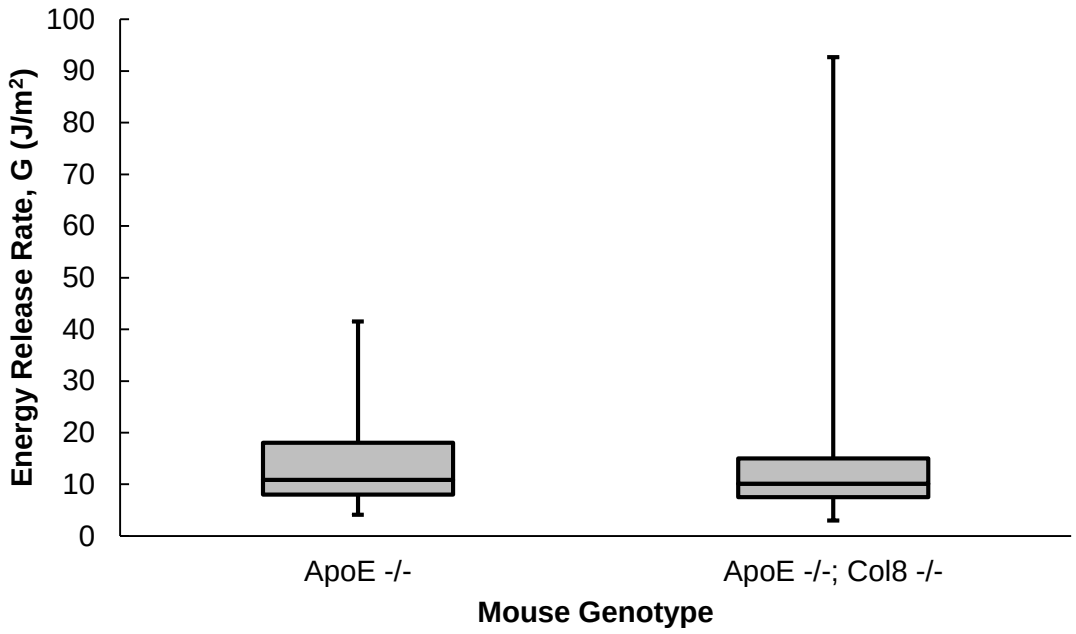

Figure 2.5 A box and whiskers plot shows that the distribution of local energy release rate (G) values is similar in both mouse genotypes.

Figure 2.6 shows that the histograms for energy release rate distribution are similar between mouse genotypes. The peak of each histogram is around 10 J/m^2,

and both distributions are positively skewed. A statistical summary of the distributions is shown in Table 2.1. Based on the results of the Shapiro-Wilk test, the distribution of plaque energy release rate values is non-normal ($p < 0.01$) in both ApoE$^{-/-}$ and ApoE$^{-/-}$ Col8$^{-/-}$ mice. A Mann-Whitney test reveals that there is no significant difference between the median energy release rates of the two populations of transgenic mice (P-value = 0.82). The stiffness parameter (calculated from equation 2.4) and failure load values for both genotypes were normally distributed. A t-test shows that stiffness is reduced in ApoE$^{-/-}$ Col8$^{-/-}$ mice compared to ApoE$^{-/-}$ mice ($P < 0.05$). The failure load values were not significantly different between the two genotypes.

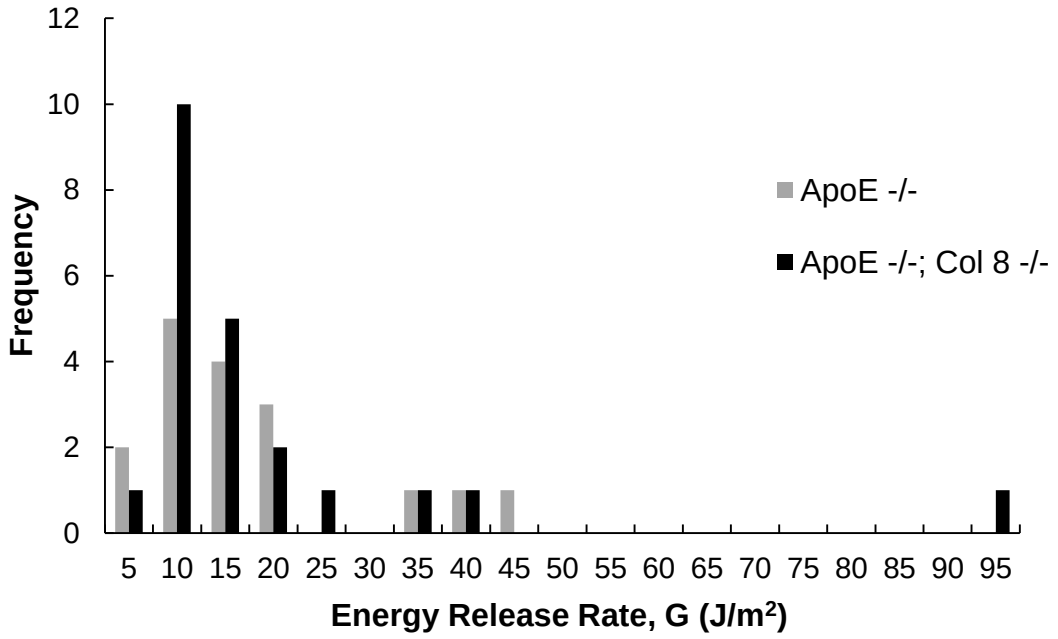

Figure 2.6 Distribution of local energy release rate, G, for ApoE$^{-/-}$ and ApoE$^{-/-}$ Col8$^{-/-}$ mice. For both genotypes, the distribution is positively skewed.

Table 2.1 Statistical parameters for local energy release rate, stiffness parameter, and failure load values for plaque delamination in ApoE$^{-/-}$ and ApoE$^{-/-}$ Col8$^{-/-}$ mice.

	Energy Release Rate (J/m^2)		***Stiffness Parameter***		***Failure Load (mN)***	
	ApoE$^{-/-}$	ApoE$^{-/-}$ Col8$^{-/-}$	*ApoE$^{-/-}$*	ApoE$^{-/-}$ Col8$^{-/-}$	*ApoE$^{-/-}$*	ApoE$^{-/-}$ Col8$^{-/-}$
Mean	15.4	16.4	1.83	1.47	6.37	5.75
Standard Deviation	11.7	18.8	0.72	0.37	2.86	2.63
First Quartile	8.03	7.51	1.27	1.23	5.10	3.46
Median	10.9	10.1	1.44	1.49	5.98	4.85
Third Quartile	18.0	15.0	2.41	1.71	8.53	7.72
Kurtosis	0.95	14.0	-1.06	0.00	0.69	-1.25
Skew	1.40	3.54	0.61	0.12	0.88	0.16

The histology performed on the delaminated tissue verifies that delamination occurred between the atherosclerotic plaque and the IEL, rather than within the media or between the media and the adventitia. Representative images of plaque alone and plaque with media are shown in Figure 2.7. Histology was performed on every delaminated specimen to confirm the plane of delamination. Specimens which delaminated outside the plaque-IEL interface were not included in this study.

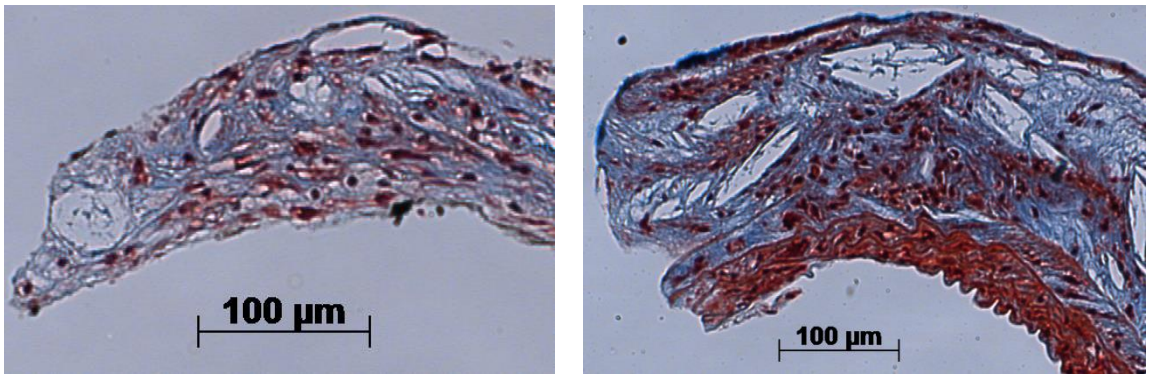

Figure 2.7 Trichrome staining on sections of peeled plaque specimens from ApoE$^{-/-}$ mice verifies the plane of delamination. Representative histological images showing plaque only, confirming delamination at the plane of interest, the plaque-IEL interface (left) and section for comparison showing plaque attached to media, showing that in this case the delamination did not occur in the plane of interest (right). Scale bar = 100 µm.

2.3.3 Human atherosclerotic fibrous cap adhesion strength results

Eleven fibrous cap delamination experiments resulted in a total of 83 delamination cycles and an average energy release rate of 343 J/m^2. There is high variability in the local energy release rates both within one plaque sample and between plaques from different patients, as shown in Figure 2.8. The histogram of energy release rate values in Figure 2.9 shows a positively skewed distribution with a frequency peak around 200 J/m^2.

Table 2.2 summarizes the key statistical parameters in the human plaque adhesion strength data set. The energy release rate measurements have a standard deviation approximately equal to the mean. Local energy release rate, failure load, and stiffness all have positively skewed distributions and exhibit positive kurtosis.

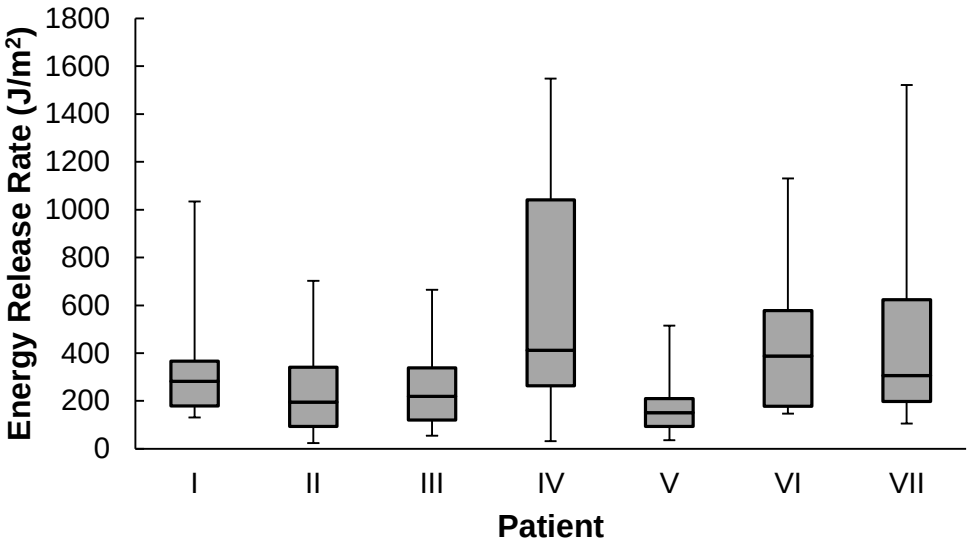

Figure 2.8 A box and whiskers plot for local energy release rate by patient. Patients I, II, IV, and V each provided two fibrous cap delamination samples.

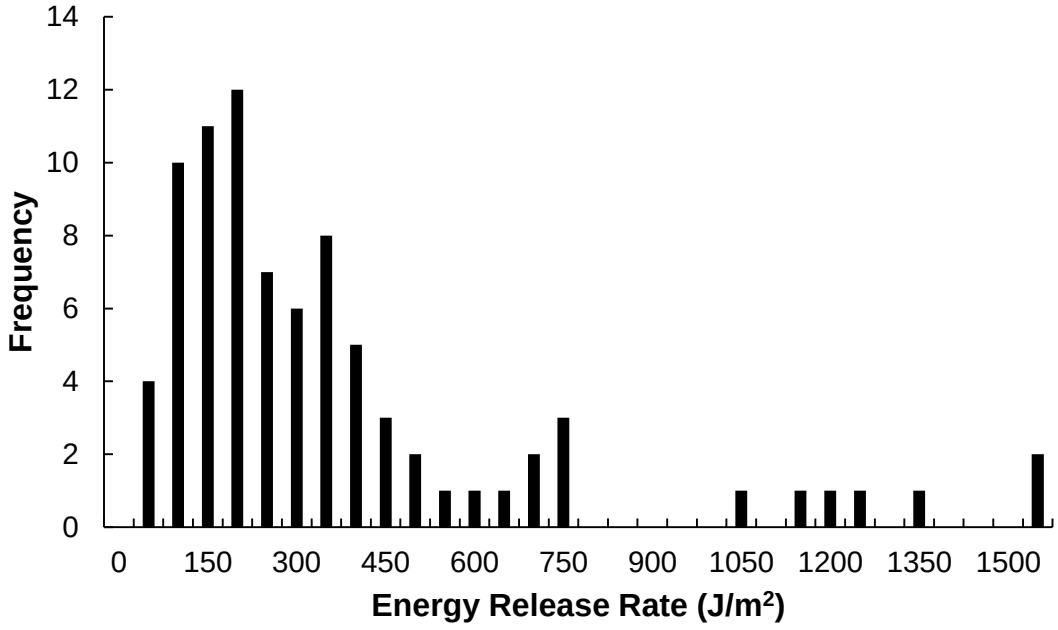

Figure 2.9 Histogram of local energy release rates during fibrous cap peeling in human carotid endarterectomy specimens.

Table 2.2 Statistical parameters for local energy release rate, stiffness parameter, and failure load values for human fibrous caps

	Energy Release Rate (J/m^2)	Stiffness Parameter	Failure Load (mN)
Mean	343	2.13	360
Standard Deviation	338	0.90	276
First Quartile	123	1.66	148
Median	221	2.00	262
Third Quartile	386	2.38	504
Kurtosis	3.9	19.6	1.5
Skew	2.0	3.48	1.3

Trichrome staining on delaminated fibrous caps was analyzed to confirm that delamination occurred between the fibrous cap and the underlying plaque. A representative image of both the fibrous cap and the underlying plaque is shown in Figure 2.10.

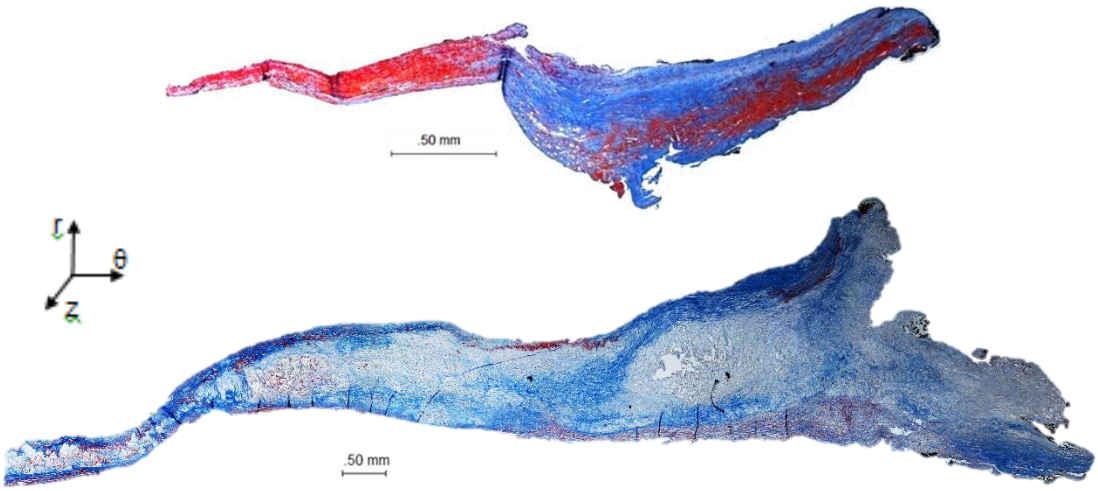

Figure 2.10 A representative image of delaminated human fibrous cap (top) and underlying plaque and media (bottom) stained with Masson's Trichrome. Blue = collagen. Scale bar represents 0.5 mm.

2.4 Discussion

2.4.1 Mouse plaque adhesion strength is unaffected by collagen VIII

The adhesion strength between the atherosclerotic plaque and IEL as well as the load at which tearing initiates are unchanged between ApoE$^{-/-}$ and ApoE$^{-/-}$ Col8$^{-/-}$ mice. However, the plaques in ApoE$^{-/-}$ Col8$^{-/-}$ mice are less stiff than those in ApoE$^{-/-}$ mice. Stiffness is a structural property that depends on both material properties and specimen geometry, in this case the thickness and width of the plaque. We have not isolated the influence of material properties and geometry on the stiffness parameter measurements. However, Lopes et al. have previously shown that plaque size and burden of atherosclerosis are similar between ApoE$^{-/-}$ and ApoE$^{-/-}$ Col8$^{-/-}$ mice [42]. While these results suggest that material properties may solely be responsible for the change in stiffness, further studies are needed to confirm this. Lower plaque stiffness in the ApoE$^{-/-}$ Col8$^{-/-}$ mice is consistent with previous observations of impaired fibrous cap formation in this genotype [42].

The local energy release rate for delamination of atherosclerotic lesions in ApoE$^{-/-}$ mice after 8 months on diet has previously been reported with average values of 19.2 J/m^2 and 24.5 J/m^2 [36], [37]. The current study finds an average value for the local energy release rate of plaque delamination in ApoE$^{-/-}$ mice after 6 months on diet to be 15.4 J/m^2. In general, our results agree with previous studies, however it is important to note the difference in time points. While there is a slight increase in adhesion strength with increased time on western diet (Figure

2.11), a Mann-Whitney nonparametric test confirms that there is not a statistically significant difference in the energy release rate of these two populations.

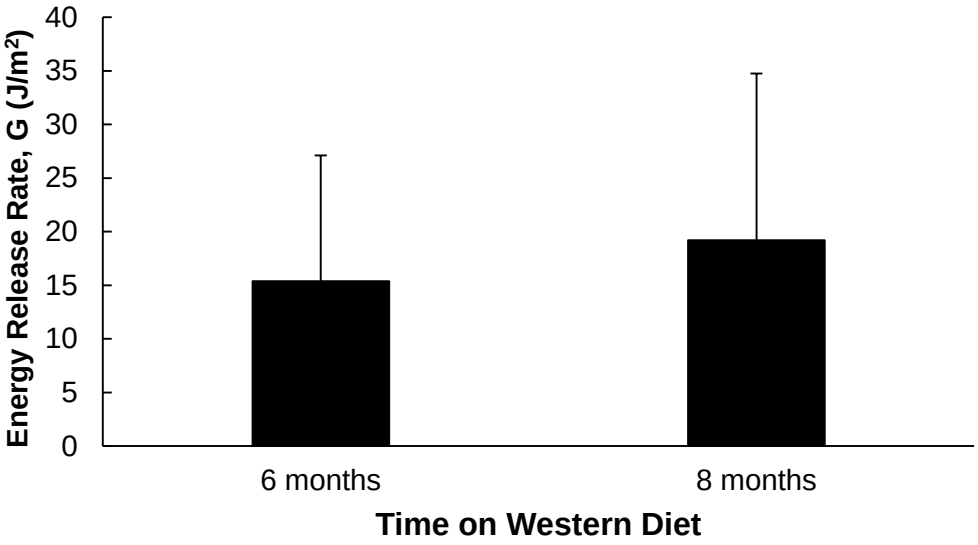

Figure 2.11 The effect of time on western diet on plaque adhesion strength in ApoE$^{-/-}$ mice. Data for the adhesion strength from ApoE $^{-/-}$ mice on western diet for 8 months was obtained from [37]. Error bars represent standard deviation.

Previous studies have shown that there is a positive correlation between local energy release rate and total collagen content as measured by Picrosirius Red staining [37]. Our study shows that the energy release rate is unaffected by the absence of type VIII collagen and suggests that other types of collagen may be responsible for the differences in adhesion strength previously reported. We have shown that the ApoE$^{-/-}$ Col8$^{-/-}$ plaques are less stiff than the ApoE$^{-/-}$ plaques, which may be caused by the lack of type VIII collagen or by impaired migration of SMCs and resulting matrix deposition, as previously reported.

This study shows that the absence of type VIII collagen does not reduce plaque adhesion strength and thus does not reduce the mechanical likelihood of plaque failure by delamination at the plaque shoulder. However, these studies have not ruled out the possibility that plaques in ApoE$^{-/-}$ Col8$^{-/-}$ mice may be more susceptible to failure by tensile rupture of the fibrous cap.

2.4.2 Comparison between human and mouse results

The current study shows that energy release rate and failure load are one to two orders of magnitude higher in human fibrous cap delamination than in mouse aortic plaque delamination. While this finding may indicate structural differences in tissue types between species, it is also important to note several differences in methodology in the two sets of experiments. First, plaque adhesion strength is measured in the longitudinal direction at the plaque-IEL interface in mice, while it is measured in the circumferential direction between the fibrous cap and the underlying lipid core in human tissue. Logistically, the diameter of the mouse aorta is too small to readily test circumferential plaque adhesion strength. Additionally, mouse plaques generally do not have distinct and thickened fibrous caps as do human atherosclerotic plaques. Human plaques are highly heterogeneous, and many plaques contain a very weak lipid core that can not withstand the loads applied during experimental delamination. In these instances, the lipid core disintegrates rather than delaminating cleanly from the IEL.

Other studies investigating delamination strength in human arteries have found adhesion strength values ranging from 20 J/m^2 to 100 J/m^2 [56]–[58]. These

studies investigated delamination within the layers of an artery rather than plaque fibrous cap delamination, which could explain the higher results obtained in our study.

While the human atherosclerotic plaques are much stronger than those found in mice, the plaque adhesion strength data sets are qualitatively similar, in terms of having positively skewed distributions of energy release rate and standard deviations which are approximately equal to the means. While the quantitative values of the mouse plaque adhesion strength may not be representative of human samples, many of the qualitative behaviors observed during plaque delamination are similar in both species.

2.5 Future Work

This study has examined plaque adhesion strength in both mouse and human tissue; however, the microscopic mechanism for failure at this interface is still unknown. Likely potential determinants of plaque adhesion strength are adhesive proteins binding the two layers or bridging fibers extending between the two layers. Thus, failure may involve either de-cohesion of protein-protein interactions, fiber breakage, or both. Both of these failure mechanisms should be investigated further.

In addition to plaque adhesion strength, other plaque rupture mechanisms should be investigated to assess plaque stability, such as tensile rupture of the fibrous cap. Both adhesive and tensile failure can potentially lead to clinical events, such as stroke or myocardial infarction, and all measurements are valuable in

providing mechanical properties for computational simulations of atherosclerotic plaque behavior.

Acknowledgements

I would like to acknowledge Bilal Merei for his assistance with the plaque adhesion strength mechanical testing in mice, John Johnson for his histological staining on all of the samples, and Xiaochang Leng for his efforts in obtaining images of the human histological results. This work was funded by the National Science Foundation through grant CMMI-1200358.

CHAPTER 3

ADHESIVE PROTEIN CONTRIBUTIONS TO THE MECHANICAL STRENGTH AND INTEGRITY OF THE PLAQUE-INTERNAL ELASTIC LAMINA (IEL) INTERFACE IN A MOUSE MODEL OF ATHEROSCLEROSIS[1]

[1] L.A. Davis, M.A. Sutton, S.M. Lessner. To be submitted to Annals of Biomedical Engineering.

3.1 Introduction

Atherosclerotic plaque failure is one of the leading causes of myocardial infarction. There are at least two potential failure mechanisms for atherosclerotic plaques. The first involves tensile rupture of the fibrous cap and the second, which is prominent during angioplasty, involves plaque delamination from the internal elastic lamina (IEL) at the plaque shoulder. During balloon angioplasty, a catheter is inserted into the blood vessel and a small balloon is inflated at the lesion. The goal is to flatten the plaque and to increase the lumen area; however, in some cases this results in intimal dissection at the plaque shoulder. The resulting arterial damage is commonly treated with the implantation of a stent over the dissected tissue to hold the intimal and medial surfaces together and to recreate a smooth lumen [25], [26], [59].

Identifying the matrix proteins responsible for adhesion between the plaque and the IEL may provide insight into the delamination mechanism for atherosclerotic plaque failure at the shoulder. Wang et al. have used plaque peeling experiments to determine the local energy release rate, G, a measure of adhesive strength between the plaque and the IEL [36], [37]. A significant positive correlation was found between local collagen content in the plaque and adhesion strength between the plaque and the IEL, suggesting that collagen is an important determinant of plaque adhesion strength [37].

Tsamis et al. have shown that during vascular remodeling of the extracellular matrix (ECM) due to aneurysm, collagen and elastin fibers become

radially oriented [60]. Vascular remodeling also occurs due to atherosclerotic plaque formation and may result in a similar reorganization of fibers. If radially oriented fibers are present at the plaque-IEL interface, they may be responsible for the adhesion strength at this interface. Previous studies in our lab have shown that IEL degradation increases adhesion strength between the plaque and the IEL, raising the possibility that fiber bridges extending between the intima and media contribute to interfacial toughness [37]. The composition of these potential bridges is unknown, though they likely form from proteins found in the surrounding ECM. Contributions to adhesion strength may also come from adhesive proteins that link ECM components together. Potential failure mechanisms at the plaque-IEL interface include a) fiber breakage, b) fiber pull out or decohesion from the surrounding ECM, c) adhesive failure mediated by glycoproteins, or d) any combination of the three.

In this study, we seek to characterize the ECM composition at the mouse plaque-IEL interface and to investigate the potential contribution of specific matrix constituents to interfacial adhesion strength. The matrix proteins selected for investigation are collagen I, collagen IV, fibrillin-1, fibronectin, and osteopontin. These proteins were chosen to include both adhesive glycoproteins and fibrillar ECM proteins known to be present within atherosclerotic plaques. In addition, we used biomechanical methods to investigate the adhesive/cohesive strength of thin films of purified protein to determine how strongly these matrix proteins adhere to decellularized aortic matrix.

Based on the results in Wang et al. [37], collagen is a potential contributor to plaque adhesion strength. Collagen I, a fibrillar collagen, is the most abundant protein in vascular tissue. Collagen IV is a basement membrane protein that forms structural networks or scaffolds which interact with proteoglycans [61], [62] and cells [63], [64] and. In healthy tissue, collagen IV is found at the intimal-medial border, and we hypothesize that collagen IV will also be present at the plaque-IEL interface in the atherosclerotic diseased state.

Fibrillin-1 is a key component of microfibrils, which provide a scaffold for elastic fiber formation. Though microfibrils are primarily associated with mature elastic fibers [8], they are found in the absence of elastin in ciliary zonula of the eye and superficial regions of the skin [9]. In the absence of elastin, microfibrils contribute to the structural integrity of the tissue [10] and exhibit nonlinear material behavior [65]. Microfibrils frequently interact with the basement membrane via perlecan [66] and can adhere to cells [67]. Additionally, microfibrils have been shown to link endothelial cells to the internal elastic lamina in developing mouse aorta [11], [12].

Fibronectin and osteopontin may contribute to the strength of the plaque-IEL interface through adhesive interactions with other ECM components. Fibronectin has a multidomain structure which enables binding to cell surfaces as well as to other extracellular matrix molecules, such as collagen, and proteoglycans [13], [68], [69]. Osteopontin is a secreted adhesive protein, commonly expressed in inflammatory and auto-immune diseases, that binds to cellular integrins and can mediate cell-cell and cell-ECM adhesion [70].

Osteopontin may be an important adhesive molecule at the plaque-IEL interface because of its ability to bind directly to fibronectin [71] and collagen [72]. Therefore, both fibronectin and osteopontin may be structural links between ECM components and cells at the plaque-IEL interface.

In situ blotting, or histoblotting, has been used previously to transfer protein directly from frozen or fixed tissue sections to nitrocellulose or polyvinylidene difluoride (PVDF) membranes and stain with histochemical or immunological methods to detect specific proteins [73], [74]. This study builds on those techniques by blotting fresh, unsectioned tissue on PVDF membranes along with a series of protein standards to allow for approximate protein quantitation. More specifically, we investigate the protein concentration at the plaque-IEL interface by blotting fresh atherosclerotic plaques peeled from the IEL onto PVDF membranes.

Khayer Dastjerdi et al. developed an elegant technique, the rigid double cantilever beam (RDCB) test, for measuring the fracture toughness during cohesive failure of soft biological adhesives [75]. This RDCB technique also allows for direct determination of the full traction-separation function. The RDCB technique is slightly modified in this study, by adding a layer of decellularized aorta between each beam and the protein layer. Using this modified technique, the fracture toughness of isolated proteins can be determined for failure at the interface between the protein layer and the matrix or within the protein layer itself.

Combining these two techniques allows for an interesting study on the contributions of specific proteins to mechanical strength. For this study specifically,

we have investigated the contributions of adhesive proteins to the delamination strength, or adhesive strength, of the plaque-IEL interface. However, this technique can be applied to a broad range of biological materials.

3.2 Materials and Methods

3.2.1 Immunohistochemistry

All procedures involving vertebrate animals were approved by the USC Institutional Animal Care and Use Committee. Apolipoprotein E knockout ($ApoE^{-/}$) mice were put on a Western (42 kcal% fat, Harlan-Teklad, Indianapolis, IN) diet for eight months to develop advanced atherosclerotic plaques in the descending aorta. After eight months, two mice were sacrificed by CO_2 asphyxiation and perfused with heparinized saline for five minutes. The aorta from each mouse was harvested and fixed in neutral-buffered formalin, embedded in paraffin, and sectioned transversely at five μm.

Immunohistochemistry (IHC) was used to determine the presence and distribution of collagen I, collagen IV, fibrillin-1, osteopontin, and fibronectin in sections of the aortic wall with atherosclerotic lesions. Collagen I, collagen IV, fibrillin-1, fibronectin and osteopontin were detected with the following antibodies, respectively: rabbit anti-collagen I polyclonal antibody (1:20 dilution, Calbiochem, San Diego, CA), rabbit anti-collagen IV polyclonal antibody (1:20 dilution, Abcam, Cambridge, MA), rabbit anti-fibrillin-1 polyclonal antibody (1:20 dilution, Abcam, Cambridge, MA), rabbit anti-fibronectin antibody (1:100 dilution, Novus Biologicals, Littleton, CO), and rabbit anti-osteopontin antibody (1:100 dilution, Abcam,

Cambridge, MA). Donkey anti-rabbit rhodamine red X (RRX)–labeled secondary antibodies (Jackson Immuno Research Laboratories, Inc., West Grove, PA) were used to detect collagen I, fibronectin, and osteopontin. For collagen IV and fibrillin-1, biotin-conjugated donkey anti-rabbit IgG (Jackson Immuno Research Laboratories, Inc., West Grove, PA) was used as a secondary antibody, followed by RRX-labelled streptavidin (Jackson Immuno Research Laboratories, Inc., West Grove, PA). Lastly, the tissue sections were counterstained with Hoechst 33342 (1:10,000 dilution, Thermo Fisher Scientific, Waltham, MA). A Zeiss LSM 510 confocal microscope was used to capture images at 40X and 63X magnification.

3.2.2 Semi-quantitative plaque immunoblotting

A novel plaque immunoblotting technique was used to identify and quantify adhesive proteins present locally at the plaque-IEL interface. Five $ApoE^{-/-}$ mice were sacrificed by CO_2 asphyxiation and perfused with heparinized saline for five minutes. The descending aorta was opened longitudinally to visualize the atherosclerotic lesions. Forceps were used to make an initial flaw at one edge of the plaque-IEL interface. The free edge of the plaque was gripped and gently peeled from the aortic wall. A total of 23 plaques from 5 mice were used in these experiments. The plaque was briefly blotted three times in sequence onto adjacent areas of a PVDF membrane (the IEL interface side contacting the membrane) that had been rinsed with methanol and transfer buffer (25 mM Tris, 192 mM glycine, 20% (v/v) methanol). A set of protein standards (rat tail collagen I, EMD Millipore Corporation, Billerica, MA; mouse collagen IV, BD Biosciences, Bedford, MA; partial recombinant fibrillin-1, Novus Biologicals, Littleton, CO; human plasma

fibronectin, EMD Millipore Corporation, Billerica, MA; human recombinant osteopontin, BioVision Inc., Milpitas, CA) at known concentrations was applied to the membrane to allow for approximate quantitation of the protein transferred from the plaque-IEL interface.

After the membrane had absorbed all protein, it was rinsed in Tris-buffered saline (TBS), pH 7.4, and placed in 1% bovine serum albumin (Sigma-Aldrich, St. Louis, MO, USA) in TBS for 1 hour. The membrane was then incubated with the appropriate primary antibodies, see section 2.1, at modified dilutions (1:500, 1:3750, 1:1000, 1;1000, and 1:1000 for collagen I, collagen IV, fibrillin-1, fibronectin, and osteopontin, respectively) for 1 hour, followed by biotinylated donkey anti-rabbit IgG (1:1000 dilution, Jackson Immuno Research Laboratories Inc., West Grove, PA) for 1 hour and IR 800 labelled streptavidin (1:1000 dilution, LI-COR Biosciences, Lincoln, NE) for 45 minutes. The membranes were imaged using an Odyssey CLx Imaging System (LI-COR Biosciences, Lincoln, NE) and analyzed quantitatively using ImageJ (version 1.50c4, National Institutes of Health, USA).

The first step in determining the ex vivo protein concentration is to create a standard curve using samples of known protein concentrations. On some of the plaque blots, the protein standards at the higher concentrations spread and created a larger area of lower signal. To correct for this effect, the total signal was calculated by measuring average pixel intensity multiplied by the area of the protein dot. An adjusted average pixel intensity was calculated by dividing the total pixel intensity by the area of the smallest dot on the standards. The adjusted pixel

intensity can be viewed as the average pixel intensity, if no spreading had occurred, and was used in all subsequent calculations. An adjusted average pixel intensity was calculated for each spot, whether or not obvious spreading had occurred.

The “area concentration” of each standard spot was determined by dividing the known mass of protein added to the membrane (volume of standard x standard concentration) by the area of the smallest standard dot (the same area used to determine the adjusted average pixel intensity). The area concentration and the adjusted average pixel intensity were plotted after a logarithmic transformation of each variable, and a linear regression was performed for each set of standard proteins. The ex vivo concentration was calculated using the linear regression to determine the logarithmic transformed concentration, which was then converted to true concentration. In each case, the ex vivo area concentration was calculated based on the average pixel intensity from the first of the three adjacent plaque blot images on the PVDF membrane.

In order to confirm proteins were only transferring from the plaque-IEL interface, plaque blots were compared alongside tissue blots from within the media of the aorta and stained with anti-actin smooth muscle antibody (1:500 dilution, Thermo Fisher Scientific, Waltham, MA). Smooth muscle cells (SMCs) are present much higher levels in the media of the artery or within the fibrous cap of the plaque, but are relatively sparse at the plaque-IEL interface. Therefore, the signal should be greatly reduced in the plaque blots compared to the media plots, if the technique

only transferring protein from the interface of interest and no contamination from other tissue surfaces is occurring.

This method is described as semi-quantitative because all protein at the plaque-IEL interface does not necessarily transfer to the PVDF membrane in one blot. Each plaque was blotted onto a single PVDF membrane three times, resulting in three adjacent images. While the signal is visually similar for each plaque blot, the calculated concentrations are generally not within 10%. The collagen I concentration is generally highest in the third plaque blot while the collagen IV concentration is generally the lowest in the third blot. This suggests that protein transfer is beginning to occur in the body of the plaque at these later blots (collagen I is more abundant in the body of the plaque and collagen IV is less abundant there). For this reason, only the first plaque blot is used for quantification. These results also suggest that the majority of the protein from the plaque-IEL interface transfers to the PVDF membrane within two blots. While true quantification cannot be achieved, this technique is useful to investigate relative abundance among several interfacial matrix proteins.

3.2.3 Mechanical testing of purified protein films using rigid double cantilever beam experiments

Rigid double cantilever beam (RDCB) experiments to measure the adhesive/cohesive strength of purified protein films were adapted from Khayer Dastjerdi et al. [75]. To simulate dissection at the interface between arterial tissue layers (intima-media), purified protein films were applied between two layers of

decellularized porcine aorta prior to RDCB testing. Porcine aortas were obtained from a local slaughterhouse (Caughman's Meat Plant, Lexington, SC) and decellularized in 0.1% sodium dodecyl sulfate (SDS) for 48 hours at room temperature with gentle shaking. The tissue was placed in fresh 0.1% SDS every 24 hours.

After decellularization, the aorta was cleaned of fat and cut into a series of segments 5 mm wide by 25 mm long. The adventitial side of each segment was glued onto a glass beam of the same size using Dermabond (Ethicon Inc., Somerville, NJ, USA) (a topical skin adhesive). The glass beams were cut from microscope slides using a carbide-tipped glass cutter and a custom framing device to ensure uniform dimensions. At one end of the beam, a glass coverslip (0.17 mm thick) was placed on the decellularized aorta to control the thickness and the initial crack length of the protein film. Ten μL of protein at specified concentration (0.125, 0.25, 0.5, or 1 μg/μL) was added to the opposite end of the beam. An identical glass beam bonded to decellularized aorta was placed on top of the first beam and protein film to create a "sandwich" (see Figure 3.1). The beams and protein film were incubated overnight in a humid chamber at 4°C. Wooden tabs containing 2.25 mm diameter through-thickness holes were attached to each glass beam with standard superglue.

The beams were mounted into a Bose 3200 Test Instrument (Bose Corp, Framingham, MA) by placing 1.25 mm pins through the holes in the wooden tabs, as shown in Figure 1. The displacement of the pins was initially increased such that each pin was fully contacting the far edge of the hole in each hinge. Controlled

displacement at a rate of 0.01 mm/s was applied to the sample until complete failure occurred. Load and displacement were recorded by the Bose 3200 software at a frequency of at least 2 Hz.

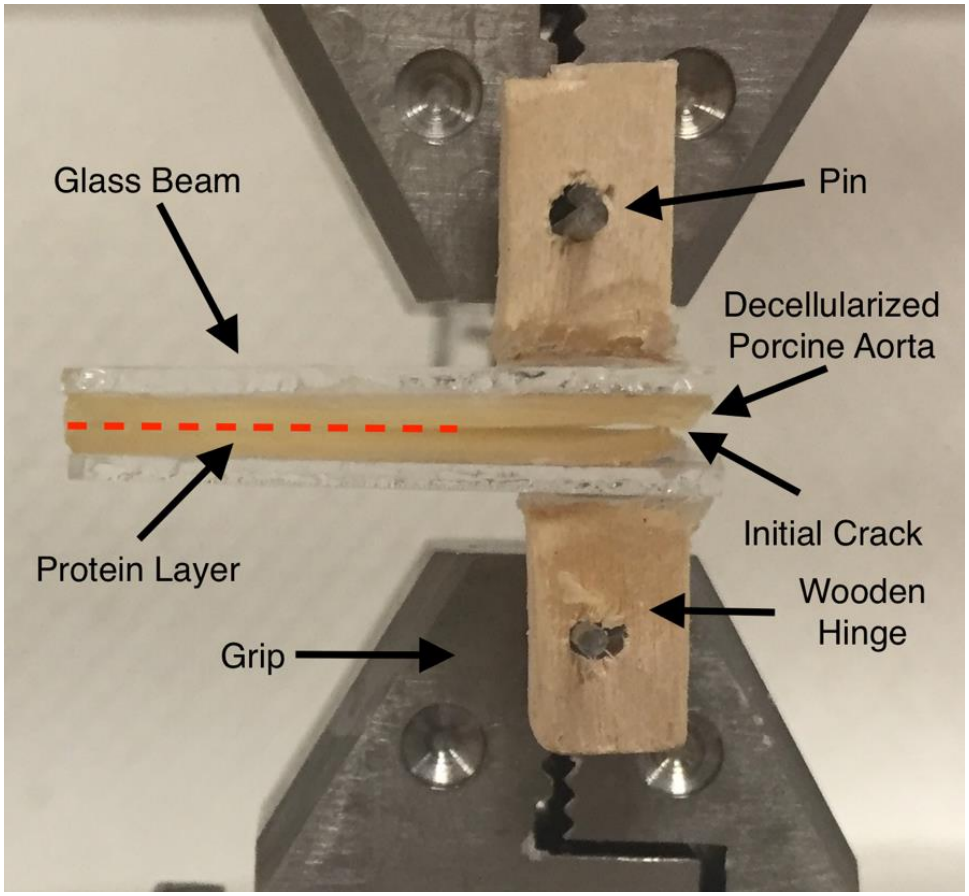

Figure 3.1 RDCB experimental setup.

3.2.3.1 Theory of Adhesion Strength Calculations

Based on the theory presented by Khayer Dastjerdi et al. [75], [76], the exact traction-separation curve for an adhesive interface can be calculated from RDCB data using the geometry of the beams and the load- displacement curves.

$$t(\delta) = \frac{L}{B(L-a_0)}\left(2F + \Delta\frac{dF}{d\Delta}\right) \tag{3.1}$$

Where t is the traction, δ is the separation at the leading edge of the protein layer, L is the length of the beams, B is the width of the beams, a_0 is the initial crack length, F is the instantaneous force, and Δ is the opening between the two ends of the beams. The separation, δ, at the crack tip is given by

$$\delta = \frac{L - a_0}{L} \Delta \tag{3.2}$$

The traction-separation curve was plotted until the traction reaches zero, at which point maximum separation distance has been reached. The energy release rate, G, was determined by measuring the area under the traction-separation curve using the trapezoidal rule,

$$G = \sum_{i=0}^{\infty} \left(\frac{t_i + t_{i+1}}{2} \right) * (\delta_{i+1} - \delta_i) \tag{3.3}$$

where t_i and t_{i+1} are sequential traction values, and δ_i and δ_{i+1} are the corresponding sequential separation values.

To combine the results from the RDCB experiments with those collected in Section 3.2.2, the equivalent volumetric concentration was determined for each of the ex vivo protein concentrations measured by plaque immunoblotting. The equivalent volumetric concentration was determined by creating a standard curve using the volumetric concentrations of the standards rather than the area concentrations.

3.2.4 Scanning electron microscopy (SEM) of partially delaminated plaques

Scanning electron microscopy (SEM) was used to examine the surface of the plaque-IEL interface. A partially delaminated plaque was prepared for SEM imaging with standard techniques for SEM images. In brief, the samples were fixed in 4% glutaraldehyde overnight, critical point dried, and sputter coated with gold. Images were taken with a JEOL 6300V scanning electron microscope (JEOL USA, Peabody, MA) at 4000X magnification.

3.2.5 Statistical Analysis

For plaque immunoblotting studies, we quantified results only from experiments in which the protein standard curve had an R^2 value greater than 0.8 and which did not require more than 10% extrapolation beyond the range of standard values to determine the concentration of unknowns (i.e., protein area concentrations of individual plaques). One-way ANOVA was used to compare average ex vivo concentrations determined from plaque immunoblotting experiments.

3.3 Results

3.3.1 Immunohistochemistry

Representative IHC results for each protein are shown in Figure 3.2. In each case, the green signal represents tissue autofluorescence, the red signal is the protein of interest and the blue signal corresponds to cell nuclei. Collagen I is present consistently at the plaque-IEL interface, in the body of the plaque, and in

the adventitia. Collagen IV is closely associated with portions of IEL. Collagen IV is strongly associated with one section of the IEL and notably absent from an adjacent segment of IEL. Fibrillin-1 is present at the plaque-IEL interface, though to a lesser extent than either collagen I or collagen IV, and within the media of the artery. There are several bright spots of signal within the body of the plaque for fibrillin-1 staining. These spots may be microfibrils oriented perpendicular to the plane of section. Fibronectin is present along the plaque-IEL interface, within the media of the artery, and near the luminal plaque edge, though absent from the plaque core. Conversely, osteopontin is most strongly associated with the plaque core and the underlying plaque-IEL interface.

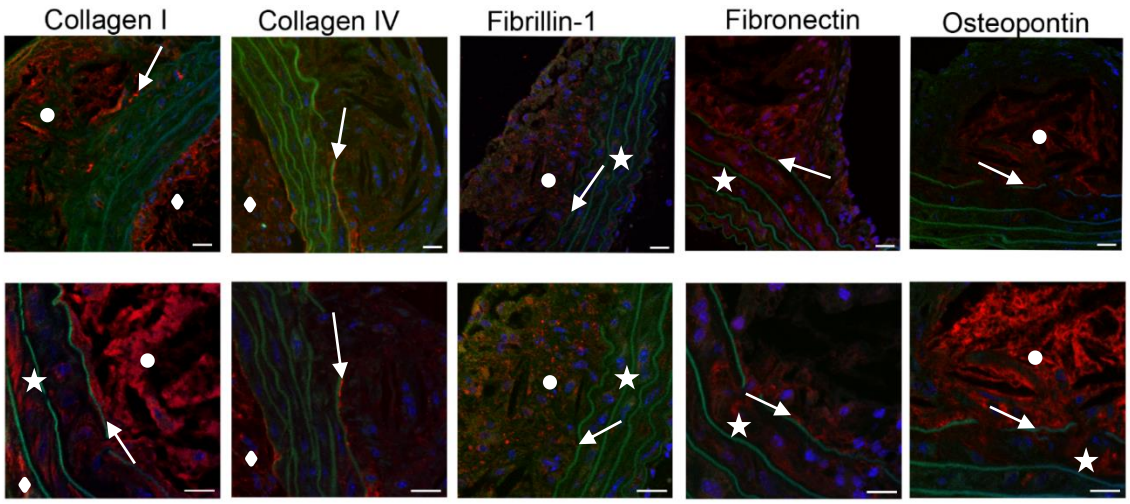

Figure 3.2 Representative Immunohistochemistry results for each matrix protein at 40X magnification (top row) and 63X magnification (bottom row). All scale bars represent 20 μm. Arrows point to protein at the plaque-IEL interface, circles denote protein in the body of the plaque, stars show protein within the media, and diamonds represent protein in the adventitia.

3.3.2 Semi-quantitative plaque immunoblotting

Representative results from the plaque immunoblotting experiments are shown in Figure 3.3. In total, we obtained three measurements of collagen I interfacial concentration, three measurements of collagen IV concentration, two measurements each of fibrillin-1 and fibronectin concentration, and no measurements for osteopontin. Osteopontin was detected at the plaque-IEL interface using the plaque immunoblotting technique; however, the protein standard curves were not of sufficiently high quality to quantitate the ex vivo concentration. The standard curves were linear at low protein concentrations, but appeared to saturate at higher concentrations in the range of the ex vivo concentration. The quantitative results (Figure 3.4, Table 3.1) show that collagen I and collagen IV are slightly more abundant at the plaque-IEL interface than fibrillin-1 and fibronectin; however, one-way ANOVA demonstrated no significant differences between the average concentrations of each protein. The standard deviation in each case is approximately equal to the mean, a trend which was also observed with the plaque adhesion strength results [36], [37]. The variation in measured interfacial protein concentrations is consistent with the observed variability in plaque adhesion strength measurements.

Comparison of plaque and media blots stained with anti-smooth muscle actin show that the signal is greatly reduced in the plaque compared to the media (Figure 3.5). These results support the notion that protein transfer is not occurring from the media or from the fibrous cap, instead protein is only transferring from the plaque-IEL interface where SMCs are expected to be relatively rare.

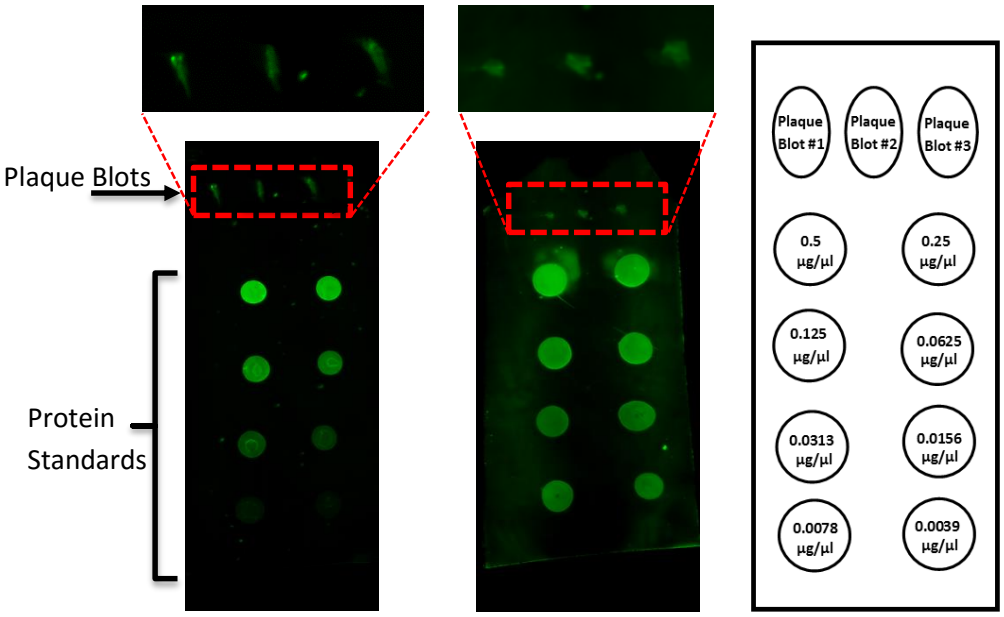

Figure 3.3 Representative plaque immunoblotting results showing standards with no spreading at high standard concentration (left) and standards which have spread at the two highest standard concentrations (middle). A schematic is shown (right). Insets show plaque blots.

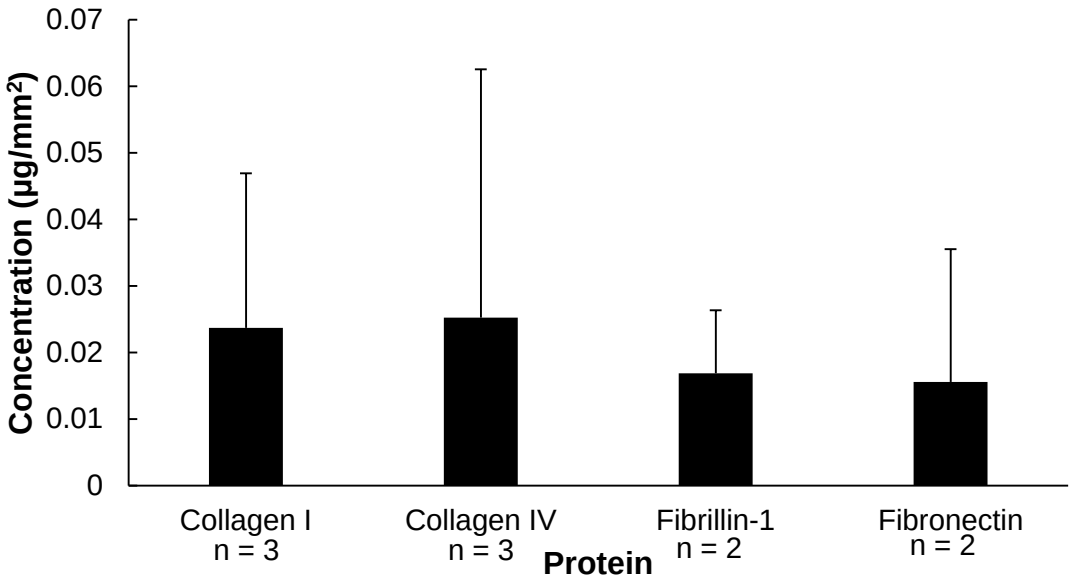

Figure 3.4 Summary of ex vivo protein concentrations at the plaque-IEL interface determined with plaque immunoblotting. Error bars represent standard deviation.

Table 3.1 Summary of ex vivo protein concentrations at the plaque-IEL interface quantified by immunoblotting

Protein	Surface Concentration (μg/mm^2)	Equivalent Volumetric Concentration (μg/μL)	Standard Curve R^2	Extrapolation from Standard Curve (%)
Collagen I	0.020	0.027	0.92	-
Collagen I	0.003	0.004	0.99	-0.39
Collagen I	0.049	0.073	0.97	-
Average	*0.024 ± 0.023*	*0.035 ± 0.035*	-	-
Collagen IV	0.001	0.002	0.92	-
Collagen IV	0.007	0.021	0.92	-
Collagen IV	0.068	0.088	0.87	-
Average	*0.025 ± 0.037*	*0.037 ± 0.045*	-	-
Fibrillin-1	0.024	0.030	0.98	-
Fibrillin-1	0.010	0.012	0.97	-
Average	*0.017 ± 0.009*	*0.021 ± 0.013*	-	-
Fibronectin	0.002	0.003	0.81	-4.43
Fibronectin	0.030	0.057	0.92	-
Average	*0.016 ± 0.020*	*0.030 ± 0.038*	-	-

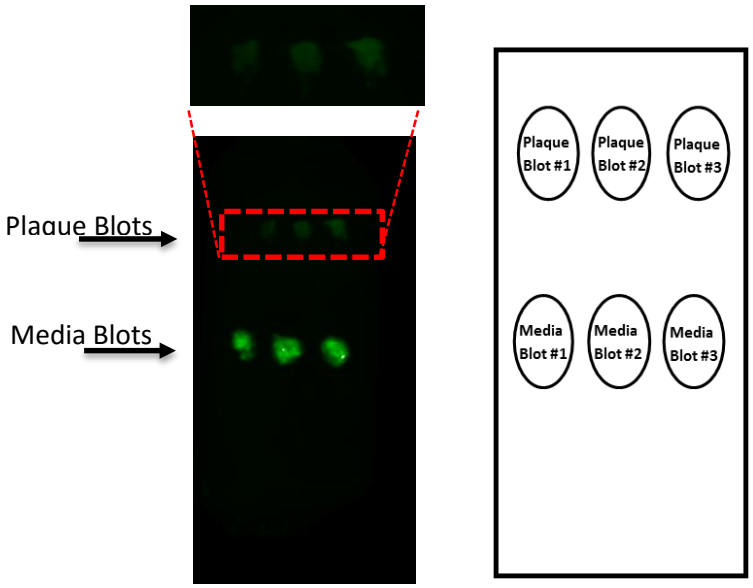

Figure 3.5 A representative blot stained with anti-SMA in the plaque and in the media (left) and schematic (right). Inset shows plaque blots.

3.3.3 Mechanical testing using RDCB experiments

RDCB experiments were performed using collagen IV protein films at several concentrations sandwiched between strips of decellularized porcine aorta. A representative load-displacement curve and traction-separation curve for collagen IV at each protein concentration is shown in Figure 3.6. The maximum load is generally reduced with deceasing protein concentration. Similarly, the maximum traction decreases with decreasing protein concentration while the maximum separation is relatively unchanged. Table 3.2 summarizes the key results from the RDCB experiments.

The results of RDCB experiments summarized in Figure 3.7 show that the adhesion strength, or energy release rate, of thin protein films increases exponentially with collagen IV concentration. Some of the variability in energy release rate may be explained by the difference in porcine tissue samples from different subjects. At the expected ex vivo equivalent concentration estimated from the plaque immunoblotting experiments (0.037 μg/μL), the corresponding energy release rate for collagen IV (0.62 J/m^2) is approximately one order of magnitude lower than the published experimental measurements of mouse plaque-IEL adhesion strength (19.3 J/m^2; 24.5 J/m^2) [36], [37]. This discrepancy suggests that while collagen IV is relatively abundant at the plaque-IEL interface, it is not a key contributor to the adhesion strength between the atherosclerotic plaque and the IEL.

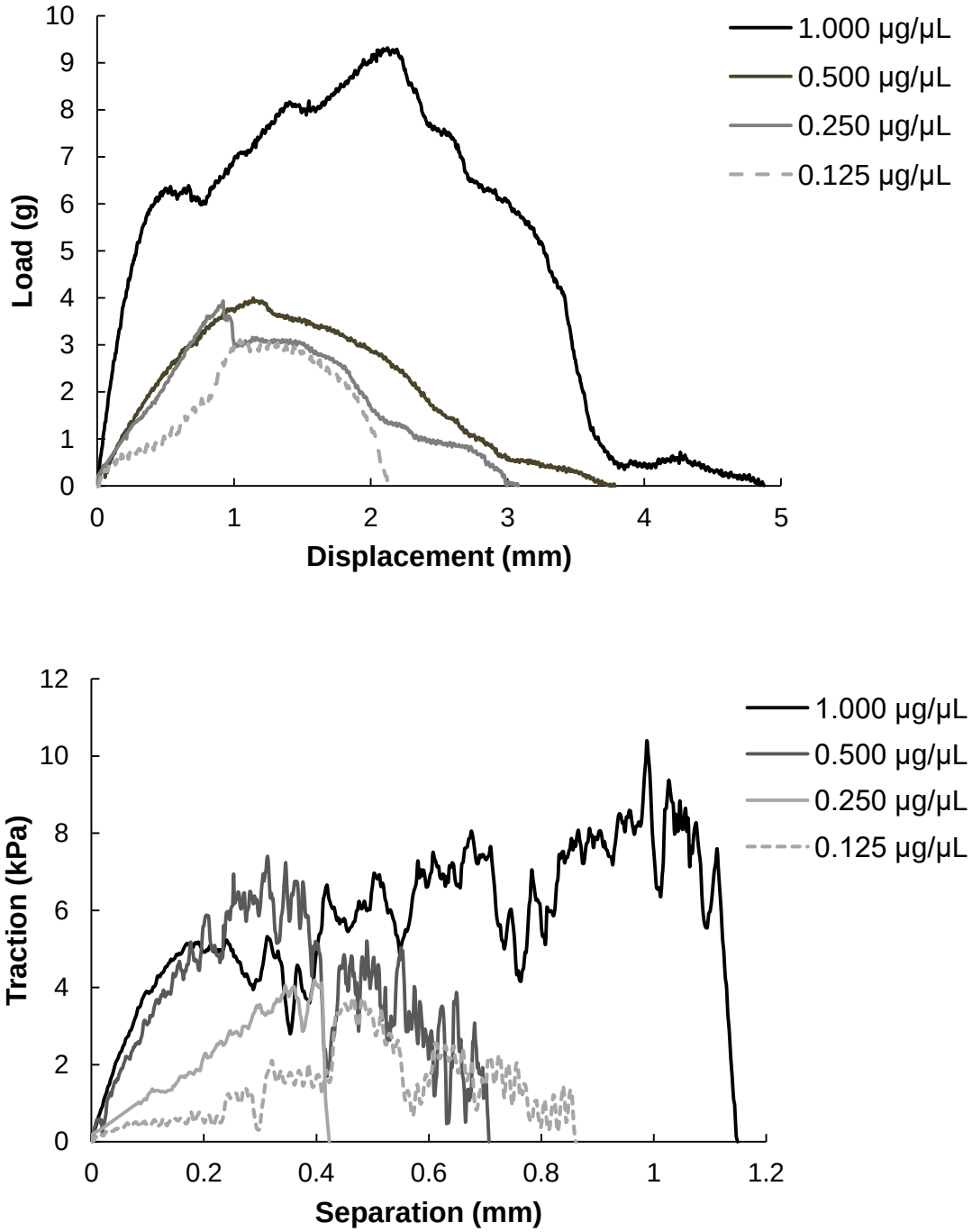

Figure 3.6 Representative load-displacement (top) and resulting traction-separation curves (bottom) at each tested protein concentration.

Table 3.2 Summary of key results from RDCB experiments.

Protein	Concentration (μg/μL)	Average Maximum Traction (kPa)	Average Maximum Separation (mm)	Average Energy Release Rate (J/m^2)
Collagen IV	1.000	25.1	0.82	9.98
Collagen IV	0.500	7.28	0.83	2.58
Collagen IV	0.250	3.58	0.51	0.66
Collagen IV	0.125	3.75	0.86	1.22

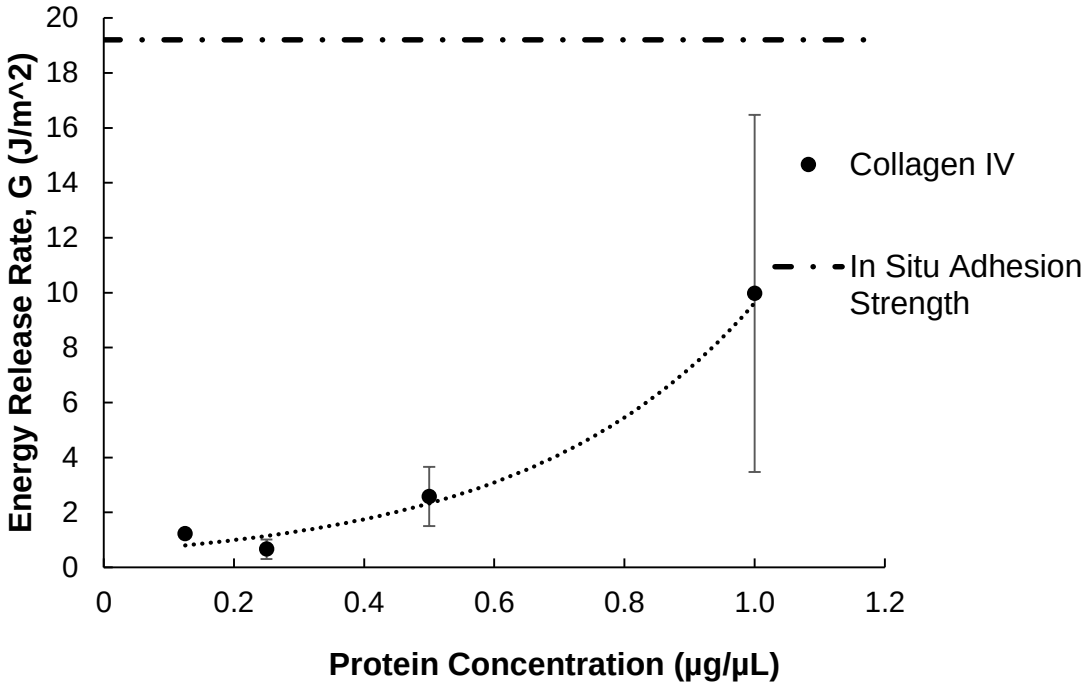

Figure 3.7 RDCB results for adhesion strength of thin collagen IV films compared to in situ adhesion strength of mouse atherosclerotic plaque (from [37]). Error bars represent standard deviation.

3.3.4 Scanning Electron Microscopy of partially delaminated atherosclerotic plaques

The results from SEM of partially delaminated atherosclerotic plaques show there are several bridging fibers at the plaque-IEL interface (Figure 3.8). These

fibers may be key structural components of the plaque-IEL interface. Radially oriented bridging fibers between the plaque and the IEL will increase adhesion strength and resist failure between these two layers. The number, diameter, and orientation of these fibers may affect the overall adhesion strength at the plaque-IEL interface.

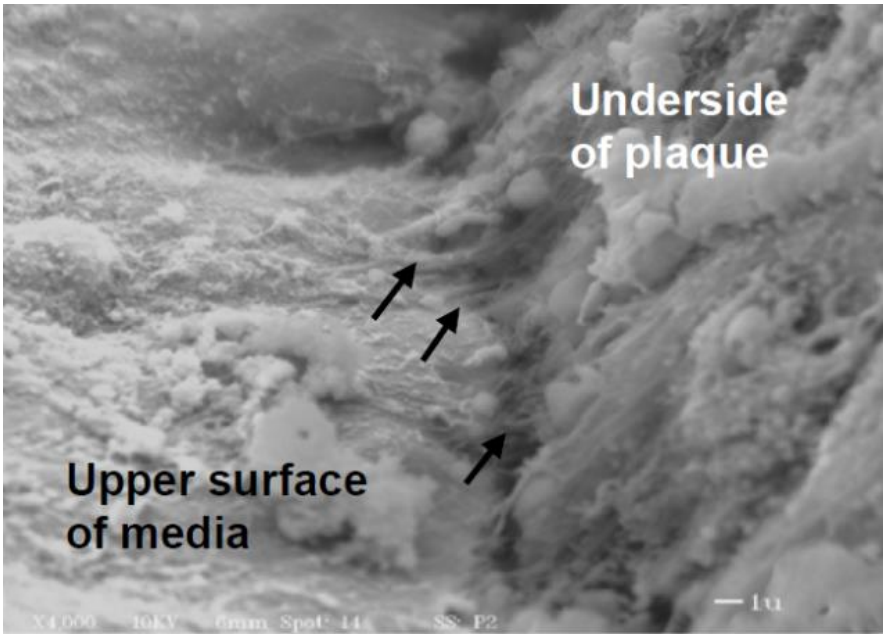

Figure 3.8 Scanning electron microscopy (SEM) of partially delaminated mouse plaque shows bridging fibers (arrows) exist at the plaque-IEL interface. Scale bar represents 1 μm.

3.4 Discussion

The results from immunohistochemistry and plaque immunoblotting studies show good agreement. Collagen I is clearly present at the plaque-IEL interface, confirmed by both IHC and plaque immunoblotting results. IHC shows that collagen IV is clearly associated with the IEL, though its distribution appears to be somewhat heterogeneous. Heterogeneous distribution of collagen IV over the

entire IEL surface could explain the large standard deviation in the plaque immunoblotting results. While both fibrillin-1 and fibronectin appear to be present at the plaque-IEL interface by IHC, the staining intensity is lower than for collagen I or collagen IV. These results are mimicked in the plaque immunoblotting results, where fibrillin-1 and fibronectin are slightly less abundant than collagen I and collagen IV. The concentration of osteopontin was not quantified; however, both IHC and plaque immunoblotting (data not shown) confirm that osteopontin is present at the plaque-IEL interface.

Examining the results from the RDCB experiments can provide insight into the mechanism of failure at the plaque-IEL interface by providing bounds on the forces required to separate surfaces adhered by a thin protein film. We hypothesize two potential sources of adhesion strength or tearing toughness at the interface: 1) bridging fibers that extend between tissue layers and/or 2) adhesive matrix proteins at the interface. The RDCB experiments can measure the mechanical toughness of a thin film of adhesive protein. The results from the RDCB experiments in this study show that collagen IV is not a likely key constituent determining adhesive strength at the plaque-IEL interface. When extrapolating the results of the RDCB experiments to the ex vivo protein concentration estimated by immunoblotting, we find that collagen IV exhibits an adhesive strength approximately one order of magnitude below previously measured in situ plaque adhesion strengths. Even at concentrations much higher than those found ex vivo, the adhesive strength of collagen IV is still weaker than the in situ plaque adhesion

results. These results clearly indicate that collagen IV is not likely to be responsible for the mechanical strength at the plaque-IEL interface.

RDCB experiments were also performed on thin films of fibronectin which resulted in a limited number of results due to the weak mechanical strength of these films (data not shown). The RDCB experiments measured the adhesive properties of human plasma fibronectin rather than cellular fibronectin. Both forms of fibronectin are encoded by a single gene and alternatively spliced to form the different variants. Cellular fibronectin is produced by fibroblasts, endothelial cells, and smooth muscle cells and is present as insoluble fibrils in the ECM, while plasma fibronectin is produced only by hepatocytes and is soluble in blood plasma and body fluids [77]–[81]. Several studies show that plasma fibronectin exhibits adhesive properties, specifically to cells [77], collagen [78], [82], and glycosaminoglycans [79], [83]. Additionally, plasma fibronectin can be incorporated into the vascular wall and form fibrils alongside cellular fibronectin [80], [81]. While plasma fibronectin may exhibit some adhesive properties, the RDCB results suggest that the adhesive strength is far weaker than collagen IV and therefore unlikely to contribute to the strength of the plaque-IEL interface. The fibrillar form of fibronectin should be further investigated as a potential contributor to adhesion strength at the plaque-IEL interface.

Other structural proteins that match the mechanical adhesive strength properties measured in situ must be localized to the plaque-IEL interface. Collagen I, fibrillin-1, and fibronectin are potential candidates for the components of the bridging fibers at the plaque-IEL interface, and this study has confirmed that these

proteins are present at the appropriate location. However, measuring the mechanical strength of fibers is fundamentally different than measuring the mechanical strength of adhesive proteins. RDCB experiments are not appropriate to directly test the mechanical strength of fibrillar proteins. First, the in vivo orientation of fibers will significantly affect their contribution to interfacial toughness. We did not make an effort to control fiber orientation in the thin films used for this study. Additionally, the number and thickness of the fibers or fiber bundles will also affect the adhesive strength of the interfacial layer. Future examination of bridging fibers in situ at the plaque-IEL interface is necessary. Atomic force microscopy (AFM) has been used to measure the mechanical properties of single collagen or elastic fibers [84]–[86]; however, computational simulations would be necessary to estimate an energy release rate from these measurements. An alternative technique that has been used to determine the energy release rate during fiber pull-out of individual carbon nanotubes from epoxy composites, using a combined micromechanical tester and SEM [87], may offer potential for determining mechanical properties of fibers at the plaque-IEL interface.

The methodology used in this study represents a novel technique that can be applied to determine the proteins responsible for the adhesive strength of other biological interfaces, such as those between layers of an artery or between cartilage and bone. The plaque immunoblotting technique can be applied to estimate protein concentrations at other biological interfaces and surfaces. Though RDCB of adhesive biological proteins was first proposed by Khayer Dastjerdi et

al., the combination of this technique with plaque immunoblotting constitutes a novel methodology that can be used to determine the adhesive strength contribution of individual proteins or protein mixtures at biological interfaces.

The results from this study include a preliminary candidate group of proteins, and examining additional adhesive matrix proteins is relevant future work. Most importantly, determining the composition of the bridging fibers and measuring their breaking strength will provide great insight into the failure mechanism at the plaque-IEL interface. Additionally, plaque adhesion strength may result from the synergistic interaction of several proteins forming matrix architectures that have emergent mechanical properties. To gain additional insight into failure mechanisms at the plaque-IEL interface, it may be necessary to evaluate cohesive/adhesive properties of protein mixtures as well as bridging fiber pull-out strength from native vascular ECM.

3.5 Conclusions

This study describes a novel technique that has been used to investigate contributions of adhesive matrix proteins to the strength of the plaque-IEL interface. We show that collagen I, collagen IV, fibrillin-1, fibronectin, and osteopontin are all present at the plaque-IEL interface. Semi-quantitative plaque immunoblotting shows that collagen I and collagen IV are present at slightly higher concentrations than fibrillin-1 and fibronectin at the plaque-IEL interface, though these differences do no reach statistical significance. RDCB experiments show that collagen IV is unlikely to be responsible for the adhesive strength of the

plaque-IEL interface. SEM images of a partially delaminated plaque show bridging fibers exist at the plaque-IEL interface. These fibers, potentially composted of collagen I, fibrillin-1 or fibronectin, are likely responsible for the adhesion strength at the plaque-IEL interface.

Acknowledgements

The authors would like to acknowledge Ying Wang and Jeffrey Davis for their work in collecting the SEM images. The authors would like to acknowledge funding from the National Science Foundation through grant number CMMI-1200358.

CHAPTER 4

CHARACTERIZATION OF FRACTURE BEHAVIOR OF HUMAN ATHEROSCLEROTIC FIBROUS CAPS USING A MINIATURE SINGLE EDGE NOTCHED TENSILE TEST[2]

[2] L.A. Davis, S.E. Stewart, C.G. Carsten, B.A. Snyder, M.A. Sutton, S.M. Lessner. Submitted to Acta Biomaterialia 2/13/2016.

4.1 Introduction

Atherosclerotic plaque rupture can lead to myocardial infarction or ischemic stroke, two of the leading causes of death in the United States [1]. It is estimated that by 2030 there will be 3.4 million strokes in American adults, a 20% increase in prevalence since 2012 [2]. Atherosclerotic plaque rupture in the carotid artery can lead to stroke or transient ischemic attack (TIA), which affect approximately 795,000 and 5 million people each year, respectively. Strokes are one of the top causes of long-term disability, while also accounting for one in every 19 deaths in the US [2].

Ischemic stroke can be induced by multiple mechanisms. One well-established cause is plaque rupture, during which a tear in the fibrous cap of an atherosclerotic plaque exposes the highly thrombogenic necrotic core material. In some cases, the resulting thrombosis causes vessel occlusion, during which the patient will experience an ischemic stroke or TIA. Plaque rupture in the carotid artery accounts for approximately 15% of all ischemic strokes [88]. This mechanism generally occurs in lesions called a thin-cap fibroatheroma (TCFA), characterized by a thin fibrous cap covering a large necrotic core [20]–[23]. Though these morphological characteristics provide a good framework for identifying vulnerable plaques, the true test of plaque vulnerability is whether or not the mechanical strength of the tissue can withstand the physiological loading conditions to which it is subjected. When loads experienced in vivo exceed the mechanical strength of the fibrous cap, the tissue will fail, often resulting in thrombus formation that may lead to ischemic stroke. The extent of damage from

plaque rupture varies. The thrombosis from plaque rupture may remain clinically silent if the thrombus does not completely occlude the vessel. However, healing of the rupture sites within the fibrous cap promotes further occlusion of the vessel, and frequently subsequent ruptures or erosions of the fibrous cap occur [22], [23]. These subsequent ruptures or erosions may result in a clinical event. Therefore, identifying which fibrous caps are more likely to tear is a good predictor of which plaques are more likely to result in a clinical event.

In order to predict likelihood of plaque rupture, the first step is to identify the best metric to assess fracture toughness of the fibrous cap. While there is some information in the literature regarding quantitative measures of fibrous cap failure, such as ultimate tensile strength, the detailed failure mechanism of fibrous caps is not well understood. It is important to understand how the tissue fails in order to select the best method to assess the failure of these tissues. Examining the fracture behavior of the tissue will provide more insight into plaque rupture than previous studies.

With regard to quantitative metrics, several groups have previously used energy release rate to characterize fracture toughness in soft biological tissues, both in an adhesive layer [36], [37], [89], and within a biological tissue [30], [34], [35]. Though not used previously to characterize fracture toughness in vascular tissue, crack tip opening displacement (CTOD) was first proposed by Wells at the British Welding Institute to characterize failure in elastic-plastic yielding conditions [90]. Wells observed that plastic deformation resulted in blunting at the crack tip, and that the extent of crack-tip blunting increased in proportion to the toughness

of the material. Later, Dawes showed that CTOD is linearly related to the J-integral in elastic-plastic conditions and that both are valid fracture parameters [91].

Since the fracture toughness of fibrous caps has not been studied, this study aims to quantitatively characterize the fracture behavior of fibrous caps using both the CTOD metric and the stress in the un-cracked segment (UCS) to assess fracture toughness. To the authors' knowledge this is the first application of CTOD in vascular tissue.

4.2 Materials and methods

4.2.1 Sample preparation and dissection

The current study was approved by the IRB at Greenville Health System on September 3, 2013 and all patients gave written informed consent. In order to be considered for this study, patients must have greater than 50% stenosis in the carotid artery and a prior stroke or TIA, or greater than 70% carotid artery stenosis. Human carotid endarterectomy specimens were obtained from 8 patients at the time of surgery at Greenville Memorial Hospital (patient demographics in Table 4.1). Two plaque specimens generated multiple samples from the same patients (Samples III and IV; Samples VII and VIII). The excised specimens were immediately immersed in Belzer UW Cold Storage Solution (Bridge to Life Ltd., Columbia, SC, USA) and were kept cool until testing. All mechanical testing was completed within 48 hours of tissue harvest. The intact specimen, shown in Figure 4.1 (left), ranges from approximately two to five cm in length. The specimen is nominally centered in the carotid artery bifurcation and usually contains portions

of the common carotid artery (CCA), the internal carotid artery (ICA), and the external carotid artery (ECA). The intact specimen was sliced into a series of transverse slices nominally 5-mm thick (Figure 4.1, right) using a custom slicing device.

Table 4.1 Patient demographics

Sample ID	Gender	Age	Region of Sample Used for Mechanical Testing
I	M	46	Carotid Bulb
II	F	89	Common Carotid Artery
III	M	84	Carotid Bulb
IV	M	84	Carotid Bulb
V	M	60	Carotid Bulb
VI	M	74	Carotid Bulb
VII	M	86	Internal Carotid Artery
VIII	M	86	Internal Carotid Artery
IX	F	74	Internal Carotid Artery
X	F	56	Carotid Bulb

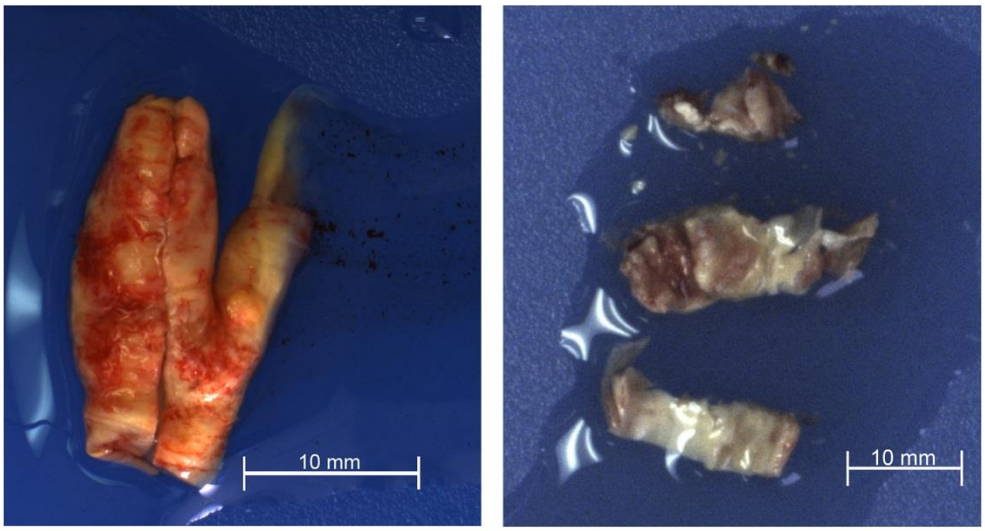

Figure 4.1 Typical examples of specimens obtained from carotid endarterectomy. An intact specimen immediately following harvest is shown on the left, with the common carotid artery at the bottom. The specimens are sliced into a series of 5 mm rings, as shown on the right.

4.2.2 Mechanical testing of isolated fibrous cap

The fibrous cap was isolated for mechanical testing by dissection from the remaining plaque. All samples were subjected to tensile loading in the circumferential direction, corresponding to the direction of maximum wall stress (hoop stress). Two types of mechanical tests were performed. First, uniaxial tensile tests on the fibrous cap were performed to determine the stress-strain response of the fibrous cap. Then, the fracture behavior within the fibrous cap was examined. Immediately following the uniaxial tensile tests, a scalpel was used to introduce an initial flaw on one edge in the longitudinal direction, approximately at the midpoint between the two grips. The flaw orientation is nominally perpendicular to the longitudinal edge, with the loading applied parallel to the longitudinal edge (i.e., along the in-vivo circumferential direction).

4.2.2.1 Experimental setup

The isolated fibrous cap was mounted into a set of metal grips, with 100 grit sandpaper on the inner surface to minimize slippage. The grips were connected to a Bose 3200 Test Instrument (Bose Corp., Framingham, MA, USA). One grip was stationary and connected to a load cell, while the other grip was connected to an actuator. All experiments were performed in displacement control. Both the uniaxial load and displacement were recorded at a rate of 2 Hz or higher during the experiment. Due to the unique geometry of each plaque specimen, in some cases the length of the isolated fibrous cap was very short (less than 15 mm). In the case of these short specimens, Dermabond Advanced (Ethicon Inc.,

Somerville, NJ, USA) (a topical skin adhesive) was added to the grips in order to further reduce the potential for specimen slippage within the grips.

Two charge-coupled device (CCD) cameras (Grasshopper GRAS-50S5M, Point Grey Research, Richmond, BC, Canada) were positioned at a 90° offset from each other, one providing a front view and the other providing a side view of the tissue. Images were acquired at 1 Hz throughout each experiment. Small dots of black tissue marking dye were applied to the front face of the tissue in order to perform marker tracking and to measure the stretch ratio. The experiments were performed at a loading and unloading rate of 0.05 mm/s, with additional Belzer UW solution applied to the tissue at regular intervals (i.e., approximately every two minutes) during testing to prevent drying.

4.2.2.2 Uniaxial tensile experiments

Uniaxial tensile testing was performed to obtain the stress-strain response of the tissue. Cyclical displacements of approximately 20% - 30% of the specimen length were applied, resulting in global strains on the order of 0.20 to 0.30 during the cyclic strain process. The tissue was preconditioned through multiple loading and unloading cycles until the maximum load at the end of each cycle reaches steady state. The loading portion of the last cycle from each experiment was used to calculate the stress-strain response of the tissue. The stretch ratio was determined every second using the applied dot pattern. The Cauchy stress is determined by dividing the instantaneous force by the deformed cross-sectional area. The cross-sectional area was estimated using specimen width and thickness

measurements from the images captured by the cameras. The resulting experimental stress-strain data points were fitted by a second order polynomial hyperelastic model using Abaqus (Version 6.13-2, Dassault Systèmes Simulia Corp., Providence, RI, USA) material data fitting tools.

4.2.2.3 Miniature single edge notch tension experiments

As discussed earlier, miniature single edge notch tension (MSENT) experiments were performed on plaque specimens that were prepared with an initial crack perpendicular to the direction of the applied load. In these studies, the initial crack length was between 45% and 70% of the overall width of the tissue. Cyclical controlled displacement was applied such that the crack extended slowly during several cycles of loading; each crack extension is approximately 0.4 mm in length. For the ten specimens where crack extension in the nominally longitudinal direction occurred from the notch root region, the crack tip opening displacement (CTOD) is obtained as the crack extends using images acquired during the MSENT experiments[3]. CTOD is calculated by measuring the distance between the intersections of a 90 degree vertex centered at the crack tip with the crack edges, as first suggested by Rice [92]; a schematic is shown in Figure 4.2. Additionally, the uniaxial average Cauchy stress in the UCS, σ, is determined at the initiation of tearing in each cycle as

[3] Of the 34 specimens used in our experiments, 13 specimens (38%) failed in the grip region, 6 (18%) specimens failed in regions away from both the grips and the notch root and 5 (15%) specimens exhibited tearing across the thickness. Results from these experiments are not included in this paper.

$$\sigma = \frac{F}{w*t} \tag{4.1}$$

where *F* is the instantaneous measured load, *w* is the instantaneous current remaining width of the UCS and *t* is the instantaneous current measured thickness in the UCS.

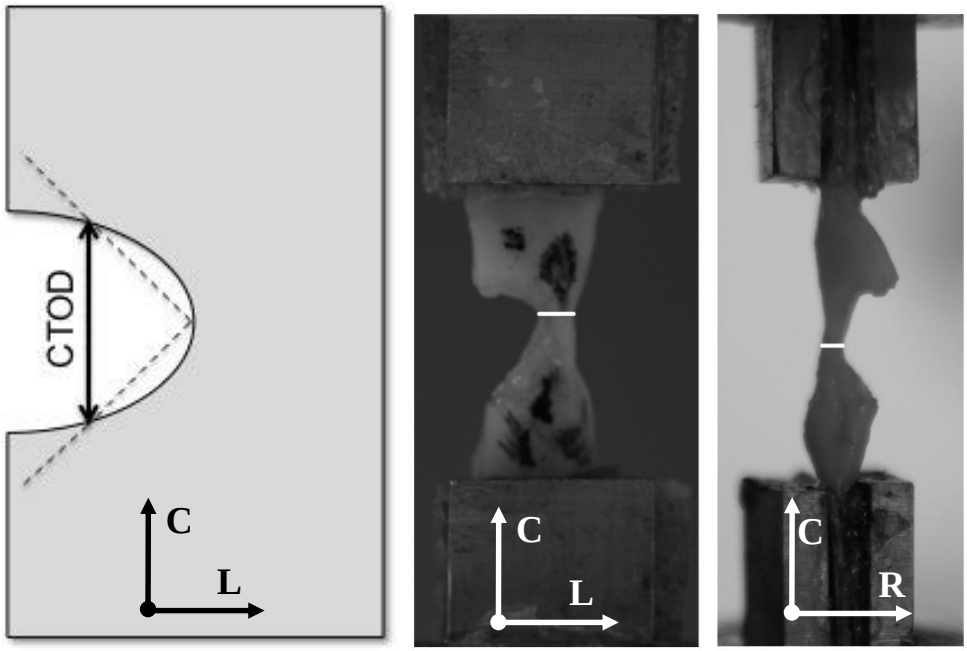

Figure 4.2 A depiction of the CTOD measurement (left) and the geometry measurements required for the stress in the UCS calculations (middle and right). CTOD is calculated by measuring the distance between the intersections of the sides of a 90 degree vertex centered at the crack tip. The current cross-sectional area of the UCS is determined by measuring the current width (white line, center panel) and the current thickness (white line, right panel) of the UCS at the crack tip. The longitudinal (L), circumferential (C), and radial (R) directions are as shown.

4.2.3 Histological studies

After mechanical testing, the samples were fixed in a solution of 4% paraformaldehyde in 0.1 M phosphate buffer, pH 7.4, embedded in paraffin, and sectioned at a thickness of 5 μm. The sections were stained in 0.1% Picrosirius Red (PSR) in saturated picric acid for 90 minutes, washed for 2 minutes in 0.01 M hydrochloric acid, dehydrated, cleared, and mounted in Permount. The sections were analyzed under cross-polarized transmitted light on a Zeiss Axio Imager microscope. A 10X objective lens was used to collect images from the samples. Images were captured with a Zeiss AxioCam CCD camera and analyzed for collagen content using Image-Pro Plus software (Version 5.1.0.20, Media Cybernetics, Rockville, MD, USA).

Collagen content was determined based on the fractional area of birefringence observed in the PSR-stained tissue sections. First, an image was collected in brightfield and the total tissue area was measured using Image-Pro Plus. Then the same field was examined under cross-polarized light and an image was collected. The area of the sample that showed green, yellow, or orange-red birefringence characteristic of collagen was then measured. The collagen content of the sample as a whole was calculated by comparing the birefringent area to the total tissue area. This analysis was applied to several regions of each section, as the sections are sometimes too large to be completely visualized at 10X magnification. Values of fractional collagen area from the different quadrants were then averaged to produce a final value for the sample.

4.2.4 Statistical analysis

Data from multiple samples are reported in terms of the median, first quartile (IQR1), and third quartile (IQR3) values. Significant relationships between measured parameters were assessed using linear regression to test the null hypothesis that the slope is equal to zero. The null hypothesis was rejected, with statistical significance, if $P < 0.05$.

4.3 Results

4.3.1 Stress-strain curves

Figure 4.3 presents the stress-strain curves for tensile loading of individual fibrous cap specimens. As shown in Figure 4.3, there is substantial scatter in material response that is consistent with previous observations [17-24]. In our studies, each specimen exhibits non-linear response that is typical of vascular tissue. Further study of the data shown in Figure 4.3 led the authors to extract subsets of the overall data that represent (a) the low-strain region and (b) the high-strain region. The low and high strain data sets are separated by manually identifying the midpoint between the two regions, depicted in Figure 4.4. In addition, linear regression is performed on the data points in each of these subsets to identify the tangent modulus. Table 4.2 presents both the tangent moduli and the stretch ratio at which the shift between the two regions occurs. Results show that the median [IQR 1, IQR 3] low-strain tangent modulus is 63.1 [29.5, 87.0] kPa, the median [IQR 1, IQR 3] high-strain tangent modulus is 1006.6 [288.1 1805.1] kPa, and the median [IQR 1, IQR 3] stretch ratio at the shift between the two data

sets is 1.13 [1.09, 1.15]. More detailed investigation of the data in Figure 4.3 suggests that there are three major sub-groups in the stress-strain response; a stiff group (III, V), an intermediate group (II, VI, VII, VIII), and a compliant group (I, IV).

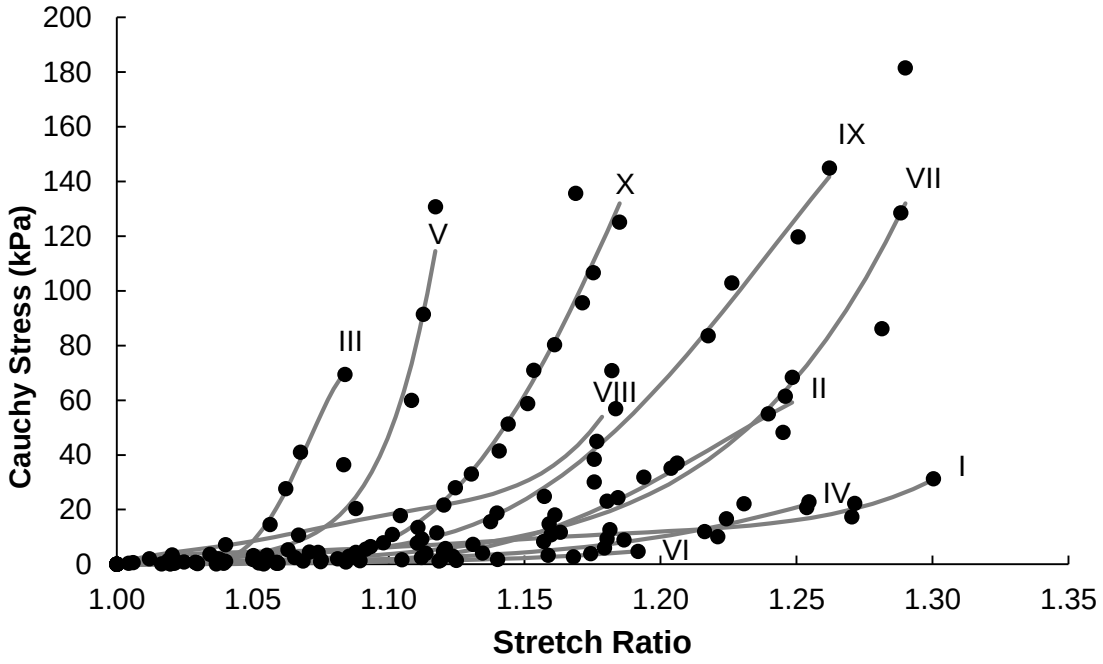

Figure 4.3 The stress-strain response of several fibrous caps. The dots represent experimental data points The solid curves represent predictions based on material model data fitting performed in Abaqus.

Table 4.2 Parameters describing the stress-strain response for each sample

Sample ID	Low-Strain Tangent Modulus (kPa)	High-Strain Tangent Modulus (kPa)	Stretch Ratio at Shift
I	60.7	142.8	1.15
II	16.3	536.8	1.14
III	90.9	1972	1.05
IV	20.5	205.2	1.15
V	75.4	2086	1.07
VI	6.64	44.77	1.09
VII	65.6	1303	1.18
VIII	149.1	963.0	1.10
IX	100.7	1050	1.16
X	56.8	1995	1.12

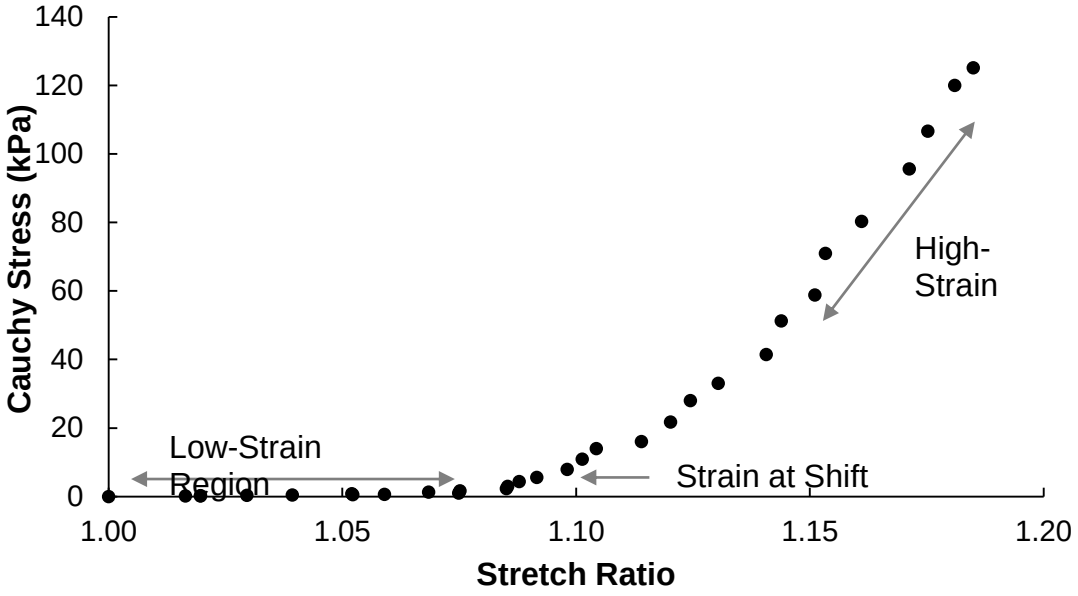

Figure 4.4 The low-strain tangent modulus (LSTM), high-strain tangent modulus (HSTM) and the stretch ratio at shift are determined from the stress-strain curves. Data from the low-strain region and high-strain region of each stress-strain curve are fit by linear regression to determine the low-strain tangent modulus and high-strain tangent modulus, respectively. The stretch ratio at shift is determined by identifying the stretch at the midpoint between the two regions.

4.3.2 Crack tip opening displacement

Figure 4.5 presents the CTOD measurements during crack extension for the plaque specimens. As shown in Figure 4.5, CTOD increases with increasing crack extension. This behavior is consistent with ductile materials that exhibit crack tip blunting. In these studies with relatively small specimens, the overall amount of crack extension is limited by the geometry of the sample and by the size of the initial crack. Inspection of the data in Figure 4.5 suggests that CTOD is a linearly increasing function of crack extension. The median [IQR 1, IQR 3] initial CTOD is 0.54 [0.42, 0.71] mm, and the median [IQR 1, IQR 3] slope of the CTOD

measurements is 1.30 [0.59, 1.51]. It is important to note that in almost all of the plaque specimens the initial CTOD values are clustered around 0.5 mm, with the exception of samples IV, VI and X, which have higher initial CTOD values (0.96 mm, 2.73 mm, and 1.01 mm, respectively).

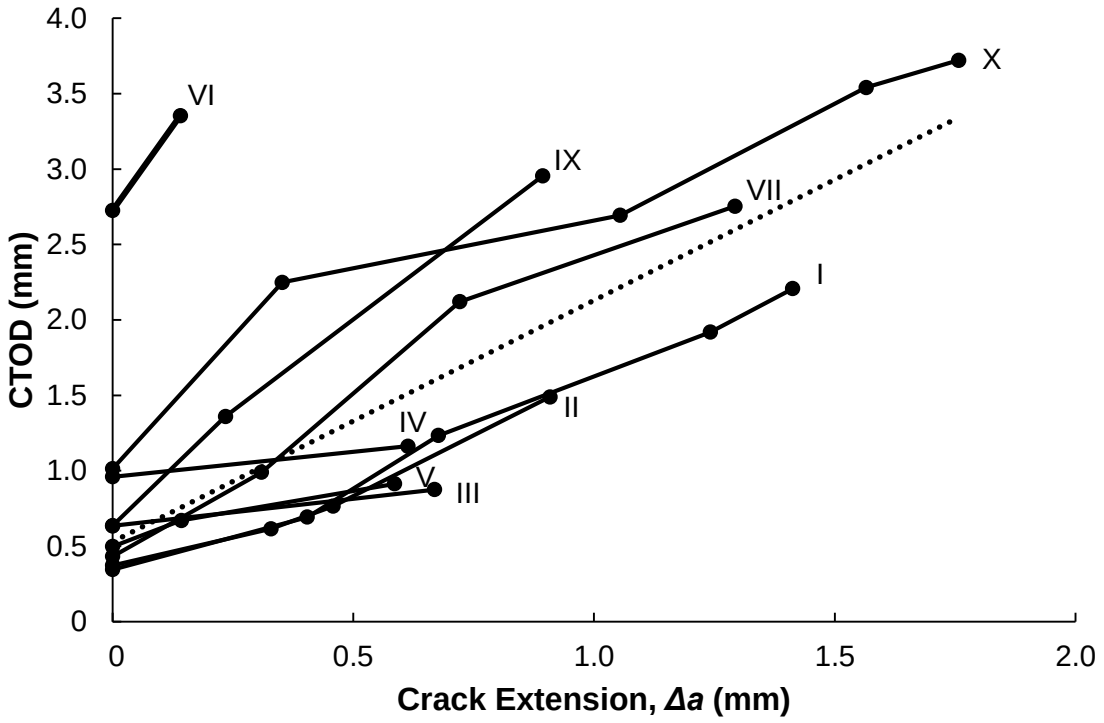

Figure 4.5 The CTOD increases with crack extension (Δa) for each specimen. The dashed line shows a trendline through all CTOD data points.

In addition to the CTOD measurements, the radius of curvature of the crack tip is quantified at the initiation of tearing for each sample as a metric for the degree of crack tip blunting. Two samples exhibited such a high degree of blunting that a 90 degree vertex did not intersect the edges of the crack. In these cases, CTOD could not be calculated using the 90^{o} intersection definition (a) for the entire duration of crack extension in sample VIII and (b) for the final part of crack

extension in sample VI. Even so, in all cases the radius of curvature of the crack tip at the initiation of tearing was measured. The median [IQR 1, IQR 3] radius of curvature of the crack tip at initial tearing is 0.24 [0.13, 0.27] mm.

4.3.3 Stress in the un-cracked segment

Stress in the UCS was calculated at the initiation of tearing for each cycle, with median [IQR 1, IQR 3] values of 0.366 [0.279, 0.648] MPa. The stress in the UCS is plotted versus crack extension in Figure 4.6. There appear to be two groups of responses. One group (I, V, VII) has a high initial stress in the UCS, followed by much lower stresses at the initiation of additional crack extension. The other group (II, VI, VIII, IX, X) has relatively constant stresses in the UCS. Samples III and IV only had one cycle of tearing and therefore only one stress calculation.

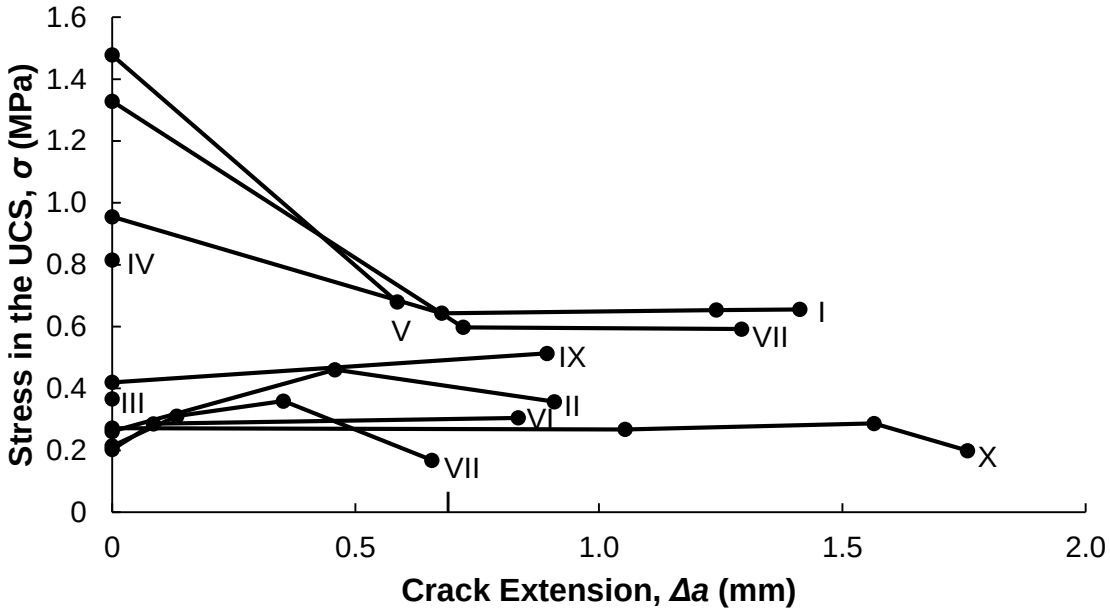

Figure 4.6 Stress in the UCS versus crack extension for each specimen. Samples III and IV only had one cycle of tearing and therefore were not evaluated at multiple crack extensions.

The initial decrease in stress in the UCS in samples I, V, and VII could arise from calcification, local variations in collagen content, or varying orientation of collagen fibers. Additionally, when Figure 4.5 and Figure 4.6 are compared it is clear that CTOD and stress in the UCS are not directly related. While CTOD is a strictly increasing function of crack extension, stress in the UCS is essentially constant, after an initial decrease in some cases.

4.3.4 Collagen content trends

Collagen content was measured in each specimen after mechanical testing and compared to patient age, initial stress in the UCS, initial CTOD, and initial radius of curvature at the crack tip (Figure 4.7, Table 4.3). The median [IQR 1, IQR 3] value of fractional collagen content is 32.8 [30.0, 42.0] percent. While there is a slight decrease in collagen content with age, this is not a significant relationship. However, there is a statistically significant relationship between collagen content and the stress in the UCS ($P = 0.003$ that slope is zero). In addition, there is a statistically significant inverse trend between the initial CTOD value and total collagen content ($P = 0.019$).

The effect of collagen content on CTOD at fixed values of crack extension was assessed and no significant trends were found (Figure 4.8), suggesting that other material constituents may be responsible for the slope of the CTOD curve, or rate of crack tip blunting. The radius of curvature at the crack tip, which is a measure of the degree of blunting at the crack tip, also is shown to have a statistically significant inverse relationship with collagen content ($P = 0.009$). These

results suggest that samples with higher collagen content begin tearing with a sharper, narrower crack and exhibit higher stresses at the initiation of tearing.

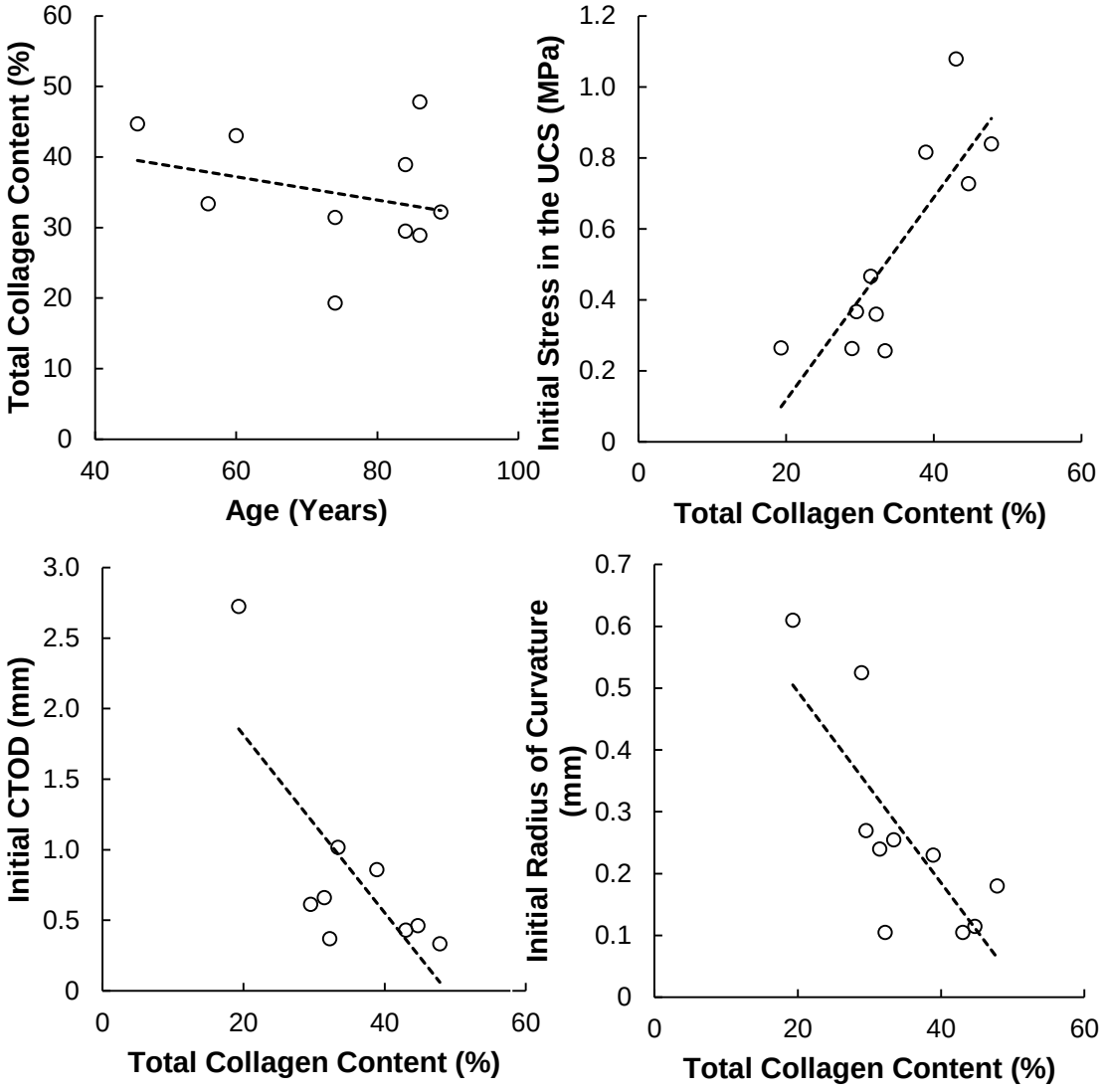

Figure 4.7 The effect of total collagen content on age, initial stress in the UCS, initial CTOD and initial radius of curvature of the crack tip. While total collagen content generally decreases with age, this is not a significant trend (top left). There is a significant linearly direct relationship between the stress in the UCS and total collagen content ($P < 0.05$) (top right). The initial CTOD decreases with increasing total collagen content and this is a statistically significant relationship ($P < 0.05$) (bottom left). There is a statistically significant inverse linear relationship between the initial radius of curvature of the crack tip and the total collagen content ($P < 0.05$) (bottom right).

Table 4.3 Summary of key statistical relationships between selected parameters

Parameter 1	Parameter 2	Relationship	Statistically Significant
Collagen Content	Age	Inverse Linear	No (P = 0.425)
Collagen Content	Initial CTOD	Inverse Linear	Yes (P = 0.019)
Collagen Content	Initial Stress in the UCS	Direct Linear	Yes (P = 0.003)
Collagen Content	Initial Radius of Curvature at the Crack Tip	Inverse Linear	Yes (P = 0.009)
Initial Radius of Curvature at the Crack Tip	Initial CTOD	Direct Linear	Yes (P = 0.038)

4.3.5 Other observations of tissue behavior

During the MSENT experiments, the crack tip exhibited blunting in each sample. Figure 4.9 shows a representative series of images of the crack both before and during tissue failure. The radius of curvature of the crack tip is measured at the initiation of tearing for each cycle. The radius of curvature of the crack tip increased with each consecutive cycle in every specimen, showing that the degree of crack tip blunting increases with crack extension. Wells noted that crack tip blunting increased directly with an increase in toughness of the material [90]. To examine whether or not our results also show this trend, the initial CTOD and the initial radius of curvature of the crack tip were compared. We find a significant direct correlation (P = 0.038), shown in Figure 4.10, that matches Wells' observations.

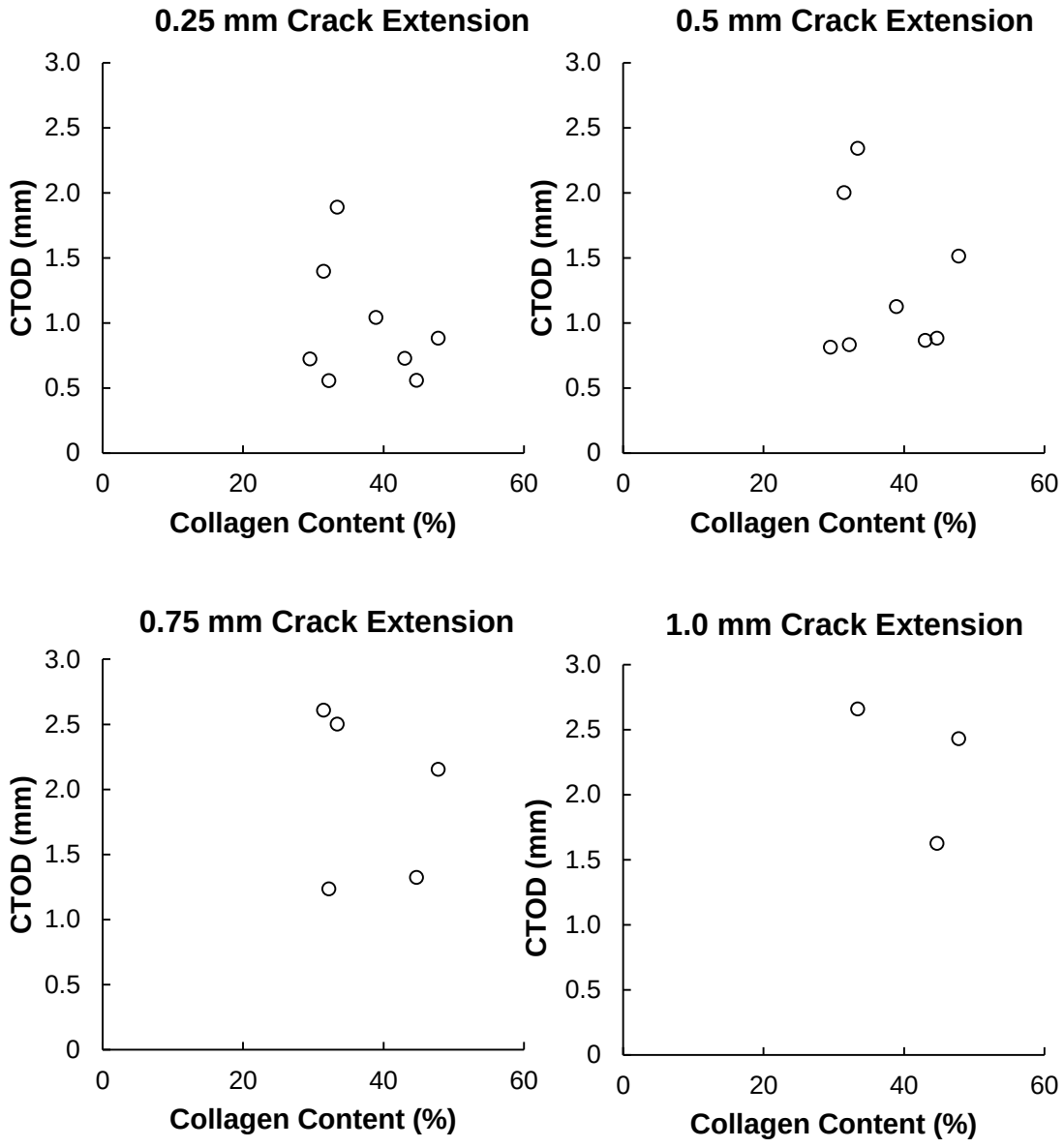

Figure 4.8 Collagen content versus CTOD at selected crack extension values. The CTOD at selected values of crack extension is determined by linear interpolation for each specimen. These values are plotted versus collagen content to determine if collagen content affects CTOD values at other crack extensions. Collagen content versus initial CTOD (before crack extension) is shown in Figure 4.7. None of the relationships in this figure are statistically significant.

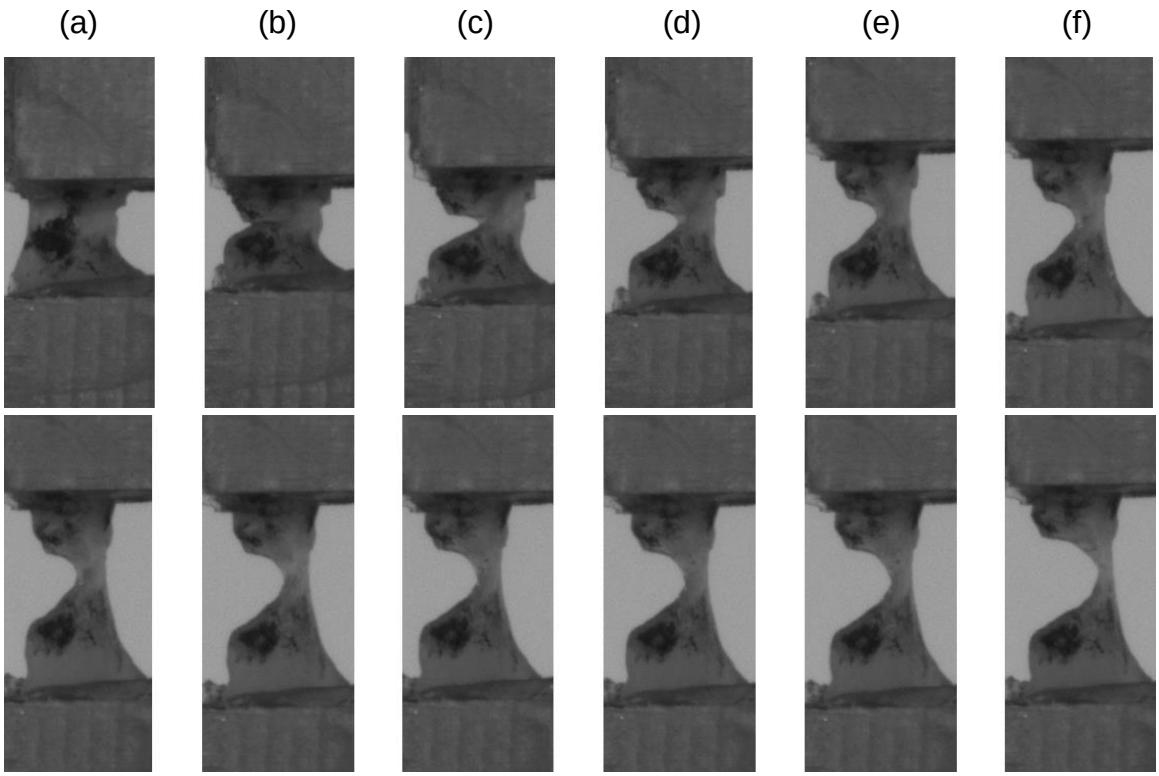

Figure 4.9 Blunting of the crack tip progresses as the tissue tears. The first row shows the initial, intact specimen (a), the specimen immediately after the notch is made (b), and the specimen during the deformation before tearing initiated (c-f). The bottom row shows the progression of blunting as tearing progresses in the tissue (a-f).

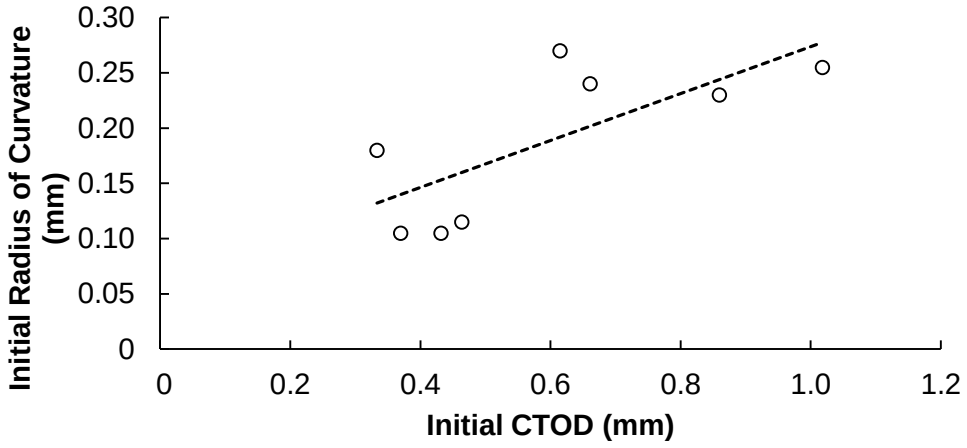

Figure 4.10 The initial radius of curvature of the crack tip and the initial CTOD have a significant linearly direct relationship ($p < 0.05$).

4.4 Discussion

To the authors' knowledge, this is the first study that has investigated the fracture behavior of fibrous cap tissue and the first to use CTOD as a fracture parameter in vascular tissue. The results show that collagen content plays a significant role in determining the material's fracture response, in terms of stresses observed at fracture, CTOD, and blunting of the crack tip. These results suggest that collagen fibers are responsible for increasing the load-bearing capacity of fibrous caps and resisting plastic deformation of the crack tip during fibrous cap failure.

4.4.1 Validity of results

Obtaining valid fracture toughness measurements in soft biological materials is inherently difficult, primarily due to limitations of specimen size. The results in this study show that CTOD increases with crack length, due to an increase in blunting of the crack tip with each increment of crack extension. There is no observable significant change in CTOD when the initial crack length is varied. While the size limitations of fibrous cap specimens make it difficult, if not impossible, to obtain adequate samples for ASTM standardized testing for fracture toughness experiments, these results can still be used to add to the understanding of fibrous cap failure. Atherosclerotic fibrous caps are notoriously heterogeneous tissues [93]. For this reason, a metric that can provide insight into the relative mechanical strength of fibrous caps is beneficial. The fracture parameters quantified in this study can be used to compare resistance to failure between

samples from different patients and to infer which fibrous caps are more likely to rupture under specific loading conditions.

4.4.2 Effect of collagen content

The fibrous cap is composed of smooth muscle cells, macrophages, and an extracellular matrix made up primarily of collagen and proteoglycans [20]. Collagen type I and collagen type III are the primary structural components [94] in fibrous caps and are responsible for much of the mechanical response of the tissue. The results from this study show that collagen content plays a significant role in the blunting of the crack tip at crack initiation and in the magnitude of stress in the UCS that is required to initiate tearing. These results predict that a fibrous cap with higher collagen content will fail at a higher stress with a sharper crack and a lower initial CTOD. Previous studies have shown that increased collagen content in fibrous caps leads to a greater stress at tearing and decreased extensibility of the tissue [95], [96]; these trends are consistent with our observations.

Fibrous caps can be viewed as a fiber-reinforced material with collagen fibers embedded in the surrounding extracellular matrix. Since collagen is the primary load bearing protein in the ECM of the fibrous cap, and the remaining matrix is much weaker than the collagen fibers, the non-collagenous matrix will be more compliant in achieving plastic deformation and blunting of the crack tip. In this context, an abundance of collagen fibers will require either breakage of the collagen fibers or debonding between the fibers and the matrix for the crack tip to blunt. Thus, the orientation of collagen fibers becomes critical. If collagen fibers

are aligned parallel to the direction of loading (circumferential orientation), as seen in the arterial media, then the fibers will increase tensile strength and resist crack tip blunting prior to the initiation of tearing. However, if collagen fibers are oriented perpendicular to the loading direction (longitudinal orientation), they will have very little impact on the material response. In this case, the mechanical response will be controlled by the interactions between the fibers and the remaining extracellular matrix, rather than by the fibers themselves. The collagen fiber organization has not been examined in this study and is relevant future work. Generally, collagen organization is assumed to be isotropic in the fibrous cap. However, if this is not the case, the organization of the collagen fibers will play a critical role in characterizing the material response of fibrous cap tissue.

While collagen content significantly affects the initial CTOD and the initial stress in the UCS, the importance of collagen content may diminish with crack extension. Figure 4.8 shows that collagen content has no effect on CTOD beyond the initial crack extension. Figure 4.6 demonstrates that the range in magnitude of stress in the UCS is reduced with additional crack extension. Collagen content may be a good predictor of the initial failure conditions only. After the initial increment of crack growth, other unidentified material constituents may be responsible for the fracture behavior.

This study was a portion of a larger study on mechanical properties of atherosclerotic plaque tissue. Mechanical test data and histological results from additional fibrous cap and isolated media specimens is shown in Appendix A.

4.4.3 Notch sensitivity

The effect of the presence of a notch on the mechanical strength of a material oftentimes is measured by the notch sensitivity ratio (NSR). NSR is the ratio of the notch strength, or stress required to tear the material when a notch is present, to the ultimate tensile strength (UTS), which is the stress at which failure initiates in an un-cracked material. A NSR of 1 is indicative of a material that is not weakened by the presence of a notch and is known as a notch-insensitive material [97], [98]. Ideally, the tensile strength would be measured in an un-cracked specimen and in a cracked specimen with the same material properties, and the results would be compared pairwise. This approach is logistically difficult in fibrous cap tissue due to the small size of the specimens and heterogeneity of material properties. Even samples from the same patient can have noticeably different results (for example: samples III and IV, samples VII and VIII in this study).

Since our current study has not obtained ultimate tensile strength data for the small plaque specimens, previous results from the literature may provide some insight. A few studies measured the UTS of whole plaque specimens [46]–[48] and at least one study measured UTS in isolated fibrous cap tissue [54]. Teng et al. report a median [IQR 1, IQR 3] UTS of 0.158 [0.0721, 0.259] MPa in fibrous caps from symptomatic patients [54], which is much lower than the stress measurements presented in this study of 0.366 [0.279, 0.648] MPa in fibrous caps from asymptomatic patients. These results suggest a NSR of approximately 2.3, which is indicative of a notch-strengthening material. It should be noted that an apparent NSR greater than one in this case may reflect a difference in material

properties between plaques from symptomatic versus asymptomatic patients, rather than the effect of the notch. Future work should include measuring the UTS of fibrous caps from asymptomatic patients. Additionally, the frequent observation of failure away from the crack tip supports the idea of a relatively high NSR (≥ 1). In such cases, tissues with a higher NSR do not have a significant stress concentration at the crack tip. Therefore, the material is not predisposed to fail preferentially at the notch tip. It is further noted that notch insensitivity or defect tolerance is expected to occur in highly fibrous tissues with a relatively uniform fiber orientation when loaded parallel to the predominant fiber direction. If the bonding between fibers is relatively poor, then the stress cannot be transmitted between fibers and the tissue essentially acts as a series of independent fibers [99].

Clinically, notch insensitivity could be a very beneficial material behavior for fibrous caps. If a flaw does not create a stress concentration in the fibrous cap, this gives the tissue an opportunity to heal over time, as long as the critical fracture criterion is not exceeded during the healing process. For example, if high blood pressure is experienced for a short time and a small tear occurs in the fibrous cap, the event may remain clinically silent since the tear will not readily propagate. If the blood pressure is then lowered, the fibrous cap could repair this tear over time without an increased risk for future plaque rupture events. However, if high blood pressure is uncontrolled and maintained long term, the critical failure criterion of the tissue may be exceeded and the tissue could continue to tear, resulting in a clinical event such as a stroke or TIA. It is important to note that this analysis does

not consider the effects of material fatigue, which may also play a significant role in plaque rupture.

4.4.4 Fracture parameters for fibrous caps

Materials that fracture at a higher stress are considered to be stronger than materials that fracture at a lower stress. A material with a higher CTOD is considered more resistant to fracture than a material with a lower CTOD. The results from this study show that tissues with greater collagen content fail at a higher stress and a smaller CTOD than those with a lower collagen content. These divergent fracture parameters suggest a conflicting ranking for the fracture resistance of fibrous caps. Generally, fibrous cap stability has been assessed by the stress at which failure occurs, rather than the CTOD or the strain, but our results and the following discussion suggest that stress may not always be the most appropriate metric to use. Plaque rupture will occur when the fibrous cap tissue cannot withstand the loading conditions imposed upon it. While collagen-rich fibrous caps are able to withstand higher forces, they are less extensible. Deformation of an artery, particularly the carotid artery from which these samples are obtained, is important in vascular health. If the fibrous cap is significantly stiffer than the underlying media and unable to deform to the same extent, the discrepancy in material properties may lead to plaque dissection at the shoulders, a prominent event during balloon angioplasty [24]–[26]. This effect has also been demonstrated in a finite element model where the plaque tissue is approximately one order of magnitude stiffer than the medial layer [100]. A mismatch in material properties between the media and the intima may contribute to the high frequency

of plaque ruptures at the plaque shoulders. Conversely, fibrous caps with lower collagen content may deform more readily with the underlying media but may fail at lower stress values.

Ultimately, the optimal fracture parameter for assessing plaque vulnerability will depend on the material properties of the fibrous cap, rather than the conditions to which it is subjected. Our results do not show which fracture parameter will be best suited for certain situations, such as high stress (high blood pressure) or high strain (balloon angioplasty, for instance). Instead, our results indicate that fibrous caps with higher collagen content are stiffer and will likely reach the critical CTOD before reaching the critical stress, suggesting that CTOD is the appropriate fracture parameter. Conversely, fibrous caps with lower collagen content will fail at a lower stress and therefore stress may be the relevant fracture parameter. For fibrous caps with an intermediate, or unknown, collagen content, it may be necessary to evaluate both fracture parameters.

Knowledge of the collagen content in the fibrous cap can give insight into the failure behavior of the material. Time-resolved laser induced fluorescence spectroscopy, a catheter-based imaging technique, has been shown to detect collagen content in atherosclerotic plaques [101]. This technique may be useful in determining collagen content, and thereby estimating material behavior of the fibrous cap, prior to clinical intervention. In particular, an estimation of the plaque mechanical properties could help assess the optimal treatment for carotid artery stenosis. Carotid endarterectomy (CEA) is generally considered the standard treatment for carotid artery stenosis, but recently carotid artery stenting (CAS) has

been suggested as an alternative, less invasive, technique. CAS has been shown to result in more strokes during the periprocedural period than CEA [27]–[29], which may be a result of the high strain applied on fibrous caps with high collagen content during balloon angioplasty. This increased risk of stroke during the periprocedural period may be reduced if the material properties of the plaque are considered prior to selecting a treatment. While CAS may be a suitable alternative to CEA in some cases, CAS may not be the optimal treatment for patients with high collagen content in the fibrous cap.

4.5 Conclusions

This study shows, for the first time, that CTOD can be used as a comparative metric for fracture toughness in atherosclerotic fibrous cap samples from individual patients. Collagen content is important in determining the mechanical behavior and response of fibrous caps in atherosclerosis. A fibrous cap with higher collagen content fails at a higher stress and lower CTOD than fibrous caps with lower collagen content. Furthermore, high collagen content is associated with a sharper crack tip, suggesting that collagen fiber-rich tissue impedes blunting of the crack tip. Additionally, the results suggest that fibrous caps may exhibit notch insensitivity or even notch strengthening behavior. Lastly, these results show that analyzing the stress in fibrous caps provides only one part of the picture when considering the problem of plaque rupture. The strain, or deformation, which a fibrous cap is able to withstand is also an important aspect of plaque stability which is often ignored in the analysis of plaque rupture.

Acknowledgments

The authors would like to acknowledge financial support from the National Science Foundation through grant number CMMI-1200358. The authors would also like to acknowledge financial support from the National Institute of Health through grant number 1R03 EB019663-01A1, and funding through the Aspire II program from the Office of the Vice President of Research at the University of South Carolina. The funding organizations played no role in the study design, data analysis, or manuscript preparation.

CHAPTER 5

CONCLUSIONS

5.1 Dissertation Summary

The overall aim of this project was to use fracture mechanics concepts to characterize atherosclerotic plaque failure. To achieve this goal, fracture toughness was measured in both mouse and human plaques to assess adhesion strength and during tearing failure of human fibrous caps from carotid endarterectomy specimens. In addition, failure behavior of thin protein films was studied in vitro to measure the adhesion strength of selected proteins,

The adhesion strength between atherosclerotic plaques and IEL as well as the failure load are unchanged between ApoE$^{-/-}$ and ApoE$^{-/-}$ Col8$^{-/-}$ mice. However, the plaques in ApoE$^{-/-}$ Col8$^{-/-}$ mice are less stiff than those in ApoE$^{-/-}$ mice. While human atherosclerotic plaques are much stronger than those found in mice, the plaque adhesion strength data sets are qualitatively similar, in terms of having positively skewed distributions of energy release rate and standard deviations which are approximately equal to the means.

Investigating the plaque-IEL interface further, this study shows that contributions of adhesive matrix proteins to the strength of the plaque-IEL interface can be measured with a novel technique. Semi-quantitative plaque immunoblotting

combined with RDCB experiments shows that collagen IV alone is not likely to be responsible for the adhesive strength of the plaque-IEL interface. SEM images of a partially delaminated plaque show bridging fibers that connect the plaque and the IEL. The adhesive strength of the plaque-IEL interface likely derives from tensile strength of these bridging fibers, potentially composed of collagen I, fibrillin-1, or other structural matrix proteins, rather than from protein adhesion/cohesion.

To characterize plaque susceptibility to tensile rupture of the fibrous cap, this study investigated the fracture toughness of human fibrous caps. The results show, for the first time, that CTOD can be used as a comparative metric for fracture toughness in atherosclerotic fibrous cap samples from individual patients. Collagen content is important in determining the mechanical behavior and response of fibrous caps in atherosclerosis. A fibrous cap with higher collagen content exhibits more brittle behavior and fails at a higher initial stress and lower initial CTOD than fibrous caps with lower collagen content. Collagen fibers act to impede blunting of the crack tip and increase tensile strength of the tissue. Knowledge of the collagen content in the fibrous cap prior to surgical intervention could predict the mechanical response of the fibrous cap and aid in determining the optimal treatment plan.

Fracture toughness was used to assess plaque resistance to two different failure mechanisms: 1) plaque delamination at the plaque-IEL interface and 2) tensile rupture of the fibrous cap. Collagen is a vital structural component of atherosclerotic plaques and is crucial in determining the mechanical response of fibrous caps. Fibrillar forms of collagen, such as collagen I, or other fibrillar

proteins, such as fibrillin-1, are likely responsible for the mechanical strength of the plaque-IEL interface.

5.2 Future Studies

There are several questions that arise from the results of the current study. The results from Chapter 3 show that collagen IV is too weak to account for the mechanical strength of the plaque-IEL interface in mice, measured in situ in Chapter 2. However, these results do not rule out all adhesive proteins as contributors to the mechanical strength at the plaque-IEL interface and therefore the mechanical strength of other adhesive proteins should be investigated. Additionally, the technique we used does not distinguish between adhesive strength between the protein and the underlying matrix and cohesive strength within the protein layer. If adhesive proteins are responsible in part for the mechanical strength of the plaque-IEL interface, distinguishing between cohesive strength and adhesive strength will be important in understanding the detailed failure mechanism.

While all adhesive proteins have not been excluded as potential contributors to plaque-IEL bonding, the role of bridging fibers at the plaque-IEL interface should also be investigated. Specifically, the number, diameter, and composition of these bridging fibers should be further investigated with immunogold SEM. Additionally, the mechanical strength of these bridging fibers should be investigated and compared to the in situ measurements from Chapter 2.

The results from Chapter 4 describe an interesting characterization of fibrous cap mechanical properties. The initial failure criteria can be predicted by collagen content; however, this trend no longer exists with additional crack extension. This change may be due to a movement or realignment of the collagen fibers ahead of the crack tip as the crack extends. Fiber realignment could be investigated using second-harmonic generation (SHG) microscopy to view collagen fiber organization after a small increment of crack growth.

If collagen fibers are in fact realigning during crack extension, the effect of displacement rate on the experimental results should also be investigated. The strain rate in vivo is much higher than the displacement rate of the experiments, and the slower experimental displacement rate may allow the tissue a chance to respond to crack extension, potentially by fiber realignment, which does not exist in vivo.

The degree of fiber realignment may be constrained by the relative stiffness of the surrounding non-collagenous matrix. For this reason, other constituents of the fibrous cap, such as macrophages, SMCs, and proteoglycans, should be investigated.

The ECM constituents quantified in plaque tissue should be related to the mechanical response of these tissues obtained from uniaxial tensile tests performed on the same specimens (see Appendix A). Specifically, the Holzapfel-Gasser-Ogden (HGO) model parameters should be determined for each sample using computational simulations. A structure based constitutive model for each

tissue type can be created by combining the HGO parameters with the material constituents in each sample. These results will be particularly useful to the computational modeling community as there is limited data available in the literature regarding material properties of atherosclerotic plaque for use in simulations.

REFERENCES

[1] M. Heron, “Deaths: Leading causes for 2010,” *National Vital Statistics Reports*, vol. 62, no. 6. Hyattsville, MD, 2013.

[2] A. S. Go, D. Mozaffarian, V. L. Roger, E. J. Benjamin, J. D. Berry, M. J. Blaha, S. Dai, E. S. Ford, C. S. Fox, S. Franco, H. J. Fullerton, C. Gillespie, S. M. Hailpern, J. A. Heit, V. J. Howard, M. D. Huffman, S. E. Judd, B. M. Kissela, S. J. Kittner, D. T. Lackland, J. H. Lichtman, L. D. Lisabeth, R. H. Mackey, D. J. Magid, G. M. Marcus, A. Marelli, D. B. Matchar, D. K. McGuire, E. R. Mohler III, C. S. Moy, M. E. Mussolino, R. W. Neumar, G. Nichol, D. K. Pandey, N. P. Paynter, M. J. Reeves, P. D. Sorlie, J. Stein, A. Towfighi, T. N. Turan, S. S. Virani, N. D. Wong, D. Woo, and M. B. Turner, “Heart disease and stroke statistics--2014 update: A report from the American Heart Association.,” *Circulation*, vol. 128, pp. 00–00, Jan. 2014.

[3] T. C. Gasser, R. W. Ogden, and G. A. Holzapfel, “Hyperelastic modelling of arterial layers with distributed collagen fibre orientations.,” *J. R. Soc. Interface*, vol. 3, no. 6, pp. 15–35, Feb. 2006.

[4] M. A. Lillie, T. E. Armstrong, S. G. Gérard, R. E. Shadwick, and J. M. Gosline, “Contribution of elastin and collagen to the inflation response of the pig thoracic aorta: assessing elastin’s role in mechanical homeostasis.,” *J. Biomech.*, vol. 45, no. 12, pp. 2133–41, Aug. 2012.

[5] J. E. Wagenseil and R. P. Mecham, “Elastin in large artery stiffness and hypertension,” *J. Cardiovasc. Transl. Res.*, vol. 5, no. 3, pp. 264–273, 2012.

[6] J. M. Clark and S. Glagov, “Transmural organization of the arterial media. The lamellar unit revisited,” *Arterioscler. Thromb. Vasc. Biol.*, vol. 5, no. 1, pp. 19–34, Jan. 1985.

[7] R. L. Armentano, J. Levenson, J. G. Barra, E. I. C. Fischer, G. J. Breitbart, R. H. Pichel, and A. Simon, “Assessment of elastin and collagen contribution to aortic elasticity in conscious dogs,” *Am. J. Physiol.*, vol. 260, no. 29, pp. H1870–H1877, 1991.

[8] J. E. Wagenseil and R. P. Mecham, “Vascular extracellular matrix and arterial mechanics.,” *Physiol. Rev.*, vol. 89, no. 3, pp. 957–89, Jul. 2009.

[9] D. Hubmacher and D. P. Reinhardt, “Microfibrils and fibrillin,” in *The Extracellular Matrix: An Overview*, R. P. Mecham, Ed. Springer-Verlag Berlin Heidelberg, 2011, pp. 233–265.

[10] M. J. Sherratt, C. Baldock, J. L. Haston, D. F. Holmes, C. J. P. Jones, C. A. Shuttleworth, T. J. Wess, and C. M. Kielty, “Fibrillin microfibrils are stiff reinforcing fibres in compliant tissues,” *J. Mol. Biol.*, vol. 332, no. 1, pp. 183–193, 2003.

[11] E. C. Davis, “Immunolocalization of microfibril and microfibril-associated proteins in the subendothelial matrix of the developing mouse aorta,” *J.*

Cell Sci., vol. 107, pp. 727–36, Mar. 1994.

[12] E. C. Davis, “Endothelial cell connecting filaments anchor endothelial cells to the subadjacent elastic lamina in the developing aortic intima of the mouse,” *Cell Tissue Res.*, vol. 272, pp. 211–219, 1993.

[13] J. Halper and M. Kjaer, “Basic components of connective tissues and extracellular matrix: Elastin, fibrillin, fibulins, fibrinogen, fibronectin, laminin, tenascins and thrombospondins,” in *Progress in Heritable Soft Connective Tissue Diseases*, J. Halper, Ed. Springer Netherlands, 2014, pp. 31–47.

[14] P. Bornstein and E. H. Sage, “Matricellular proteins: Extracellular modulators of cell function,” *Curr. Opin. Cell Biol.*, vol. 14, pp. 608–616, 2002.

[15] H. C. Stary, D. H. Blankenhorn, A. B. Chandler, S. Glagov, W. Insull, M. Richardson, M. E. Rosenfeld, S. A. Schaffer, C. J. Schwartz, W. D. Wagner, and R. W. Wissler, “A definition of the intima of human arteries and of its atherosclerosis-prone regions,” *Circulation*, vol. 85, pp. 391–405, 1992.

[16] K. J. Williams and I. Tabas, “The Response-to-Retention Hypothesis of Early Atherogenesis,” *Arterioscler. Thromb. Vasc. Biol.*, vol. 15, no. 5, pp. 551–561, 1995.

[17] M. Y. Chang, C. K. Chan, K. R. Braun, P. S. Green, K. D. O’Brien, A. Chait, A. J. Day, and T. N. Wight, “Monocyte-to-macrophage differentiation:

synthesis and secretion of a complex extracellular matrix," *J. Biol. Chem.*, vol. 287, no. 17, pp. 14122–35, Apr. 2012.

[18] Y. Nakashima, H. Fujii, S. Sumiyoshi, T. N. Wight, and K. Sueishi, "Early human atherosclerosis: accumulation of lipid and proteoglycans in intimal thickenings followed by macrophage infiltration.," *Arterioscler. Thromb. Vasc. Biol.*, vol. 27, no. 5, pp. 1159–65, May 2007.

[19] Y. Li, R. F. Schwabe, T. DeVries-Seimon, P. M. Yao, M.-C. Gerbod-Giannone, A. R. Tall, R. J. Davis, R. Flavell, D. A. Brenner, and I. Tabas, "Free cholesterol-loaded macrophages are an abundant source of tumor necrosis factor-alpha and interleukin-6: Model of NF-kappaB- and map kinase-dependent inflammation in advanced atherosclerosis," *J. Biol. Chem.*, vol. 280, no. 23, pp. 21763–72, Jun. 2005.

[20] R. Virmani, F. D. Kolodgie, A. P. Burke, A. Farb, and S. M. Schwartz, "Lessons from sudden coronary death: A comprehensive morphological classification scheme for atherosclerotic lesions," *Arterioscler. Thromb. Vasc. Biol.*, vol. 20, no. 5, pp. 1262–1275, May 2000.

[21] A. V. Finn, M. Nakano, J. Narula, F. D. Kolodgie, and R. Virmani, "Concept of vulnerable/unstable plaque," *Arterioscler. Thromb. Vasc. Biol.*, vol. 30, no. 7, pp. 1282–92, Jul. 2010.

[22] J. F. Bentzon, F. Otsuka, R. Virmani, and E. Falk, "Mechanisms of plaque formation and rupture," *Circ. Res.*, vol. 114, no. 12, pp. 1852–1866, Jun. 2014.

[23] A. P. Burke, F. D. Kolodgie, A. Farb, D. K. Weber, G. T. Malcom, J. Smialek, and R. Virmani, “Healed plaque ruptures and sudden coronary death: Evidence that subclinical rupture has a role in plaque progression,” *Circulation*, vol. 103, no. 7, pp. 934–940, Feb. 2001.

[24] D. L. Fischman, M. P. Savage, M. B. Leon, R. A. Schatz, S. G. Ellis, M. W. Cleman, P. Teirstein, C. M. Walker, S. Bailey, J. W. Hirshfeld, and S. Goldberg, “Effect of intracoronary stenting on intimal dissection after balloon angioplasty: Results of quantitative and qualitative coronary analysis,” *J. Am. Coll. Cardiol.*, vol. 18, no. 6, pp. 1445–1451, 1991.

[25] A. Schomig, A. Kastrati, R. Dietz, B. Rauch, F.-J. Neumann, H. H. Katus, and U. Busch, “Emergency coronary stenting for dissection during percutaneous transluminal coronary angioplasty: Angiographic follow-up after stenting and after repeat angioplasty of the stented segment,” *J. Am. Coll. Cardiol.*, vol. 23, no. 5, pp. 1053–1060, 1994.

[26] N. Gonzalo, P. W. Serruys, T. Okamura, Z. J. Shen, H. M. Garcia-Garcia, Y. Onuma, R. J. van Geuns, J. Ligthart, and E. Regar, “Relation between plaque type and dissections at the edges after stent implantation: An optical coherence tomography study,” *Int. J. Cardiol.*, vol. 150, no. 2, pp. 151–155, Jul. 2011.

[27] G. Lanzino, A. A. Rabinstein, and R. D. Brown, “Treatment of carotid artery stenosis: medical therapy, surgery, or stenting?,” *Mayo Clin. Proc.*, vol. 84, no. 4, pp. 362–88, 2009.

[28] J. D. Spence, “Management of patients with an asymptomatic carotid stenosis—medical management, endovascular treatment, or carotid endarterectomy?,” *Curr. Neurol. Neurosci. Rep.*, vol. 16, no. 1, pp. 1–7, 2016.

[29] J. Sun and T. S. Hatsukami, “Plaque imaging to decide on optimal treatment medical versus carotid endarterectomy versus carotid artery stenting,” *Neuroimaging Clin. N. Am.*, vol. 26, no. 1, pp. 165–173, 2016.

[30] D. Taylor, N. O’Mara, E. Ryan, M. Takaza, and C. Simms, “The fracture toughness of soft tissues,” *J. Mech. Behav. Biomed. Mater.*, vol. 6, pp. 139–147, Feb. 2012.

[31] X.-K. Zhu and J. A. Joyce, “Review of fracture toughness (G, K, J, CTOD, CTOA) testing and standardization,” *Eng. Fract. Mech.*, vol. 85, pp. 1–46, May 2012.

[32] B. Cotterell, “The past, present, and future of fracture mechanics,” *Eng. Fract. Mech.*, vol. 69, no. 5, pp. 533–553, Mar. 2002.

[33] F. Erdogan, “Fracture mechanics,” *Int. J. Solids Struct.*, vol. 37, no. 1–2, pp. 171–183, Jan. 2000.

[34] M. V. Chin-Purcell and J. L. Lewis, “Fracture of articular cartilage,” *J. Biomech. Eng.*, vol. 118, no. 4, pp. 545–556, 1996.

[35] B. Chu, E. Gaillard, R. Mongrain, S. Reiter, and J.-C. Tardif, “Characterization of fracture toughness exhaustion in pig aorta,” *J. Mech.*

Behav. Biomed. Mater., vol. 17, pp. 126–136, Jan. 2013.

[36] Y. Wang, J. Ning, J. A. Johnson, M. A. Sutton, and S. M. Lessner, “Development of a quantitative mechanical test of atherosclerotic plaque stability,” *J. Biomech.*, vol. 44, no. 13, pp. 2439–2445, Sep. 2011.

[37] Y. Wang, J. A. Johnson, A. Fulp, M. A. Sutton, and S. M. Lessner, “Adhesive strength of atherosclerotic plaque in a mouse model depends on local collagen content and elastin fragmentation,” *J. Biomech.*, vol. 46, no. 4, pp. 716–722, Feb. 2013.

[38] N. E. S. Sibinga, L. C. Foster, C.-M. Hsieh, M. A. Perrella, W.-S. Lee, W. O. Endege, E. H. Sage, M.-E. Lee, and E. Haber, “Collagen VIII Is Expressed by Vascular Smooth Muscle Cells in Response to Vascular Injury,” *Circ. Res.*, vol. 80, no. 4, pp. 532–541, 1997.

[39] G. Hou, D. Mulholland, M. A. Gronska, and M. P. Bendeck, “Type VIII collagen stimulates smooth muscle cell migration and matrix metalloproteinase synthesis after arterial injury.,” *Am. J. Pathol.*, vol. 156, no. 2, pp. 467–476, 2000.

[40] S. Sinha, C. M. Kielty, A. M. Heagerty, A. E. Canfield, and C. A. Shuttleworth, “Upregulation of collagen VIII following porcine coronary artery angioplasty is related to smooth muscle cell migration not angiogenesis,” *Int. J. Exp. Pathol.*, vol. 82, no. 5, pp. 295–302, 2001.

[41] E. Adiguzel, G. Hou, D. Mulholland, U. Hopfer, N. Fukai, B. Olsen, and M.

Bendeck, “Migration and growth are attenuated in vascular smooth muscle cells with type VIII collagen-null alleles,” *Arterioscler. Thromb. Vasc. Biol.*, vol. 26, no. 1, pp. 56–61, 2006.

[42] J. Lopes, E. Adiguzel, S. Gu, S.-L. Liu, G. Hou, S. Heximer, R. K. Assoian, and M. P. Bendeck, “Type VIII collagen mediates vessel wall remodeling after arterial injury and fibrous cap formation in atherosclerosis,” *Am. J. Pathol.*, vol. 182, no. 6, pp. 2241–53, Jun. 2013.

[43] R. Virmani, F. D. Kolodgie, A. P. Burke, A. Farb, and S. M. Schwartz, “Lessons From Sudden Coronary Death : A Comprehensive Morphological Classification Scheme for Atherosclerotic Lesions,” *Arterioscler. Thromb. Vasc. Biol.*, vol. 20, no. 5, pp. 1262–1275, May 2000.

[44] Z. Teng, Y. Zhang, Y. Huang, J. Feng, J. Yuan, Q. Lu, M. P. F. Sutcliffe, A. J. Brown, Z. Jing, and J. H. Gillard, “Material properties of components in human carotid atherosclerotic plaques: A uniaxial extension study,” *Acta Biomater.*, vol. 10, no. 12, pp. 5055–5063, 2014.

[45] H. M. Loree, A. J. Grodzinsky, S. Y. Park, L. J. Gibson, and R. T. Lee, “Static circumferential tangential modulus of human atherosclerotic tissue,” *J. Biomech.*, vol. 27, no. 2, pp. 195–204, 1994.

[46] M. G. Lawlor, M. R. O’Donnell, B. M. O’Connell, and M. T. Walsh, “Experimental determination of circumferential properties of fresh carotid artery plaques,” *J. Biomech.*, vol. 44, no. 9, pp. 1709–1715, 2011.

[47] J. J. Mulvihill, E. M. Cunnane, S. M. McHugh, E. G. Kavanagh, S. R. Walsh, and M. T. Walsh, “Mechanical, biological and structural characterization of in vitro ruptured human carotid plaque tissue,” *Acta Biomater.*, vol. 9, no. 11, pp. 9027–9035, 2013.

[48] E. M. Cunnane, J. J. E. Mulvihill, H. E. Barrett, D. A. Healy, E. G. Kavanagh, S. R. Walsh, and M. T. Walsh, “Mechanical, biological and structural characterization of human atherosclerotic femoral plaque tissue,” *Acta Biomater.*, vol. 11, pp. 295–303, 2015.

[49] E. Maher, A. Creane, S. Sultan, N. Hynes, C. Lally, and D. J. Kelly, “Tensile and compressive properties of fresh human carotid atherosclerotic plaques,” *J. Biomech.*, vol. 42, no. 16, pp. 2760–2767, 2009.

[50] C.-K. Chai, L. Speelman, C. W. J. Oomens, and F. P. T. Baaijens, “Compressive mechanical properties of atherosclerotic plaques--indentation test to characterise the local anisotropic behaviour.,” *J. Biomech.*, vol. 47, no. 4, pp. 784–92, Mar. 2014.

[51] S. R. H. Barrett, M. P. F. Sutcliffe, S. Howarth, Z.-Y. Li, and J. H. Gillard, “Experimental measurement of the mechanical properties of carotid atherothrombotic plaque fibrous cap,” *J. Biomech.*, vol. 42, no. 11, pp. 1650–1655, 2009.

[52] G. A. Holzapfel, G. Sommer, and P. Regitnig, “Anisotropic mechanical properties of tissue components in human atherosclerotic plaques,” *J. Biomech. Eng.*, vol. 126, no. 5, pp. 657–665, 2004.

[53] Z. Teng, D. Tang, J. Zheng, P. K. Woodard, and A. H. Hoffman, “An experimental study on the ultimate strength of the adventitia and media of human atherosclerotic carotid arteries in circumferential and axial directions,” *J. Biomech.*, vol. 42, no. 15, pp. 2535–2539, 2009.

[54] Z. Teng, J. Feng, Y. Zhang, M. P. F. Sutcliffe, Y. Huang, A. J. Brown, Z. Jing, Q. Lu, and J. H. Gillard, “A uni-extension study on the ultimate material strength and extreme extensibility of atherosclerotic tissue in human carotid plaques,” *J. Biomech.*, vol. 48, no. 14, pp. 3859–3867, 2015.

[55] E. Adiguzel, G. Hou, D. Mulholland, U. Hopfer, N. Fukai, B. Olsen, and M. Bendeck, “Migration and growth are attenuated in vascular smooth muscle cells with type VIII collagen-null alleles.,” *Arterioscler. Thromb. Vasc. Biol.*, vol. 26, no. 1, pp. 56–61, Jan. 2006.

[56] Y. Wang, J. A. Johnson, F. G. Spinale, M. A. Sutton, and S. M. Lessner, “Quantitative Measurement of Dissection Resistance in Intimal and Medial Layers of Human Coronary Arteries.,” *Exp. Mech.*, vol. 54, no. 4, pp. 677–683, Apr. 2014.

[57] G. Sommer, T. C. Gasser, P. Regitnig, M. Auer, and G. A. Holzapfel, “Dissection properties of the human aortic media: an experimental study,” *J. Biomech. Eng.*, vol. 130, no. 2, p. 021007, Apr. 2008.

[58] S. Pasta, J. A. Phillippi, T. G. Gleason, and D. A. Vorp, “Effect of aneurysm on the mechanical dissection properties of the human ascending thoracic

aorta," *J. Thorac. Cardiovasc. Surg.*, vol. 143, no. 2, pp. 460–467, 2012.

[59] H. J. Barnett, D. W. Taylor, M. Eliasziw, A. J. Fox, G. G. Ferguson, R. B. Haynes, R. N. Rankin, G. P. Clagett, V. C. Hacinski, D. L. Sackett, K. E. Thorpe, and H. E. Meldrum, "Benefit of carotid endarterectomy in patients with symptomatic moderate or severe stenosis," *N. Engl. J. Med.*, vol. 339, no. 20, pp. 1415–1425, 1998.

[60] A. Tsamis, J. A. Phillippi, R. G. Koch, S. Pasta, A. D'Amore, S. C. Watkins, W. R. Wagner, T. G. Gleason, and D. A. Vorp, "Fiber micro-architecture in the longitudinal-radial and circumferential-radial planes of ascending thoracic aortic aneurysm media," *J. Biomech.*, vol. 46, no. 16, pp. 2787–2794, 2013.

[61] J. Khoshnoodi, V. Pedchenko, and B. G. Hudson, "Mammalian collagen IV," *Microsc. Res. Tech.*, vol. 71, no. 5, pp. 357–370, 2008.

[62] W. Halfter, P. Oertle, C. A. Monnier, L. Camenzind, M. Reyes-Lua, H. Hu, J. Candiello, A. Labilloy, M. Balasubramani, P. B. Henrich, and M. Plodinec, "New concepts in basement membrane biology," *FEBS J.*, vol. 282, pp. 4466–4479, 2015.

[63] T. J. Herbst, J. B. McCarthy, E. C. Tsilibary, and L. T. Furcht, "Differential effects of laminin, intact type IV collagen, and specific domains of type IV collagen on endothelial cell adhesion and migration," *J. Cell Biol.*, vol. 106, no. 4, pp. 1365–1373, 1988.

[64] J. Des Parkin, J. D. San Antonio, V. Pedchenko, B. Hudson, S. T. Jensen, and J. Savige, “Mapping structural landmarks, ligand binding sites, and missense mutations to the collagen IV heterotrimers predicts major functional domains, novel interactions, and variation in phenotypes in inherited diseases affecting basement membranes,” *Hum. Mutat.*, vol. 32, no. 2, pp. 127–143, 2011.

[65] T. A. Eriksen, D. M. Wright, P. P. Purslow, and V. C. Duance, “Role of Ca2+ for the mechanical properties of fibrillin,” *Proteins Struct. Funct. Genet.*, vol. 45, no. 1, pp. 90–95, 2001.

[66] K. Tiedemann, T. Sasaki, E. Gustafsson, W. Gohring, B. Batge, H. Notbohm, R. Timpl, T. Wedel, U. Schlotzer-Schrehardt, and D. P. Reinhardt, “Microfibrils at basement membrane zones interact with perlecan via fibrillin-1,” *J. Biol. Chem.*, vol. 280, no. 12, pp. 11404–11412, 2005.

[67] D. V. Bax, S. E. Bernard, A. Lomas, A. Morgan, J. Humphries, C. A. Shuttleworth, M. J. Humphries, and C. M. Kielty, “Cell adhesion to fibrillin-1 molecules and microfibrils is mediated by a5b1 and avb3 integrins,” *J. Biol. Chem.*, vol. 278, no. 36, pp. 34605–34616, 2003.

[68] E. Engvall and E. Ruoslahti, “Binding of soluble form of fibroblast surface protein, fibronectin, to collagen,” *Int. J. Cancer*, vol. 20, no. 1, pp. 1–5, 1977.

[69] K. M. Yamada, D. W. Kennedy, K. Kimata, and R. M. Pratt,

"Characterization of fibronectin interactions with glycosaminoglycans and identification of active proteolytic fragments," *J. Biol. Chem.*, vol. 255, no. 13, pp. 6055–6063, 1980.

[70] G. A. Johnson, R. C. Burghardt, and F. W. Bazer, "Osteopontin: a leading candidate adhesion molecule for implantation in pigs and sheep," *J. Anim. Sci. Biotechnol.*, vol. 5, no. 56, pp. 1–14, 2014.

[71] B. B. Mukherjee, M. Nemir, S. Beninati, E. Cordella-Miele, K. Singh, I. Chackalaparampil, V. Shanmugam, M. W. DeVouge, and A. B. Mukherjee, "Interaction of osteopontin with fibronectin and other extracellular matrix molecules," *Ann. N. Y. Acad. Sci.*, vol. 760, pp. 201–212, 1995.

[72] S. M. Martin, J. L. Schwartz, C. M. Giachelli, and B. D. Ratner, "Enhancing the biological activity of immobilized osteopontin using a type-1 collagen affinity coating," *J Biomed Mater Res A*, vol. 70, no. 1, pp. 10–19, 2004.

[73] M. Okabe, C. Nyakas, B. Buwalda, and P. G. M. Luiten, "In situ blotting: A novel method for direct transfer of native proteins from sectioned tissue to blotting membrane: Procedure and some applications," *J. Histochem. Cytochem.*, vol. 41, no. 6, pp. 927–934, 1993.

[74] C. F. Moh, S. L. Siedlak, M. Tabaton, G. Perry, R. J. Castellani, and M. A. Smith, "Paraffin-embedded tissue (PET) blot method: Application to Alzheimer disease," *J. Neurosci. Methods*, vol. 190, no. 2, pp. 244–247, 2011.

[75] A. Khayer Dastjerdi, M. Pagano, M. T. Kaartinen, M. D. McKee, and F. Barthelat, “Cohesive behavior of soft biological adhesives: experiments and modeling.,” *Acta Biomater.*, vol. 8, no. 9, pp. 3349–59, Sep. 2012.

[76] A. Khayer Dastjerdi, E. Tan, and F. Barthelat, “Direct Measurement of the Cohesive Law of Adhesives Using a Rigid Double Cantilever Beam Technique,” *Exp. Mech.*, vol. 53, no. 9, pp. 1763–1772, May 2013.

[77] L. Zand, Q. Feng, C. D. Roskelley, P. C. K. Leung, and N. Auersperg, “Differential effects of cellular fibronectin and plasma fibronectin on ovarian cancer cell adhesion, migration, and invasion,” *Vitr. Cell. Dev. Biol. Anim.*, vol. 39, no. 3, pp. 178–182, 2003.

[78] S. Lambert Vidmar, F. Lottspeich, I. Emod, J. M. Imhoff, and V. Keil-Dlouha, “Collagen-binding domain of human plasma fibronectin contains a latent type-IV collagenase,” *Eur J Biochem*, vol. 201, no. 1, pp. 79–84, 1991.

[79] K. Lewandowska, H. U. Choi, L. C. Rosenberg, L. Zardi, and L. A. Culp, “Fibronectin-mediated adhesion of fibroblasts: Inhibition by dermatan sulfate proteoglycan and evidence for a cryptic glycosaminoglycan-binding domain,” *J. Cell Biol.*, vol. 105, no. 3, pp. 1443–1454, 1987.

[80] E. Maurer, M. Schaff, N. Receveur, C. Bourdon, L. Mercier, B. Nieswandt, C. Dubois, M. Jandrot-Perrus, J. G. Goetz, F. Lanza, C. Gachet, and P. H. Mangin, “Fibrillar cellular fibronectin supports efficient platelet aggregation and procoagulant activity,” *Thromb. Haemost.*, vol. 114, no. 6, pp. 1175–

1188, 2015.

[81] P. Singh, C. Carraher, and J. Schwarzbauer, “Assembly of fibronectin extracellular matrix,” *Annu. Rev. Cell Dev. Biol.*, vol. 26, pp. 397–419, 2010.

[82] K. Nakamura, “Characterization of the interaction between human plasma fibronectin and collagen by means of affinity electrophoresis,” *J. Chromatogr.*, vol. 597, pp. 351–356, 1992.

[83] S. C. Stamatoglou and J. M. Keller, “Interactions of cellular glycosaminoglycans with plasma fibronectin and collagen,” *Biochim. Biophys. Acta*, vol. 719, pp. 90–97, 1982.

[84] C. R. Carlisle, C. Coulais, and M. Guthold, “The mechanical stress-strain properties of single electrospun collagen type I nanofibers,” *Acta Biomater.*, vol. 6, no. 8, pp. 2997–3003, 2010.

[85] L. Yang, C. F. C. Fitié, K. O. van der Werf, M. L. Bennink, P. J. Dijkstra, and J. Feijen, “Mechanical properties of single electrospun collagen type I fibers,” *Biomaterials*, vol. 29, no. 8, pp. 955–962, 2008.

[86] M. M. J. F. Koenders, L. Yang, R. G. Wismans, K. O. van der Werf, D. P. Reinhardt, W. Daamen, M. L. Bennink, P. J. Dijkstra, T. H. van Kuppevelt, and J. Feijen, “Microscale mechanical properties of single elastic fibers: The role of fibrillin-microfibrils,” *Biomaterials*, vol. 30, no. 13, pp. 2425–2432, 2009.

[87] Y. Ganesan, H. Salahshoor, C. Peng, V. Khabashesku, J. Zhang, A. Cate, N. Rahbar, and J. Lou, “Fracture toughness of the sidewall fluorinated carbon nanotube-epoxy interface,” *J. Appl. Phys.*, vol. 115, no. 22, 2014.

[88] G. W. Petty, R. D. Brown, J. P. Whisnant, J. D. Sicks, W. M. O’Fallon, and D. O. Wiebers, “Ischemic stroke subtypes: A population-based study of incidence and risk factors,” *Stroke*, vol. 30, no. 12, pp. 2513–2516, 1999.

[89] Y. Wang, J. A. Johnson, F. G. Spinale, M. A. Sutton, and S. M. Lessner, “Quantitative measurement of dissection resistance in intimal and medial layers of human coronary arteries,” *Exp. Mech.*, vol. 54, no. 4, pp. 677–683, Dec. 2014.

[90] A. A. Wells, “Application of fracture mechanics at and beyond general yielding,” *Br. Weld. J.*, vol. 10, no. 11, pp. 563–570, 1963.

[91] M. G. Dawes, “Elastic-plastic fracture toughness based on the COD and J-Contour Integral concepts,” *ASTM STP 668*, pp. 307–333, 1979.

[92] J. R. Rice, “A path independent integral and the approximate analysis of strain concentration by notches and cracks,” *J. Appl. Mech.*, vol. 35, no. 2, pp. 379–386, 1968.

[93] A. C. Akyildiz, L. Speelman, and F. J. H. Gijsen, “Mechanical properties of human atherosclerotic intima tissue,” *J. Biomech.*, vol. 47, no. 4, pp. 773–83, Mar. 2014.

[94] B. V. Shekhonin, S. P. Domogatsky, G. L. Idelson, V. E. Koteliansky, and

V. . Rukosuev, “Relative distribution of fibronectin and type I, III, IV, V collagens in normal and atherosclerotic intima of human arteries,” *Atherosclerosis*, vol. 67, no. 1, pp. 9–16, 1987.

[95] C. L. Lendon, A. D. Briggs, G. V. R. Born, M. C. Burleigh, and M. J. Davies, “Mechanical testing of connective tissue in the search for determinants of atherosclerotic plaque cap rupture,” *Biochem. Soc. Trans.*, vol. 16, pp. 1032–1033, 1988.

[96] M. C. Burleigh, A. D. Briggs, C. L. Lendon, M. J. Davies, G. V. R. Born, and P. D. Richardson, “Collagen types I and III, collagen content, GAGs and mechanical strength of human atherosclerotic plaque caps: Span-wise variations,” *Atherosclerosis*, vol. 96, no. 1, pp. 71–81, 1992.

[97] R. T. Qu, M. Calin, J. Eckert, and Z. F. Zhang, “Metallic glasses: Notch-insensitive materials,” *Scr. Mater.*, vol. 66, no. 10, pp. 733–736, 2012.

[98] R. Qu, P. Zhang, and Z. Zhang, “Notch effect of materials: Strengthening or weakening?,” *J. Mater. Sci. Technol.*, vol. 30, no. 6, pp. 599–608, 2014.

[99] P. P. Purslow, “The physical basis of meat texture: Observations on the fracture behavior of cooked bovine M. Semitendinosus,” *Meat Sci.*, vol. 12, no. 1, pp. 39–60, 1985.

[100] P. Badel, S. Avril, M. A. Sutton, and S. M. Lessner, “Numerical simulation of arterial dissection during balloon angioplasty of atherosclerotic coronary arteries,” *J. Biomech.*, vol. 47, no. 4, pp. 878–89, Mar. 2014.

[101] L. Marcu, J. A. Jo, Q. Fang, T. Papaioannou, T. Reil, J. Qiao, J. D. Baker, J. A. Freischlag, and M. C. Fishbein, “Detection of rupture-prone atherosclerotic plaques by time- resolved laser induced fluorescence spectroscopy,” *Atherosclerosis*, vol. 204, no. 1, pp. 156–164, 2009.

APPENDIX A

ADDITIONAL MECHANICAL TEST DATA AND HISTOLOGICAL RESULTS FROM HUMAN ATEROSCLEROTIC PLAQUES

Chapter 4, a study on the fracture resistance of atherosclerotic fibrous caps, was a portion of a larger study on mechanical properties of atherosclerotic plaque tissue. This appendix presents additional mechanical test data and histological studies performed on human atherosclerotic plaque tissue.

Mechanical testing was performed on strips of isolated fibrous cap (FC), media underlying atherosclerotic lesions (diseased media, DM), and media from relatively healthy sections of tissue (normal media, NM). Stress-strain curves obtained from uniaxial tensile experiments performed on strips of atherosclerotic plaque tissue (see section 4.2.2.2 for full experimental methodology) are presented in Figure A.1.

There is a lot of scatter both within and between tissue types, similar to section 4.3.1. However, the average diseased media specimen is somewhat stiffer than the average normal media specimen. The mechanical response of the fibrous cap specimens is similar to that of the media specimens. After mechanical testing, each specimen was fixed in 4% paraformaldehyde in phosphate buffer and stored at 4 °C.

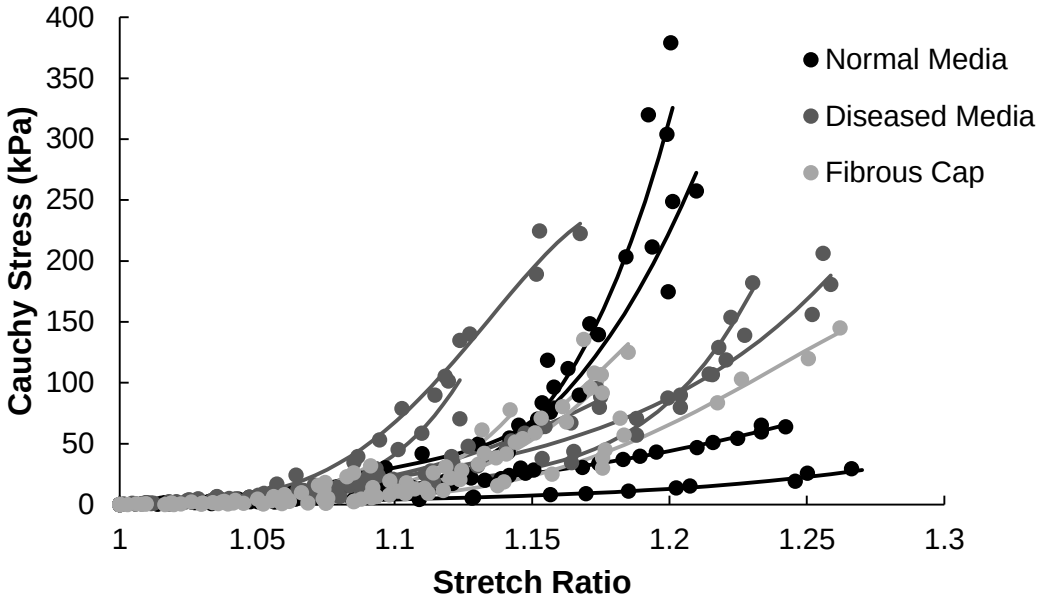

Figure A.1 Stress-strain relationships for strips of isolated normal media, diseased media, and fibrous cap from human carotid endarterectomy specimens.

Collagen content and elastin content were determined in each fixed sample saved following mechanical testing using standard histological techniques. Collagen content was determined in each sample by staining with Picrosirius Red (PSR) and following the protocol in section 4.2.3. Additionally, elastin content was determined by staining with Verhoeff solution and calculating the area of black tissue (elastin) relative to the total tissue area. Representative images of trichrome staining, PSR staining, and Verhoeff staining are shown in Figure A.2 for each tissue type. The histology performed on normal media (top row) shows some intimal thickening is present in this tissue, most clearly visible in the Verhoeff stain (right column). This is not surprising as this tissue is immediately adjacent to advanced atherosclerotic lesions and therefore is likely to exhibit some characteristics of the diseased state.

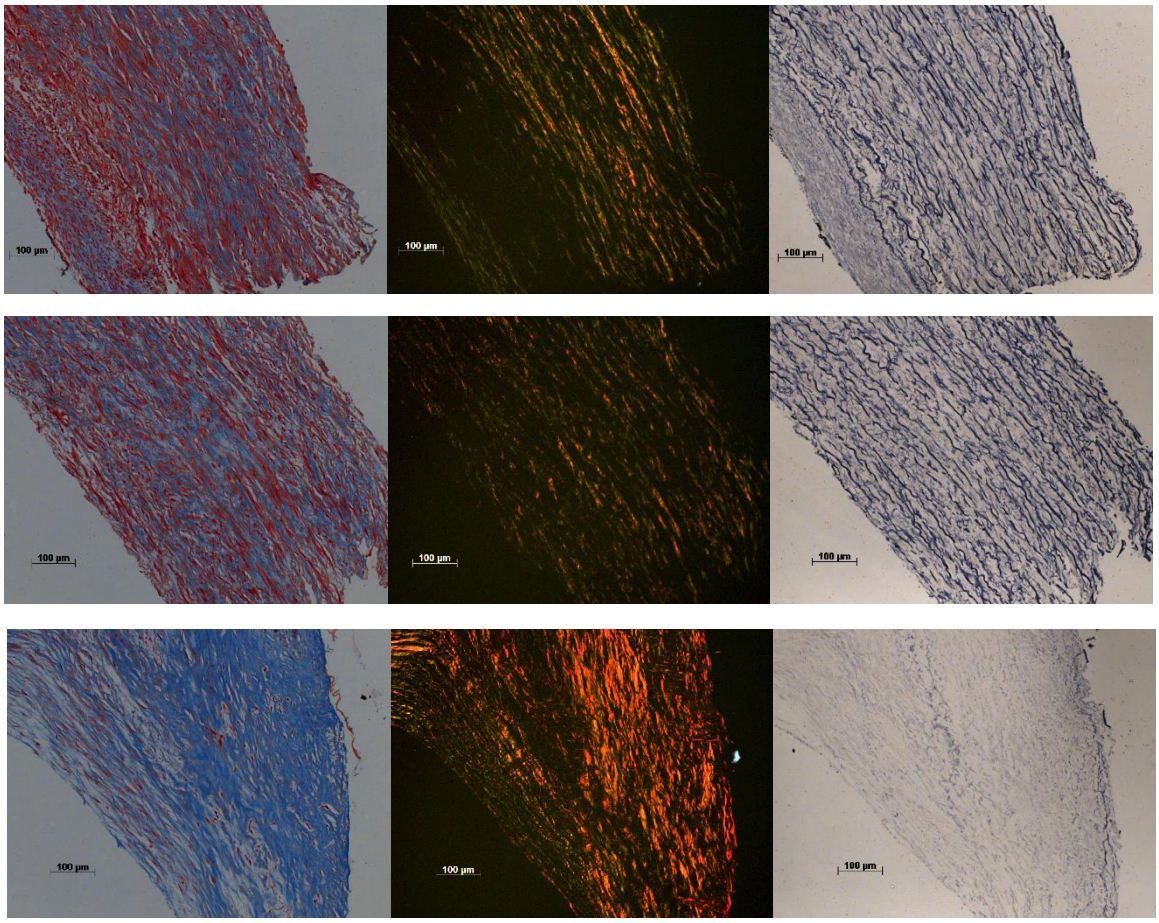

Figure A.2 Representative trichrome (left column), Picrosirius Red (middle column) and modified Verhoeff (right column) staining for normal media (top row), diseased media (middle row) and fibrous cap (bottom row). Scale bars represent 100 µm.

The results from quantification of the histological images from 5 specimens per tissue type are shown in Figure A.3 and Table A.2. One way ANOVA confirms that there are significant differences in both collagen and elastin content between tissue types. Tukey's Honestly Significant Different test confirms that collagen content in the fibrous cap is significantly different from both normal and diseased media. The elastin content in the fibrous cap is significant different from that the in normal media, but not the diseased media. There are no significant differences in collagen or elastin content between normal and diseased media.

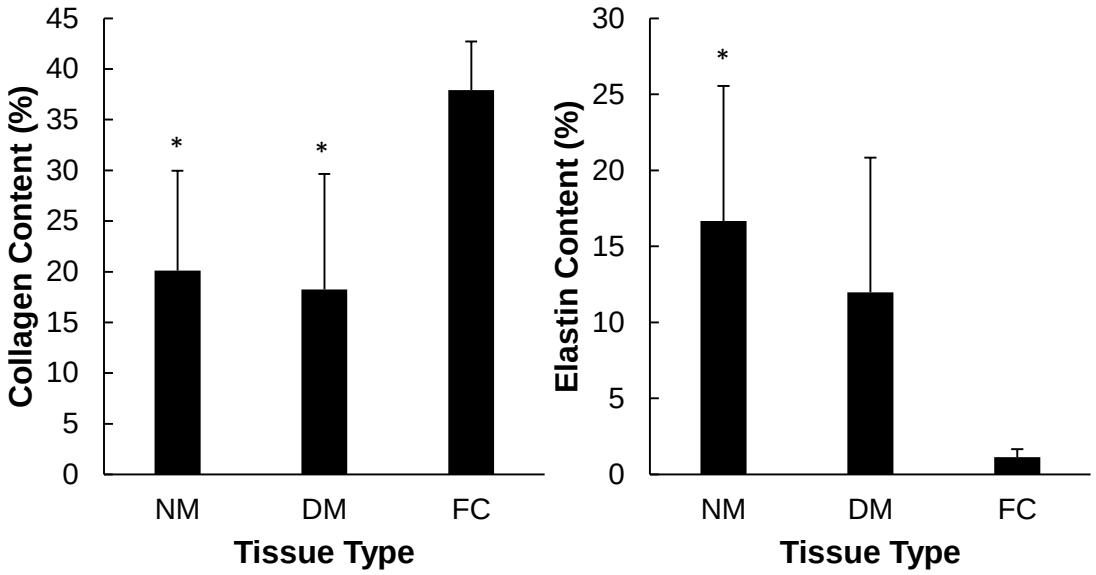

Figure A.3 Collagen and elastin content in normal media (NM), diseased media (DM), and fibrous cap (FC). Error bars represent standard deviation.

Table A.1 Summary of histological results for each tissue type

Tissue	Sample ID	Collagen %	Elastin %
Normal Media	NM1	22.1	7.0
	NM2	36.0	11.5
	NM3	12.0	17.7
	NM4	12.1	30.6
	NM5	18.4	16.5
	Average	*20.1 ± 9.8*	*16.7 ± 8.9*
Diseased Media	DM1	32.5	5.8
	DM2	26.3	6.0
	DM3	6.3	25.1
	DM4	18.4	5.7
	DM5	7.7	17.3
	Average	*18.3 ± 11.4*	*12.0 ± 8.9*
Fibrous Cap	FC1	30.4	0.72
	FC2	37.6	0.57
	FC3	38.5	1.3
	FC4	39.8	1.1
	FC5	43.4	1.9
	Average	*37.9 ± 4.8*	*1.1 ± 0.5*